Совместное использование нейтронного и синхротронного излучений для анализа структуры и динамики материалов

С.Б.Вахрушев

Нейтроны и СИ

Параметр	Нейтроны	СИ
Длина волны, nm	0.025 - 3	0.01 - ?
Энергия	0.1 – 1000 meV	? – 100 KeV
Спин	1/2	1
Магнитный момент	1.913 μ_N	0
Зависимость f(λ)	Для ядерного – нет, Для магнитного - есть	есть

Atomic Form Factor: $f^0(\vec{q}) = \int \rho(\vec{r}) e^{i\vec{q}\cdot\vec{r}} dV$

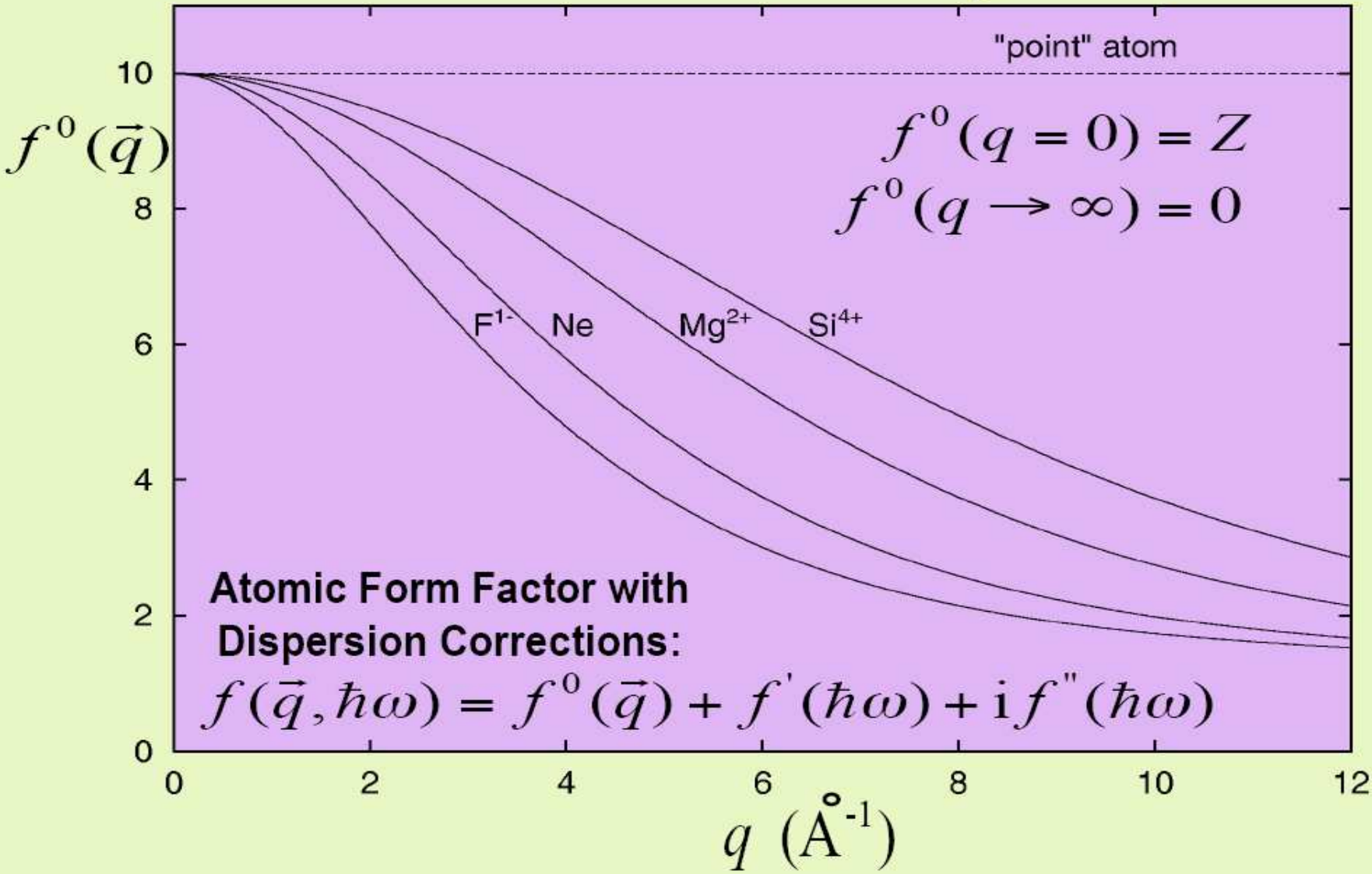

Глубина проникновения

Thermal Neutrons, 8 keV X-Rays & Low Energy Electrons:- Absorption by Matter

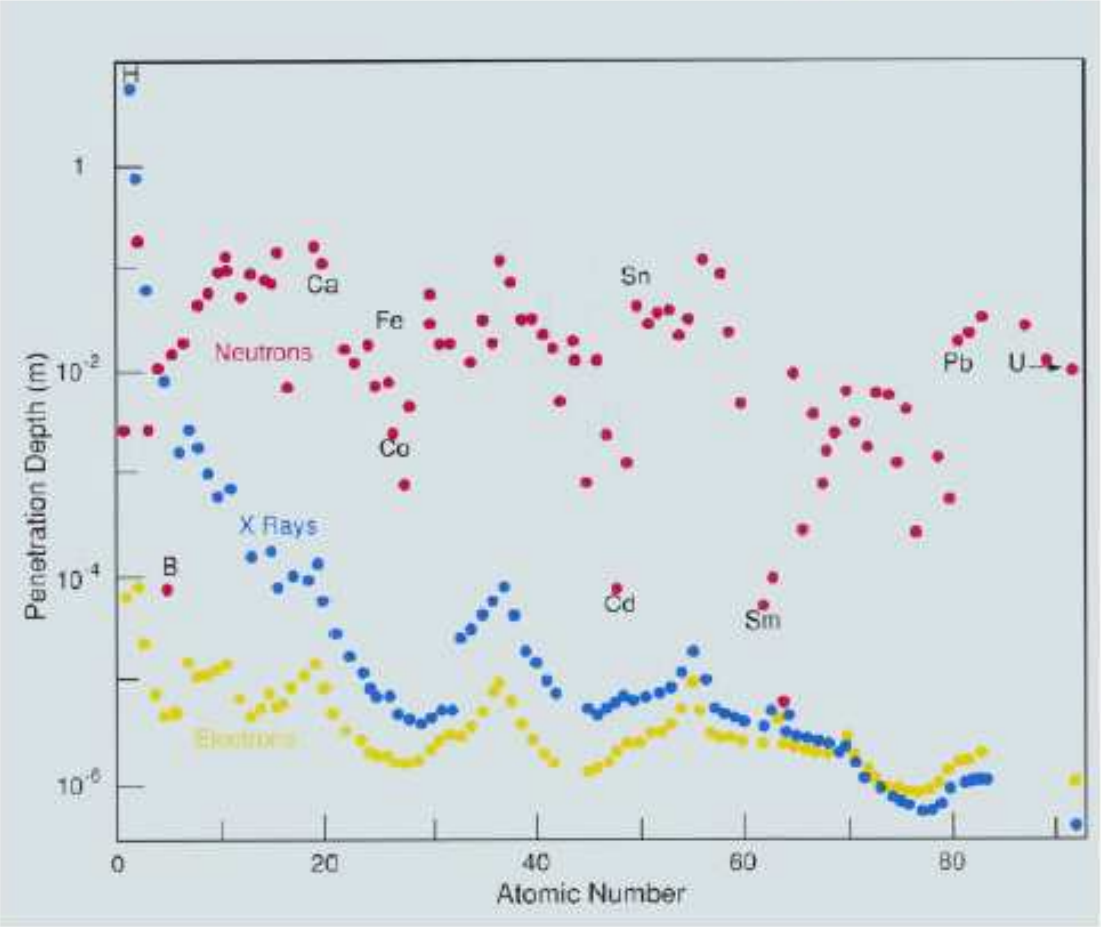

Note for neutrons:

- H/D difference
- Cd, B, Sm
- no systematic A dependence

How a Synchrotron Works

4. Storage Ring

The booster ring feeds electrons into the storage ring, a many-sided donut-shaped tube. The tube is maintained under vacuum, as free as possible of air or other stray atoms that could deflect the electron beam. Computer-controlled magnets keep the beam absolutely true.

Synchrotron light is produced when the bending magnets deflect the electron beam; each set of bending magnets is connected to an experimental station or beamline. Machines filter, intensify, or otherwise manipulate the light at each beamline to get the right characteristics for experiments.

5. Focusing the Beam

Keeping the electron beam absolutely true is vital when the material you're studying is measured in billionths of a metre. This precise control is accomplished with computer-controlled quadrupole (four pole) and sextupole (six pole) magnets. Small adjustments with these magnets act to focus the electron beam.

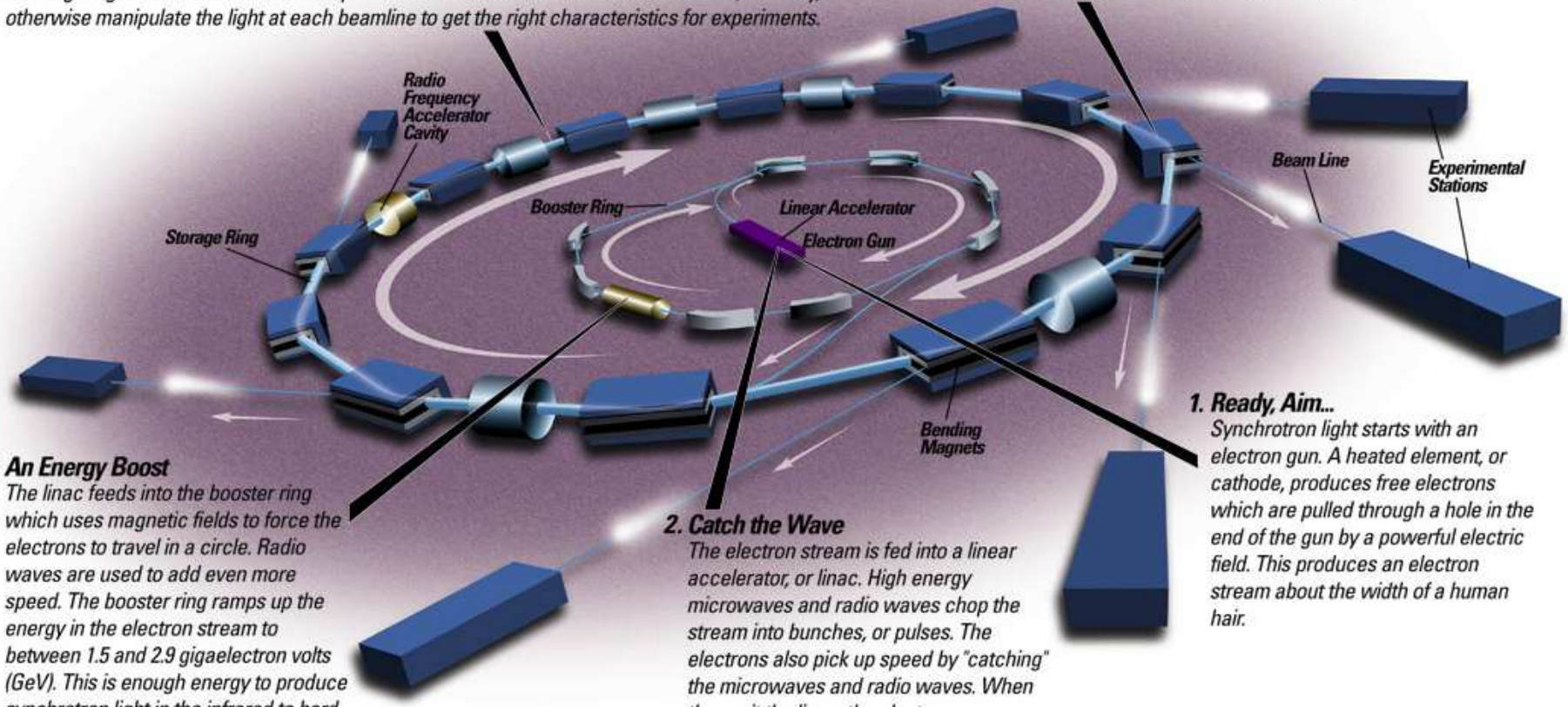

3. An Energy Boost

The linac feeds into the booster ring which uses magnetic fields to force the electrons to travel in a circle. Radio waves are used to add even more speed. The booster ring ramps up the energy in the electron stream to between 1.5 and 2.9 gigaelectron volts (GeV). This is enough energy to produce synchrotron light in the infrared to hard X-ray range.

2. Catch the Wave

The electron stream is fed into a linear accelerator, or linac. High energy microwaves and radio waves chop the stream into bunches, or pulses. The electrons also pick up speed by "catching" the microwaves and radio waves. When they exit the linac, the electrons are travelling at 99.99986 per cent of the speed of light and carry about 300 million electron

1. Ready, Aim...

Synchrotron light starts with an electron gun. A heated element, or cathode, produces free electrons which are pulled through a hole in the end of the gun by a powerful electric field. This produces an electron stream about the width of a human hair.

Source: University of Saskatchewan / Paradigm Media Group Inc.

Modern Synchrotron Radiation Facility

Older Synchrotron Radiation Facility

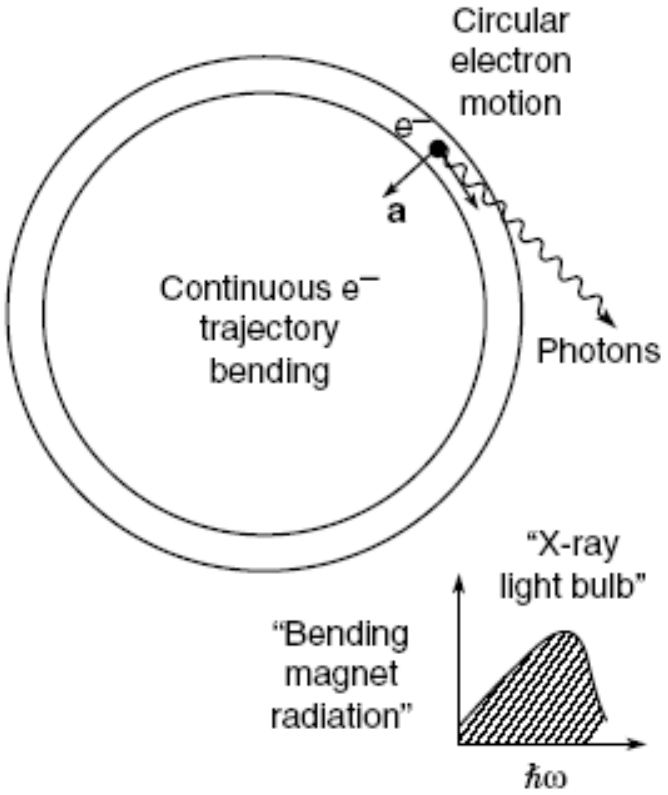

Modern Synchrotron Radiation Facility

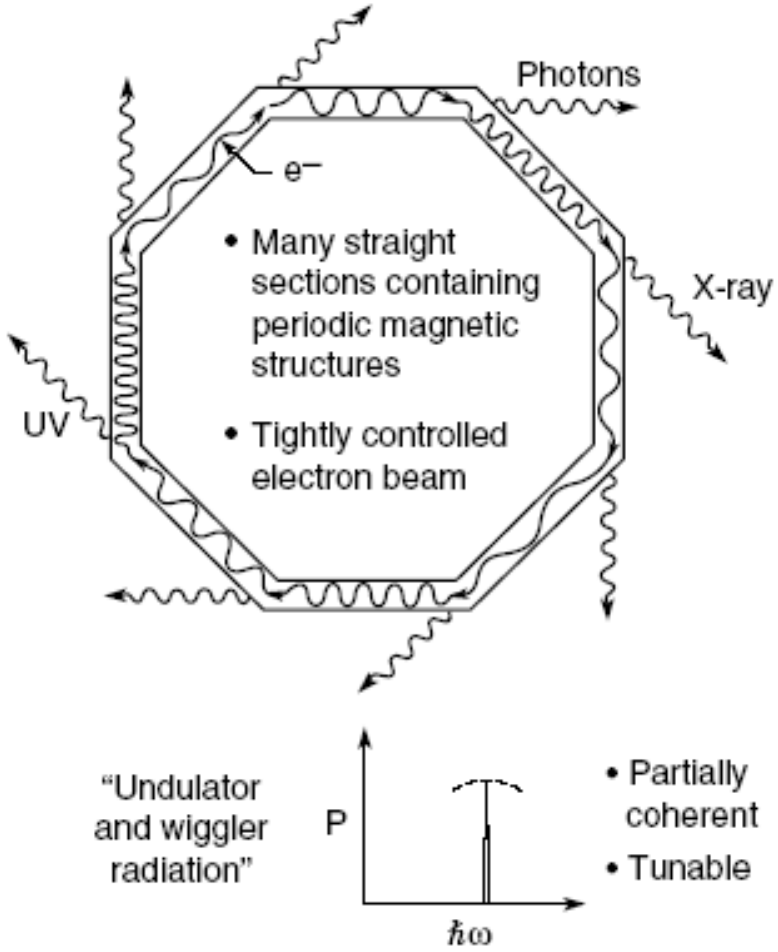

Three Forms of Synchrotron Radiation

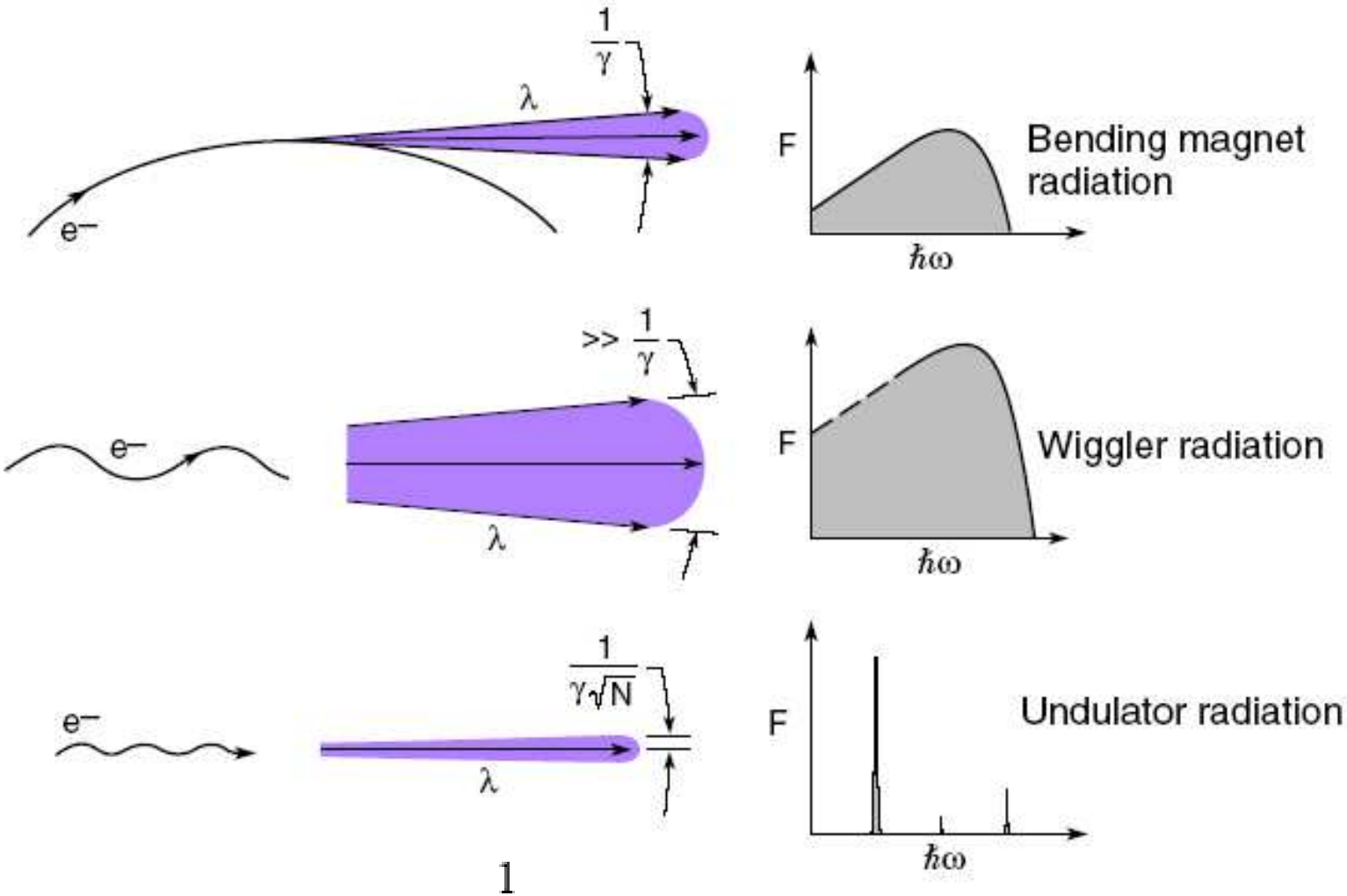

$$\gamma = \frac{1}{\sqrt{1 - \frac{v^2}{c^2}}}$$

Professor David Attwood
AST 210/EECS 213
Univ. California, Berkeley

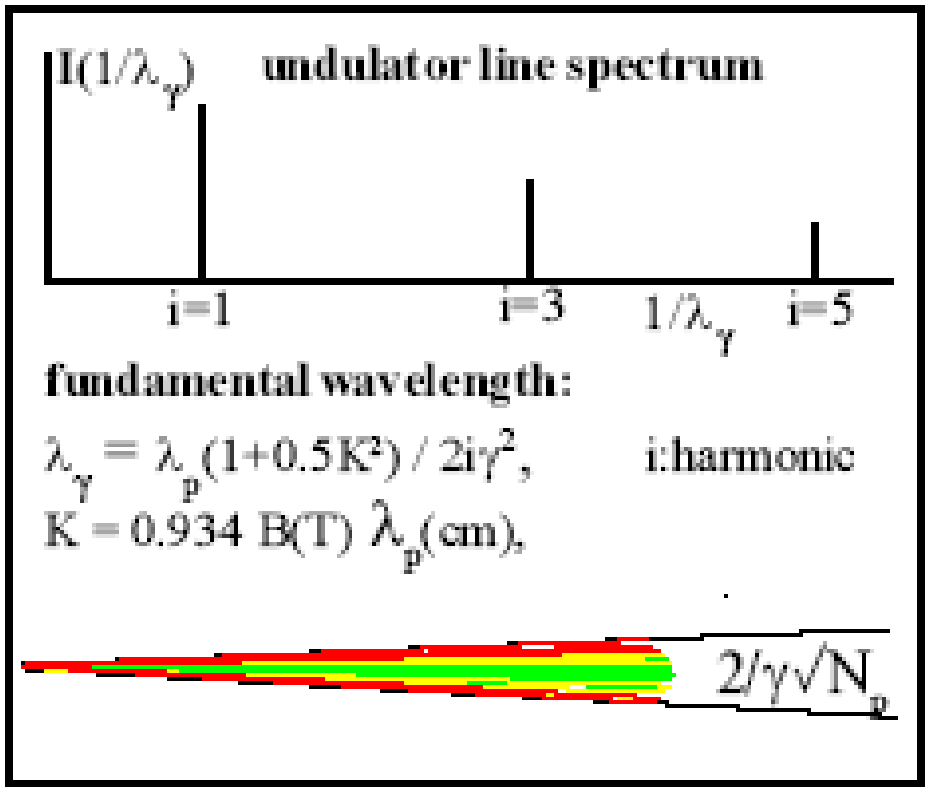
I(1/λγ)
undulator line spectrum
i=1
i=3
1/λγ
i=5
fundamental wavelength:
λγ = λp(1+0.5K²) / 2iγ², i:harmonic
K = 0.934 B(T) λp(cm).
2/γ√Np

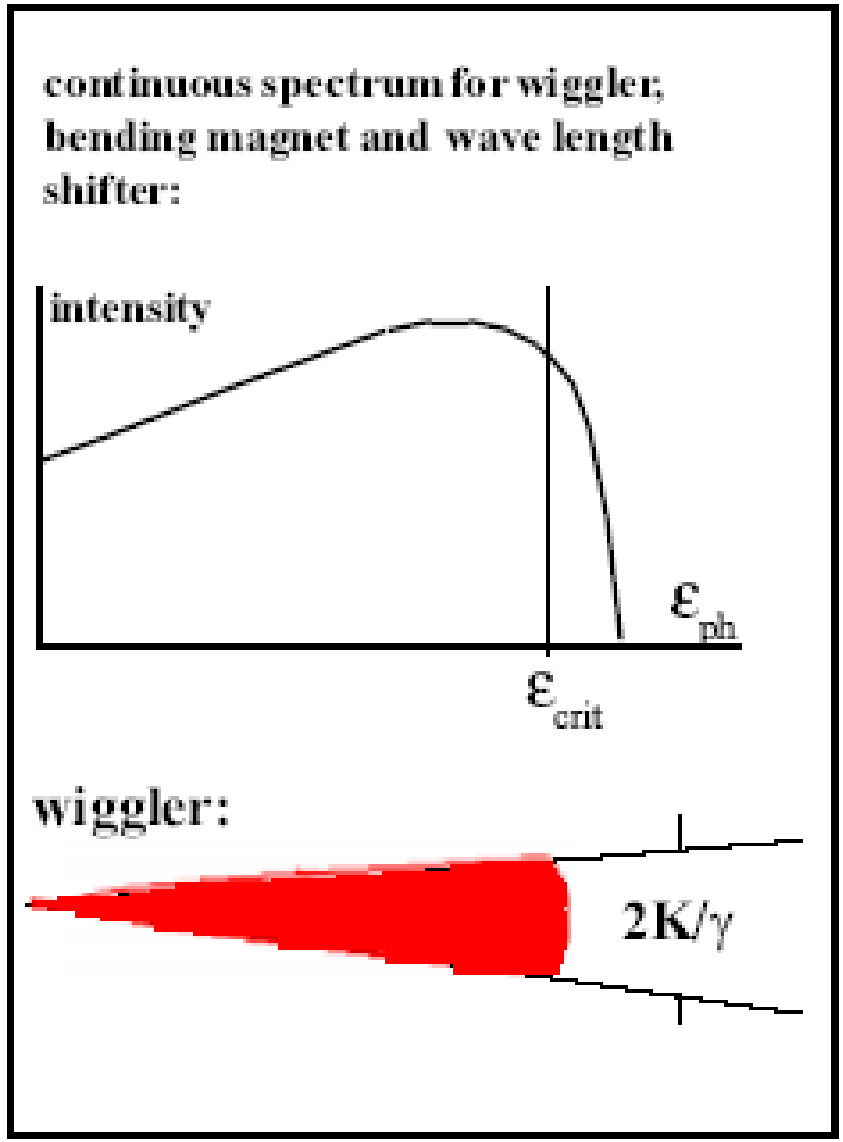
continuous spectrum for wiggler, bending magnet and wave length shifter:
intensity
εph
εcrit
wiggler:
2K/γ

Ioffe Physico-Technical Institute

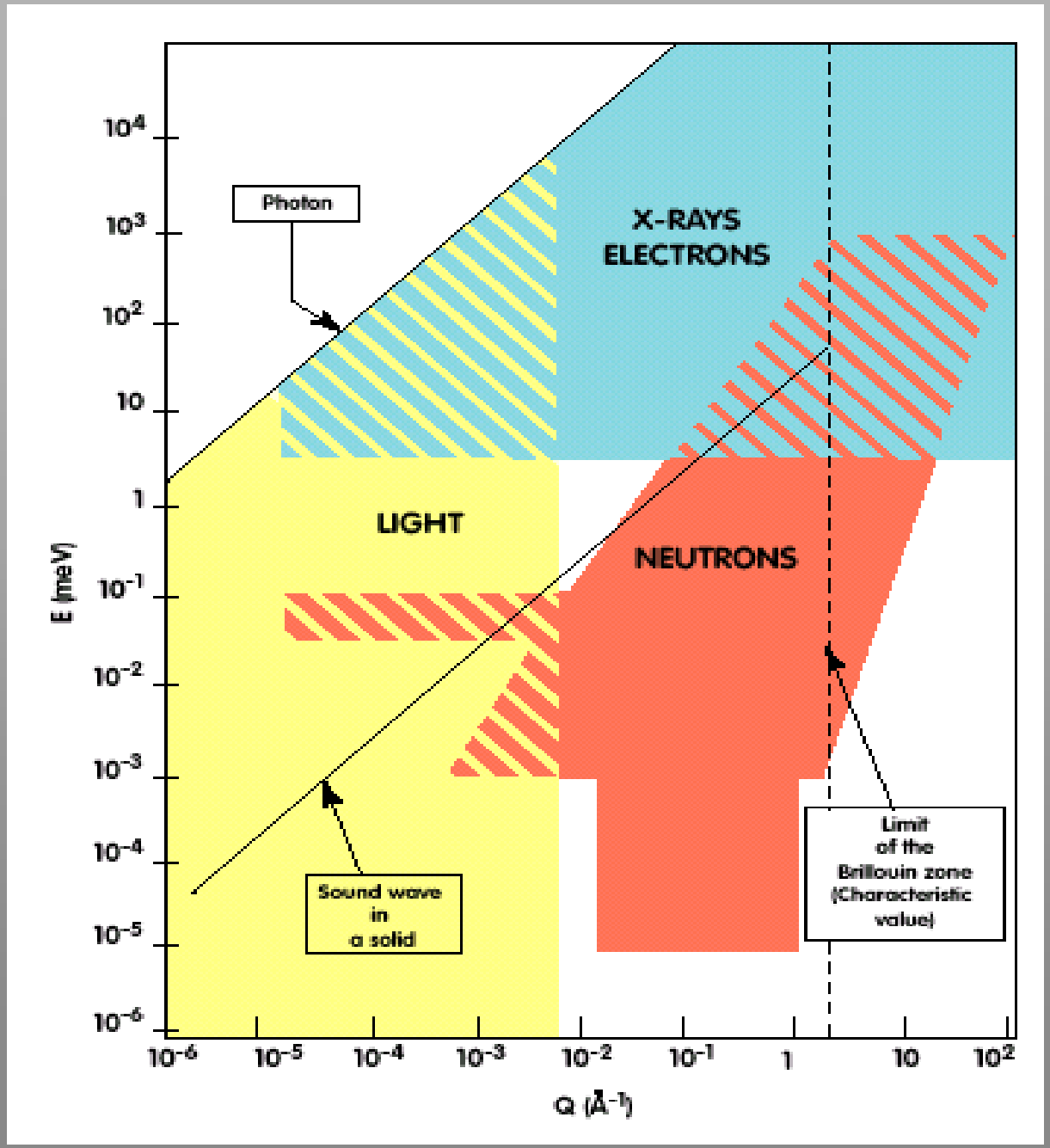

Ioffe Physico-Technical Institute

Кольцо синхротрона

Ioffe Physico-Technical Institute

Андулятор

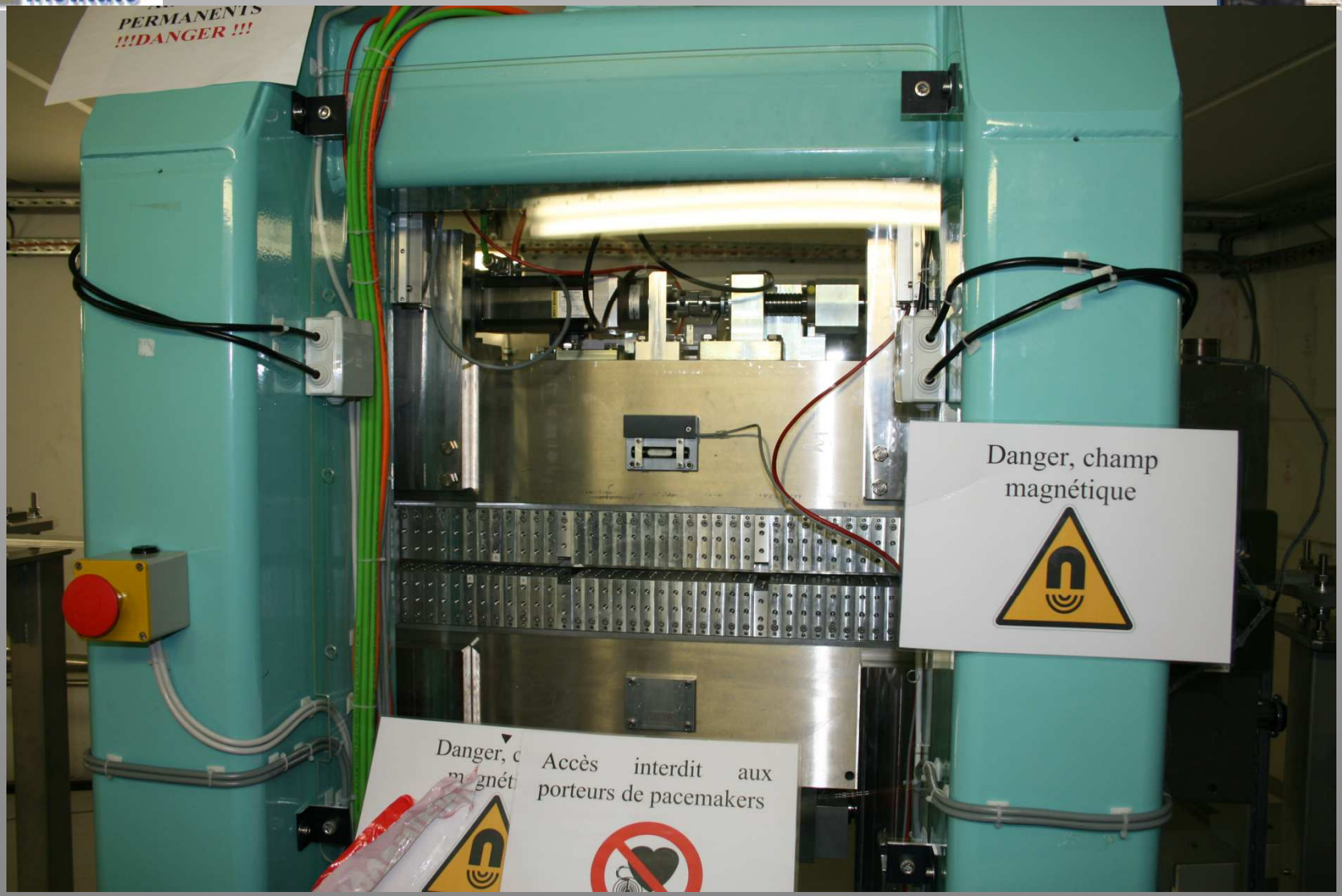

Ioffe Physico-Technical Institute

Вывод пучка

Ioffe Physico-Technical Institute

XU 22 Spring8

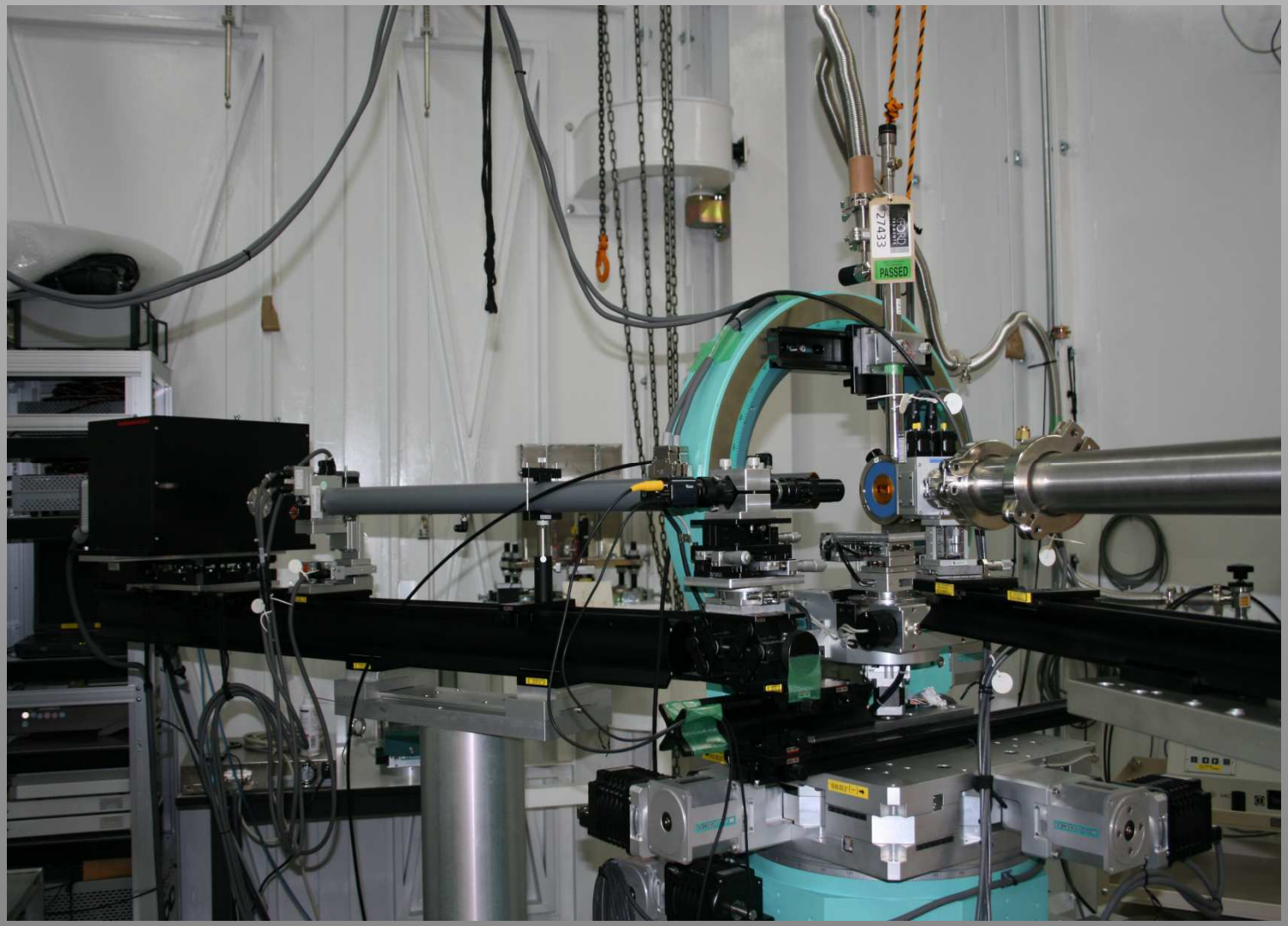

Криостат, вибрации <10nm

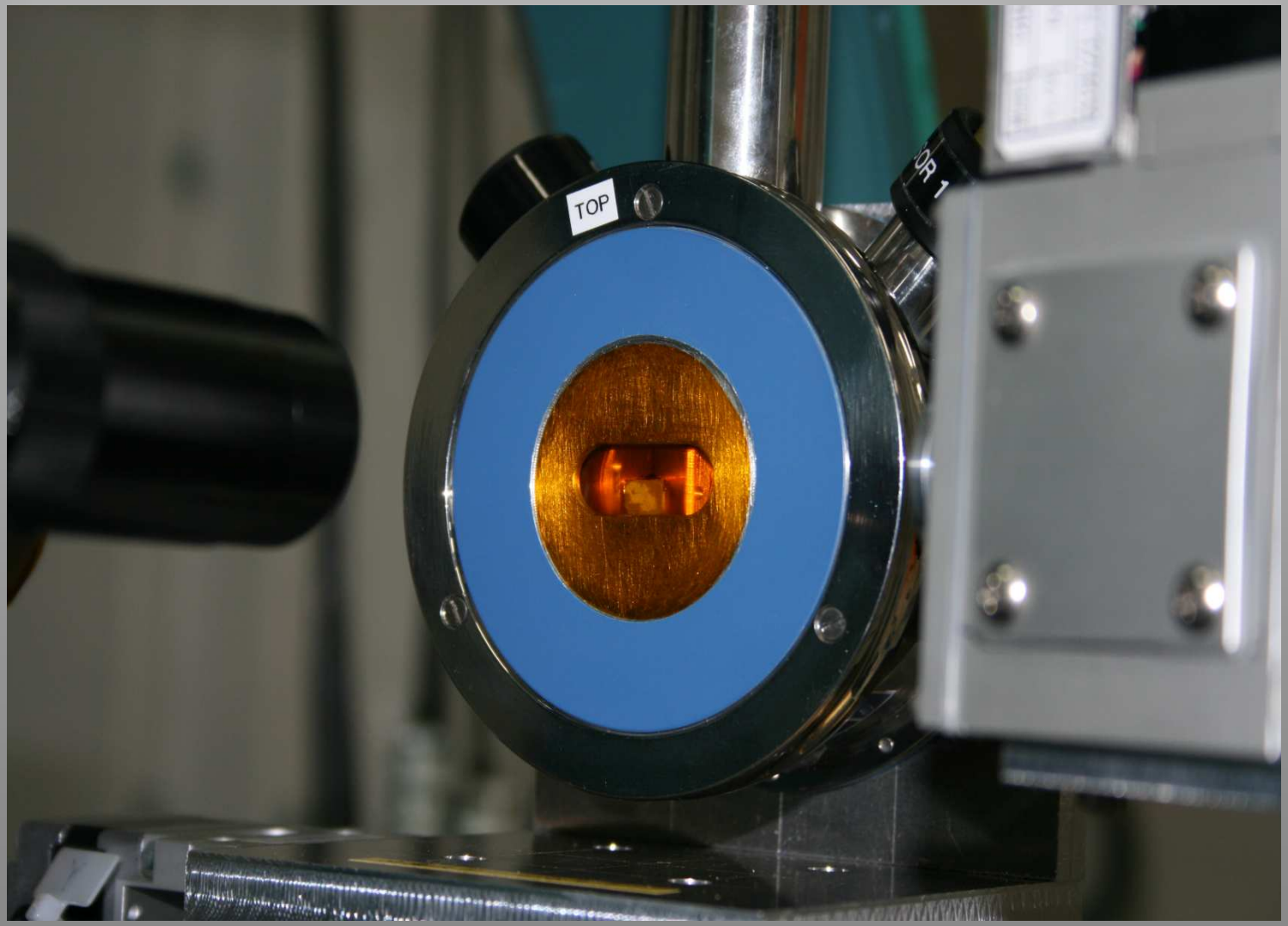

Ioffe Physico-Technical Institute

Spallation Neutron Source

Quasi-elastic Scattering

- BASIS-SNS

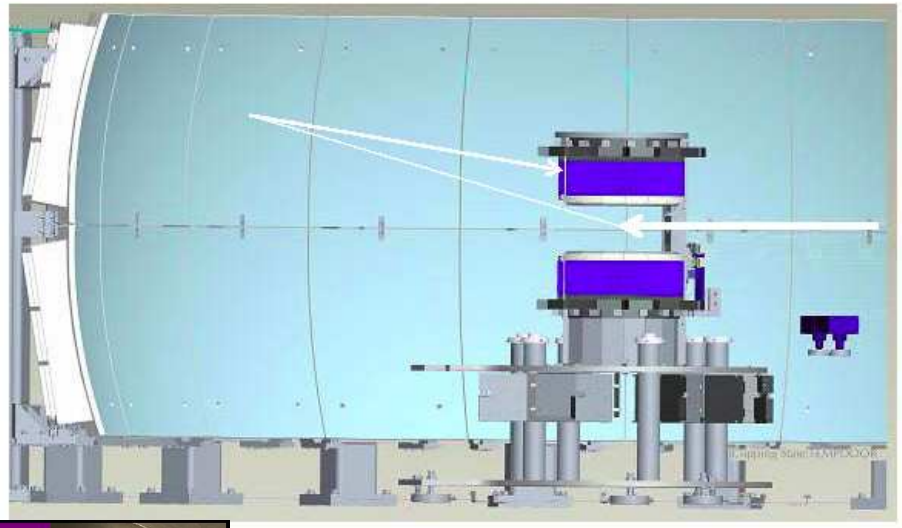

16.03.2009

Ioffe Physico-Technical Institute

Почему на примере релаксоров

Applications of Ferroelectric Single Crystals in Navy Sonar

Harold C. Robinson[1] and James M. Powers[2]
[1]Naval Undersea Warfare Center (NUWC) Division Newport, Newport, RI
[2]EDO Western Corporation, Salt Lake City, UT

		Mode	Coupling Factor	Dielectric Loss	Projector FOM Strain Energy Density (dB re PZT-8)	Sensor FOMs g*d (dB re PZT-5H)	Sensor FOMs g*d/tan δ (dB re PZT-5H)
PZT-8	ceramic	33	0.62	0.003	0.0	-3.3	4.9
PZT5H	ceramic	33	0.75	0.020	6.8	0.0	0.0
PZT5H	ceramic	15	0.68	0.020	6.0	2.8	2.8
PZT-4	ceramic	33	0.71	0.004	2.1	-1.8	5.2
PZT-4	ceramic	15	0.72	0.004	2.2	2.6	9.6
PMN-PT	crystal	33	0.92	0.003	11.1	6.5	14.7
PZN-8%PT	crystal	15	0.94	0.005	12.1	12.4	18.4
PZN-4.5%PT	crystal	15	0.97	0.005	16.1	16.0	22.0

Table 1. Comparison of sensor and projector material properties.

Диэлектрическая проницаемость (I)

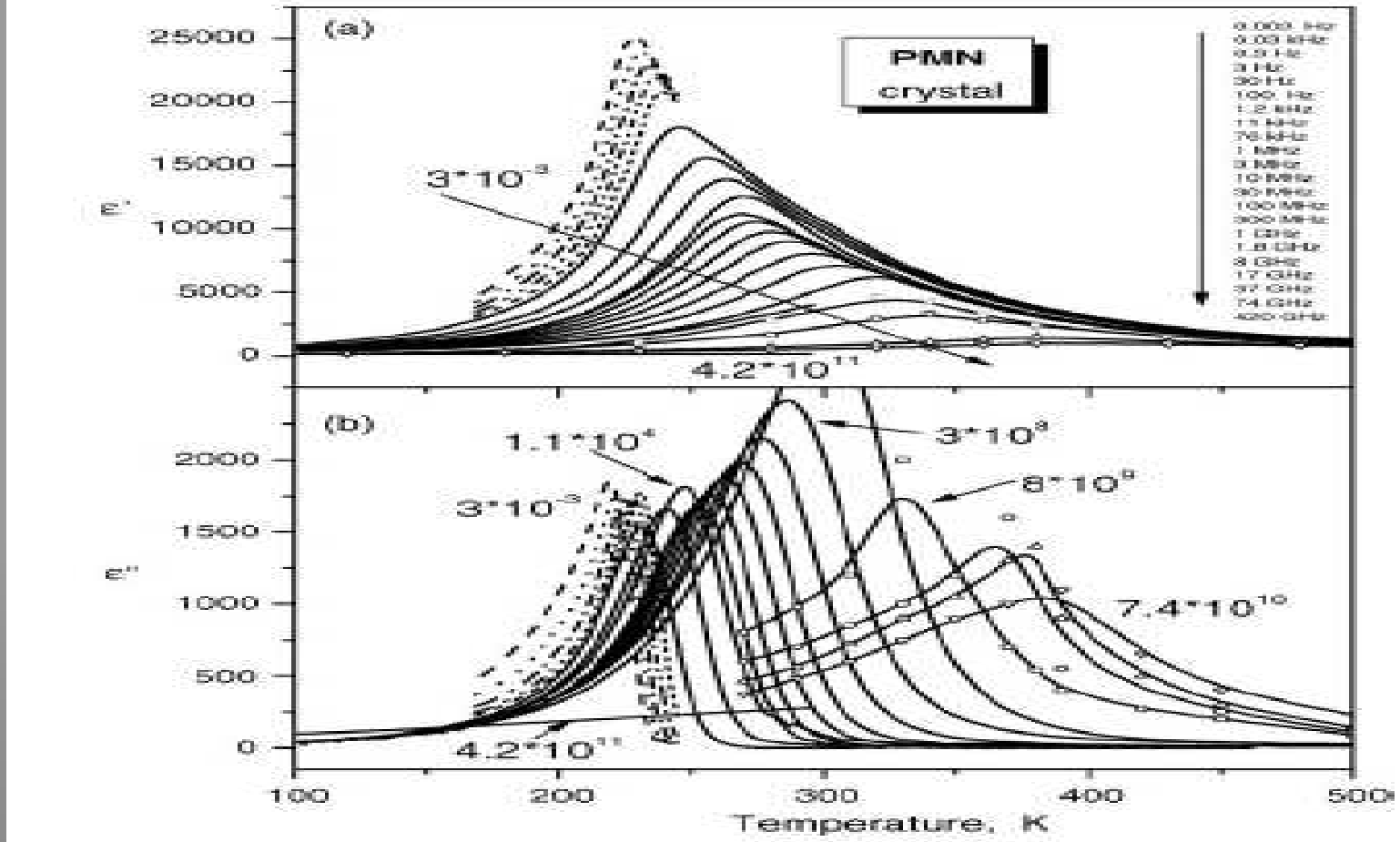

Fig. 1. Temperature dependences of dielectric permittivity ε' and loss ε'' of PMN single crystal at various frequencies. The numbers near curves denote the frequency in Hz.

PMN ideal structure

A=Pb

B=Nb/Mg

O=O

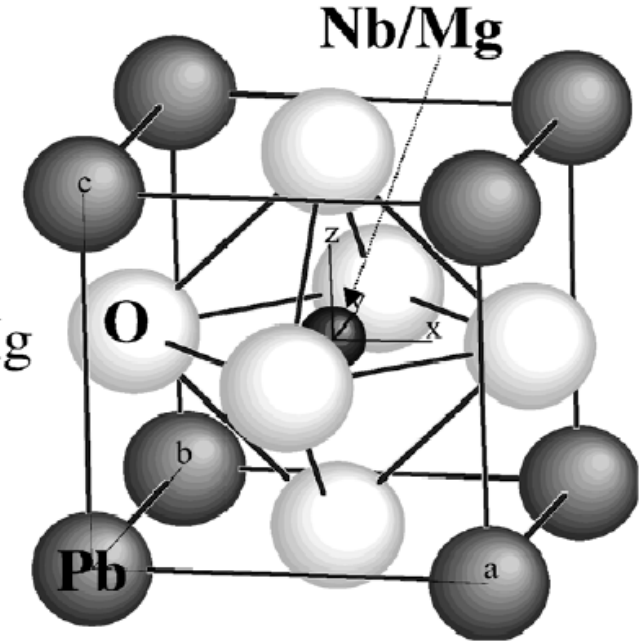

Nb^{5+} Mg^{2+} different charges, different ionic radii – should order

In the compounds without lead – tripling of the cell

In the $PbB'_{1/3}B''_{2/3}$ – cell doubling

Должно быть НАНО! (нанодомены)

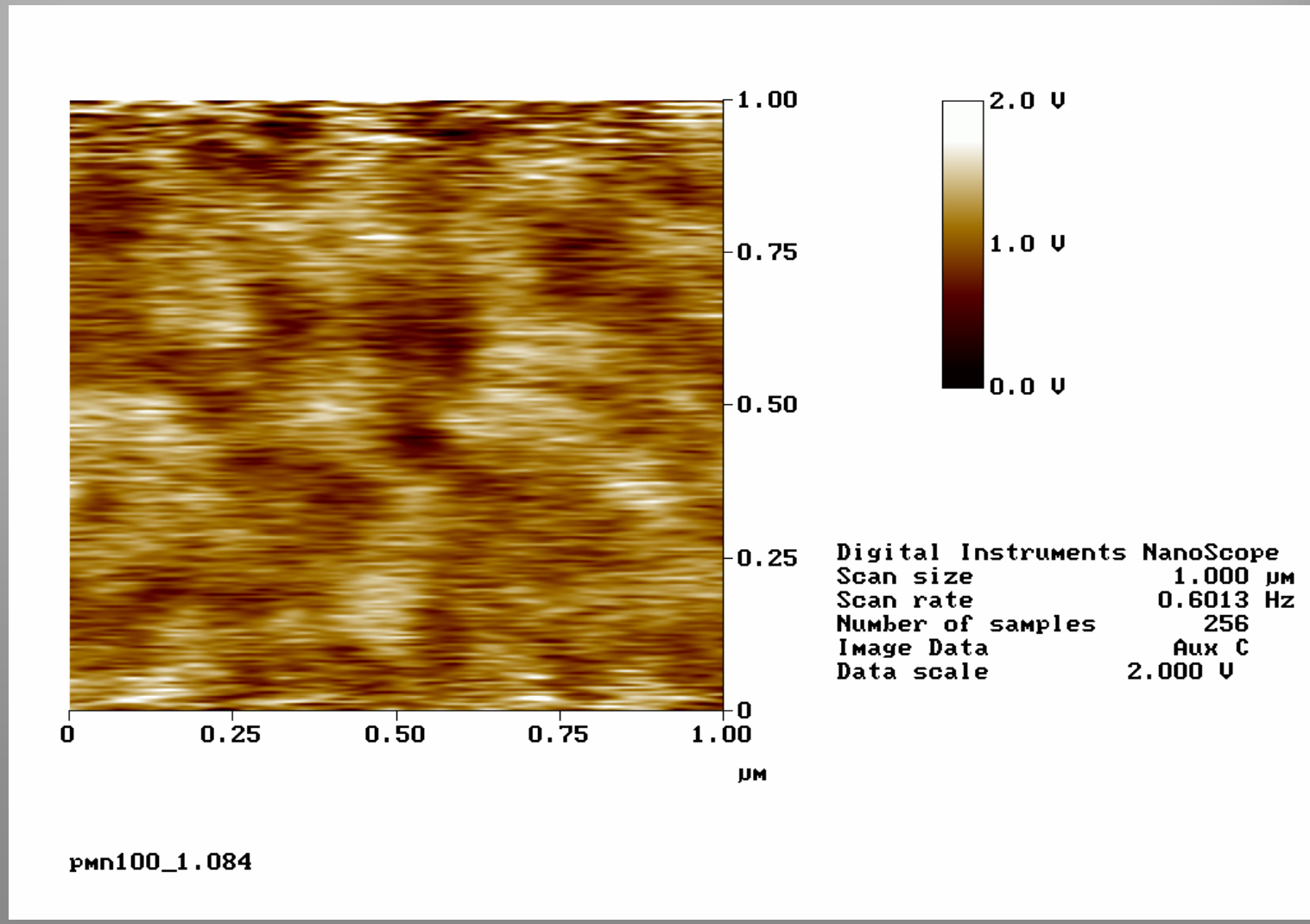

Структура

- Уточнение структуры по БРЭГГОВСКИМ ПИКАМ – неявно считаем, что упругое рассеяние доминирует, а если $\rho(r)$, т.е. Фурье образ S(Q)?

Probability density function for Pb^{2+} in PMN 300K X-rays

"Rotator model" Gram-Charli expansion"

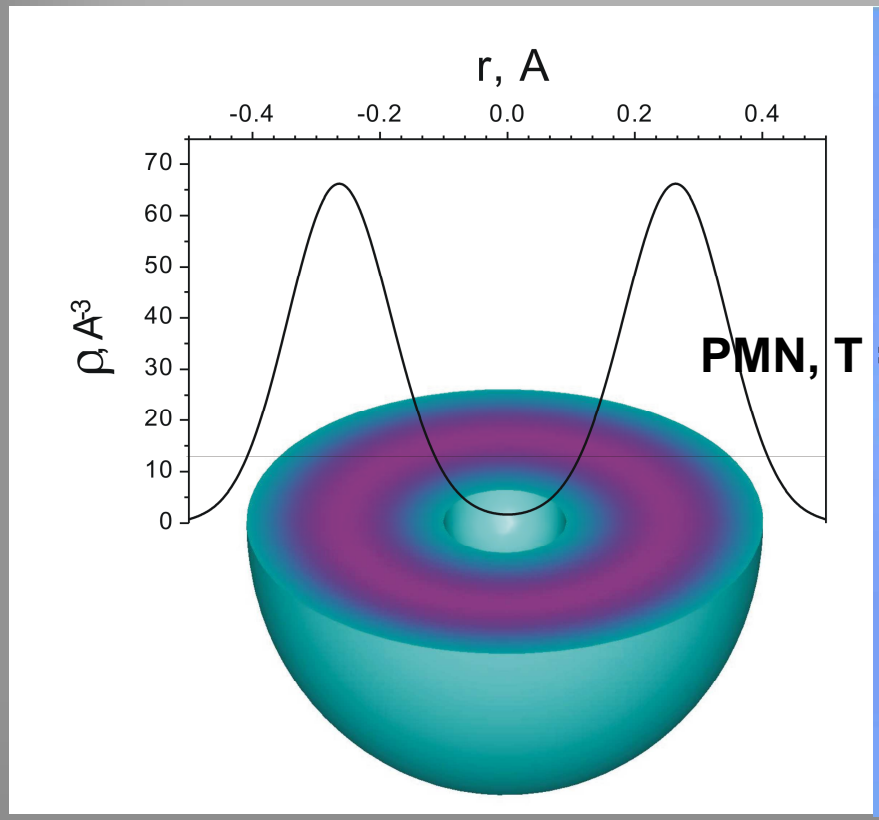

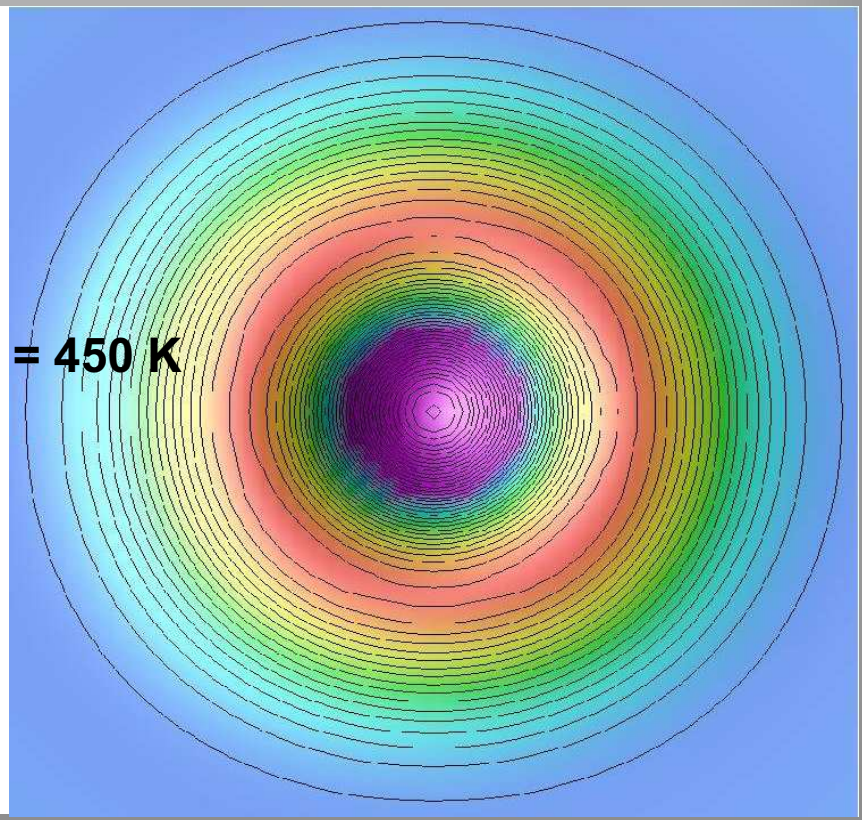

А что с кислородом? В рентгеновском эксперименте ответа не получили

Superstructural peak in PMN

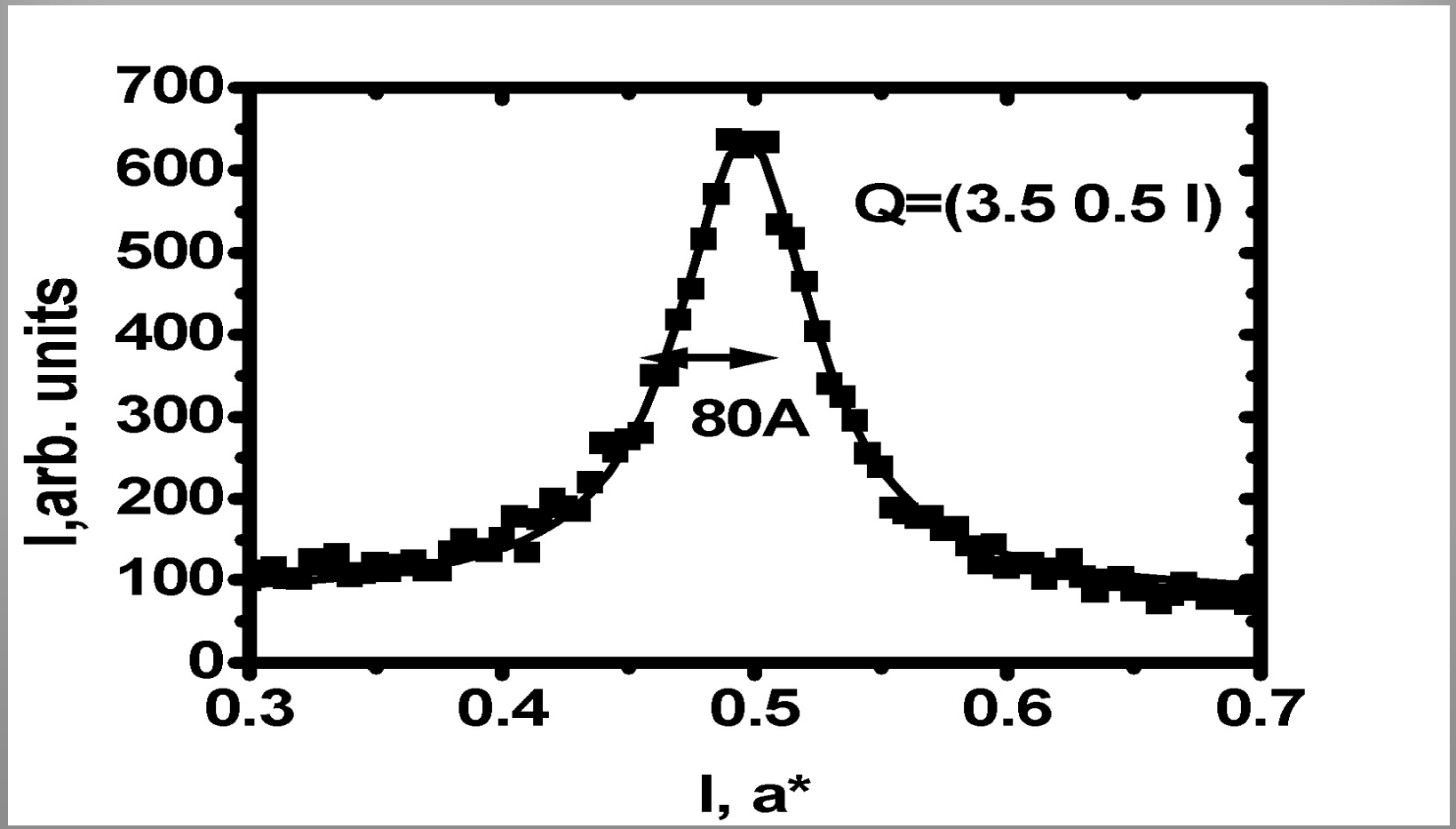

- Superstructure in PMN measured with synchrotron radiation scattering; correlation length of compositional ordering is abot 80A

Anomalous X-ray scattering in PMN

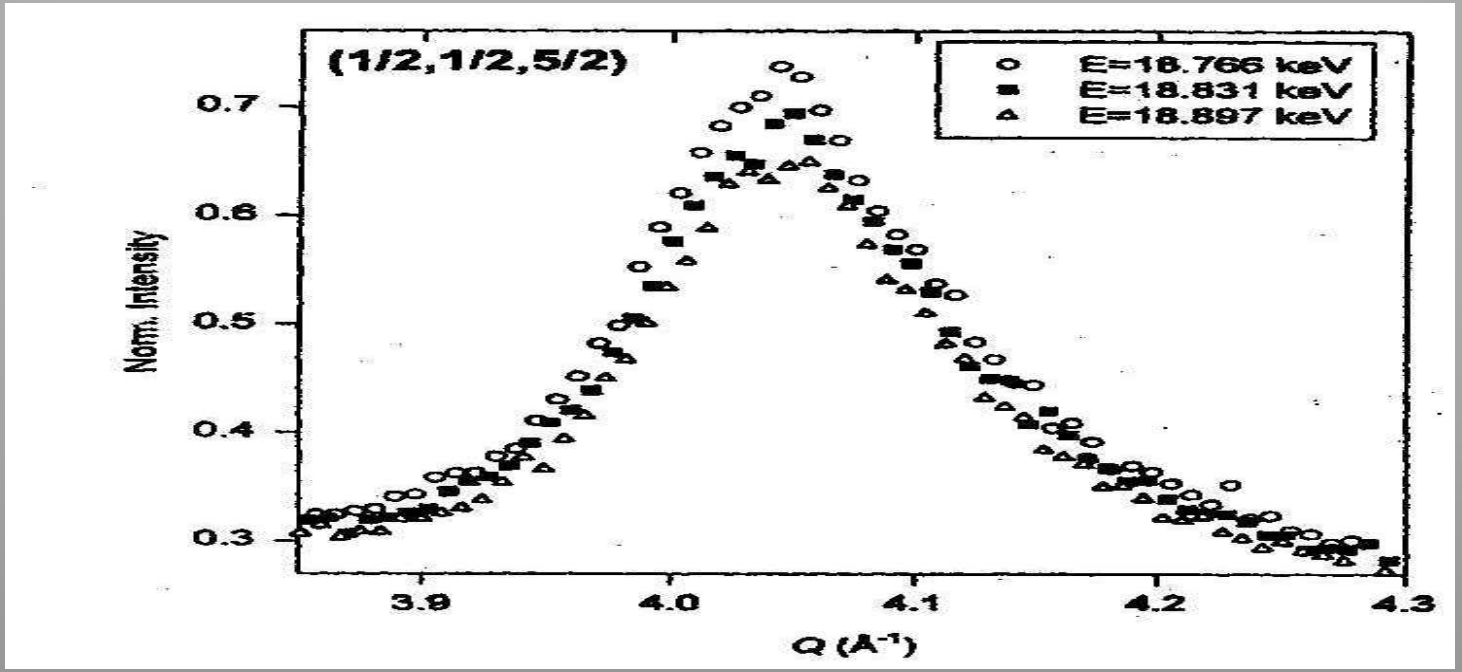

$$\frac{I(Q)}{\partial I(Q)/\partial f_{Pb}} = \frac{1}{2}(f_{Nb} - f_{Pb}) + 3\frac{Qu_O}{\alpha} f_O + \frac{Qu_{Pb}}{\alpha} f_{Pb}$$

α – degree of order, u_O, u_{Pb} – displacements

u_{Pb}/α~-0,07Å; u_O/α~0.4Å. Positive sign – toward Nb, negative – away from Nb.

Объём и поверхность

По материалам работ группы

G.Shirane

PZN, Дифракция СИ

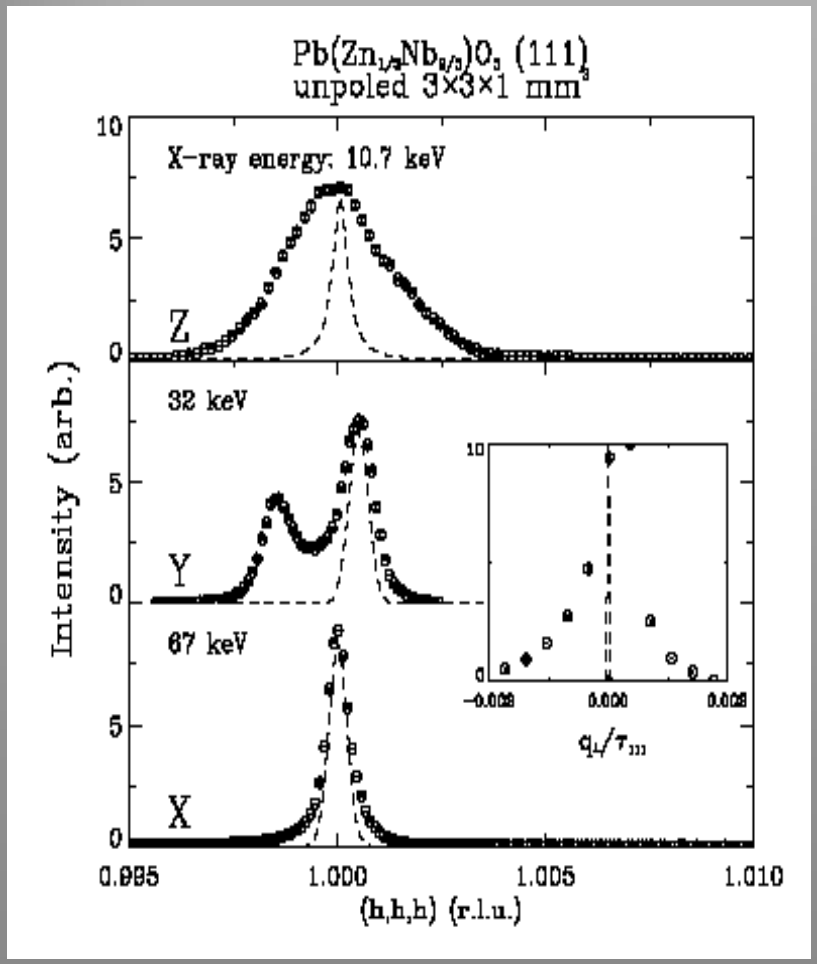

- Ромбоэдрические искажения наблюдаются только в поверностном слое толщиной порядка 50 микрон

PMNPT10 X-rays+neutrons

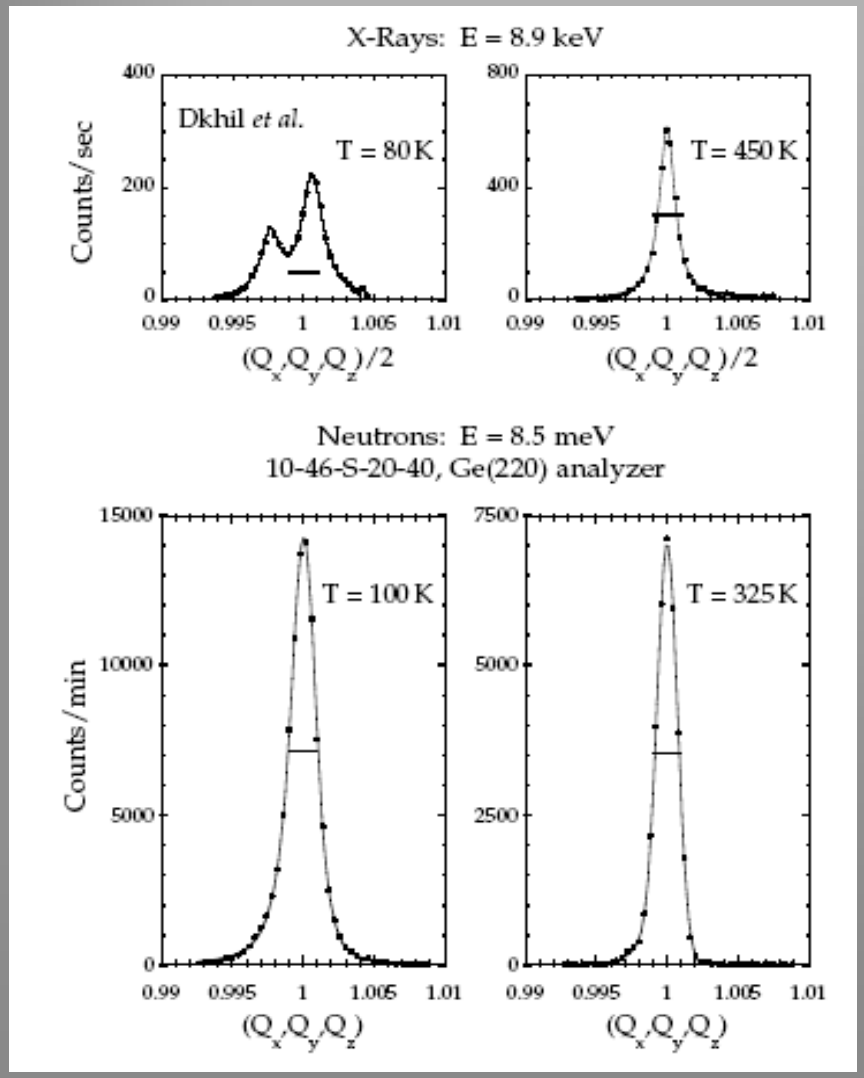

- В рентгеновских экспериментах на керамике четко наблюдается ромбоэдричесая фаза (глубина проникновения ~20 микрон).
- В нейтронном эксперименте на монокристалле кубическая фаза до 100К

Упругие напряжения в поверхностном слое PMN

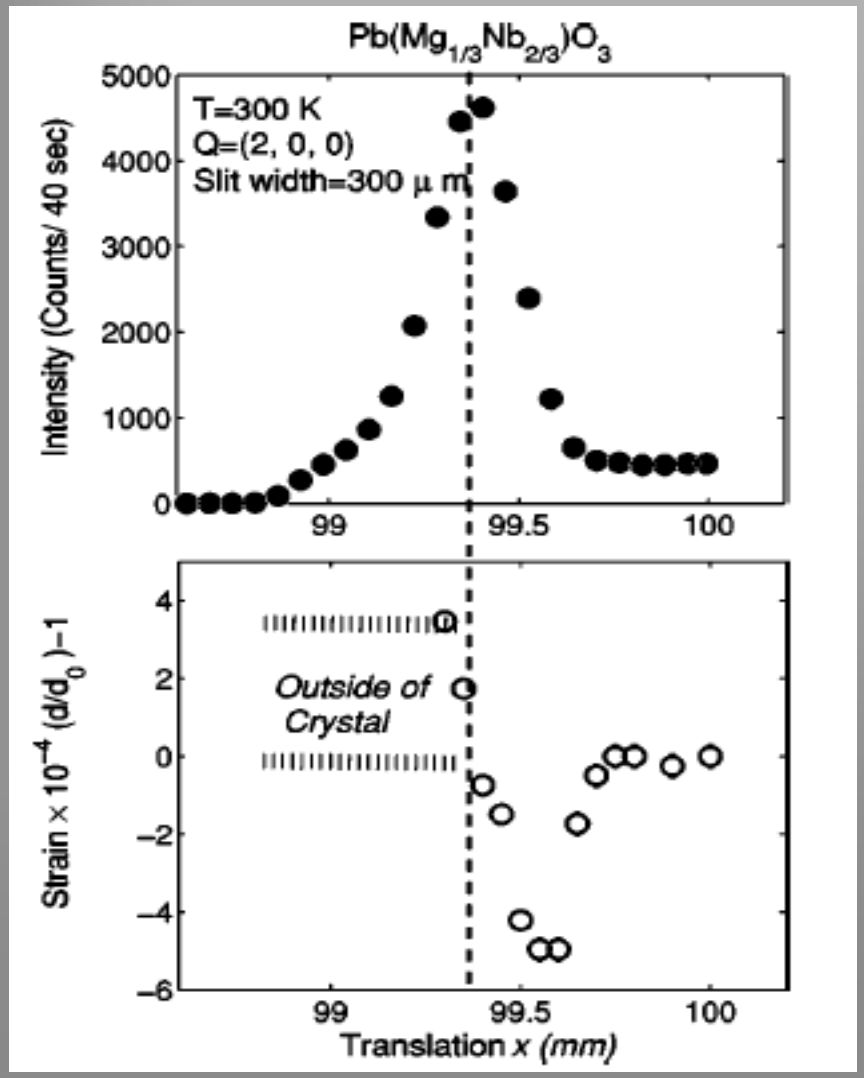

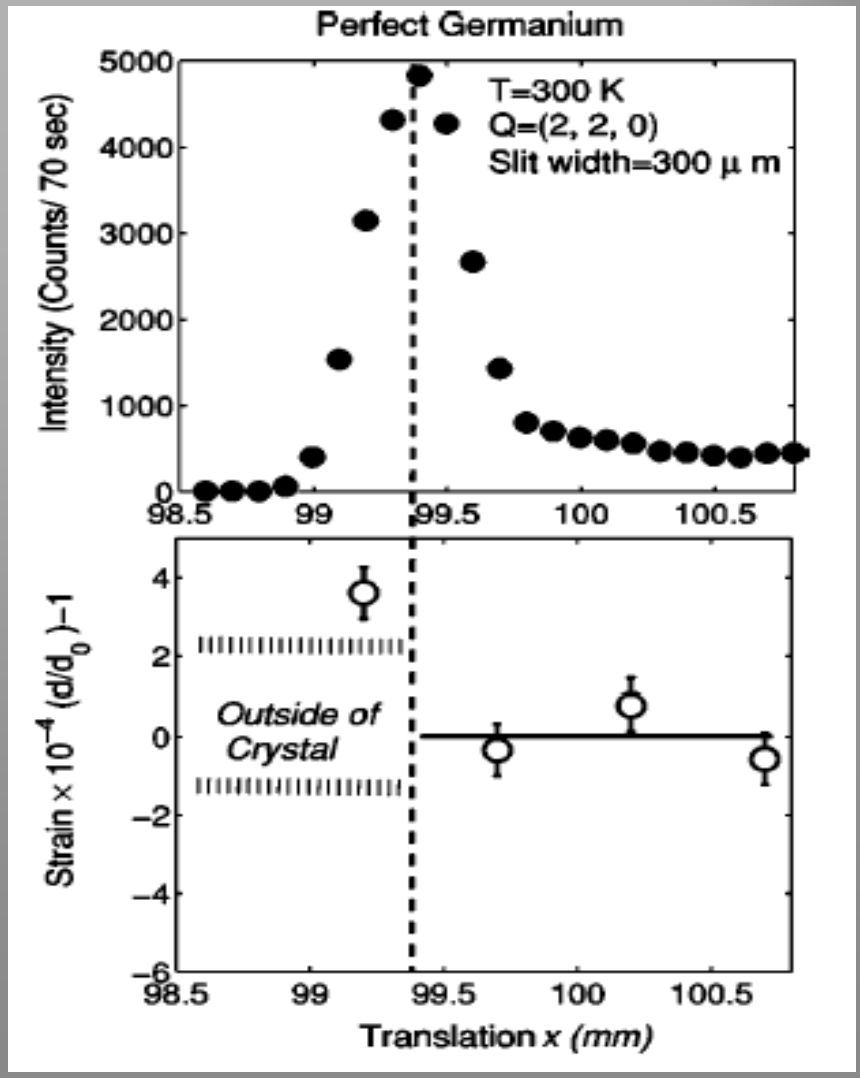

Динамика решетки

Нейтроны

Фононы в релаксорах

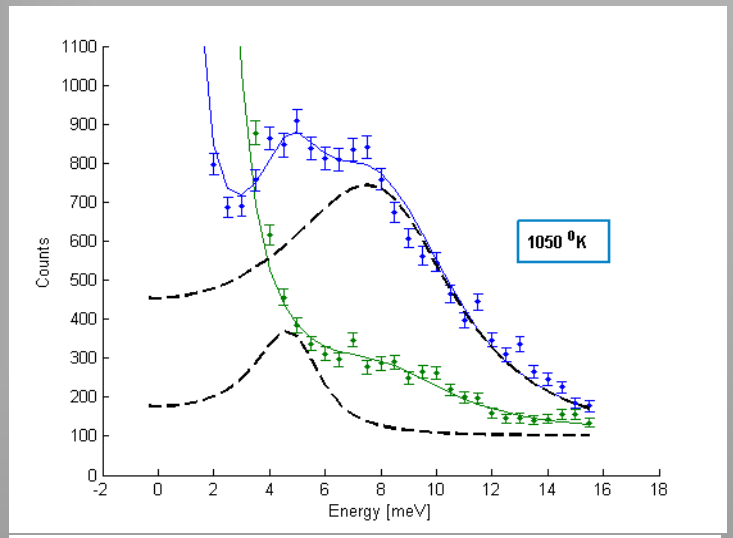

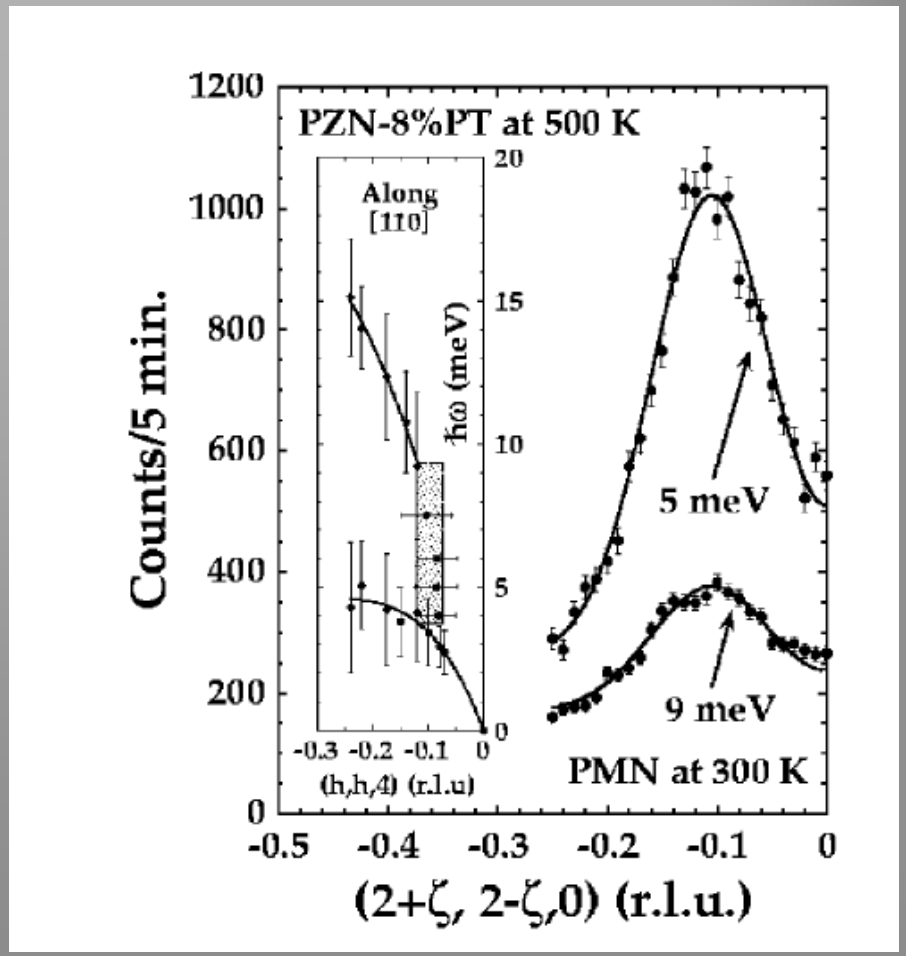

Водопад

Central Peak

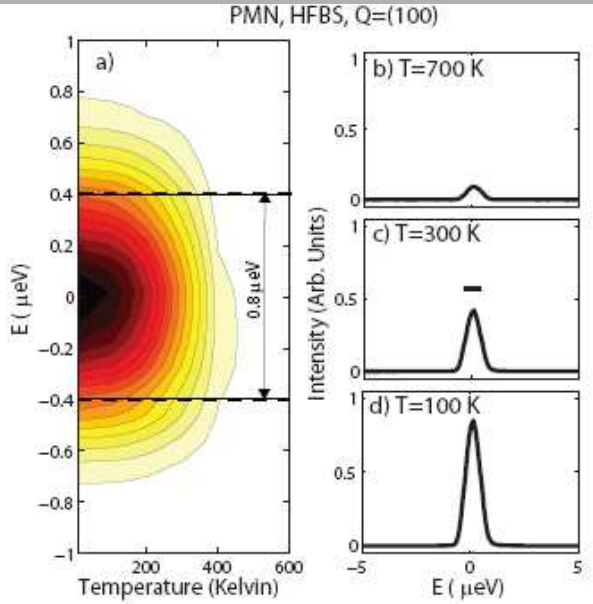

FIG. 7: (a) Contour plot of the scattering intensity as a function of energy transfer and temperature. Contours are shown on a linear intensity scale; dashed lines indicate the full-width at half-maximum (FWHM) of the peak linewidth at each temperature. The data were obtained from an integration over detectors 10-16 as illustrated in Fig. 6. Panels (b), (c), and (d) show inelastic scans at 700 K, 300 K, and 100 K. The horizontal bar in panel (c) represents the FWHM elastic energy resolution ($2\delta E$) of the spectrometer.

The energy dependence of the diffuse scattering as a function of temperature is illustrated in Fig. 7. Panel (a) shows a color contour plot of the peak linewidth in energy

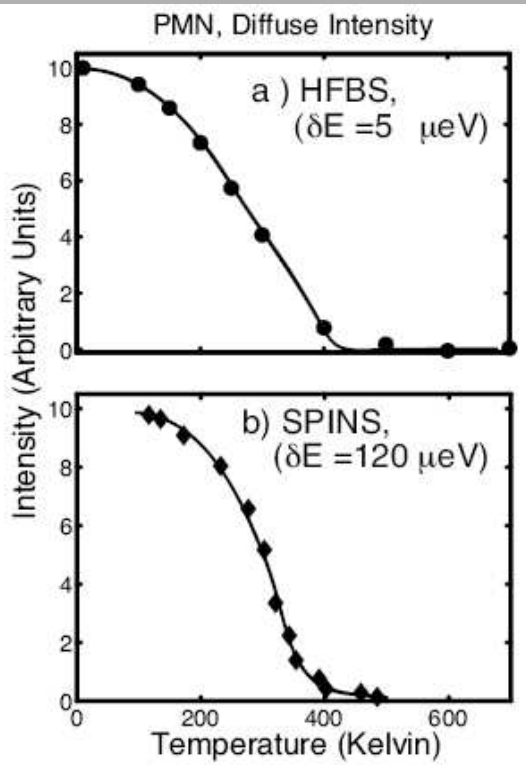

FIG. 8: (a) Temperature dependence of the diffuse scattering in PMN measured on the HFBS; data are integrated in energy from $\pm$ 5 μeV and in Q over detectors 10-16 as illustrated in Fig. 6. (b) Temperature dependence of the diffuse scattering intensity in PMN measured on SPINS at $Q = (1.05, 0.95, 0)$ by Hiraka *et al*.[31] The SPINS energy resolution of δE=120 μeV HWHM provided the energy integration.

TAS+SpinEcho

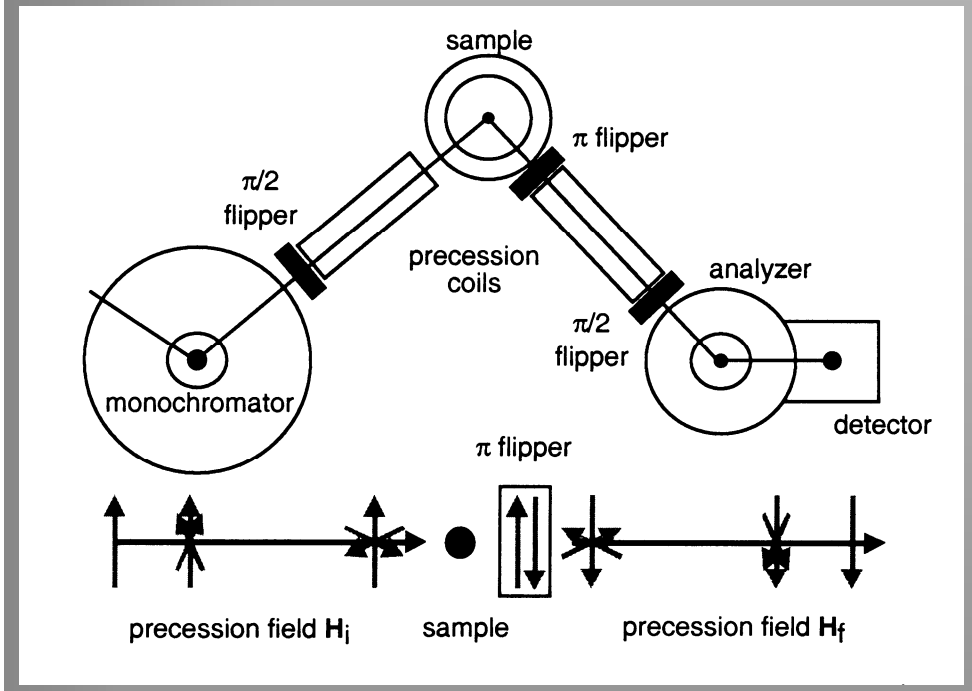

The monochromator and analyzer crystals select from the impinging beams certain energy band with defined direction of neutron polarization.
If before the analyzer the neutron polarization is inclined, the intensity in the detector will be reduced.

A typical experimental set-up for the precession field technique.

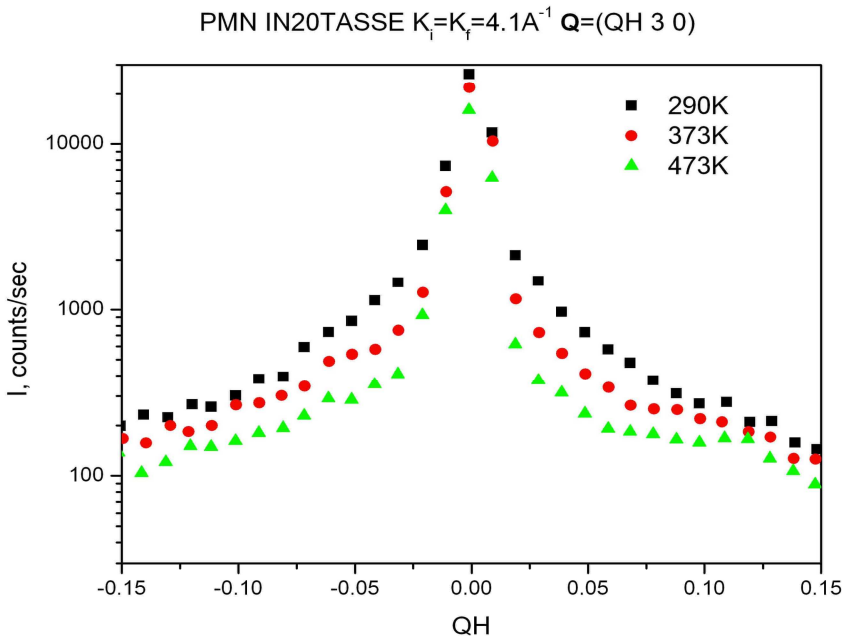
PMN IN20TASSE K_i=K_f=4.1A^{-1} **Q**=(QH 3 0)
290K
373K
473K
I, counts/sec
QH

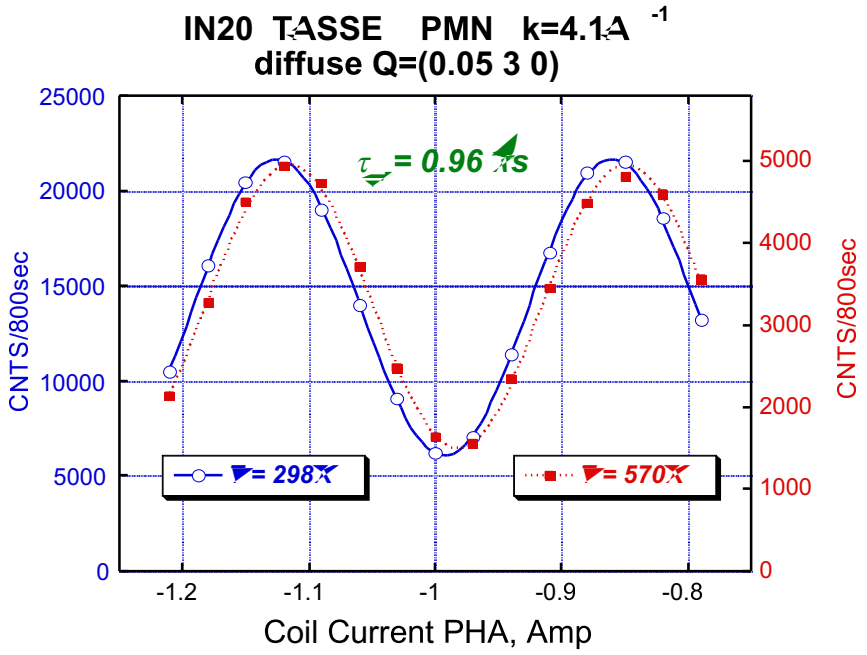
IN20 TASSE PMN k=4.1A^{-1}
diffuse Q=(0.05 3 0)
τ = 0.96 ns
T= 298K
T= 570K
CNTS/800sec
CNTS/800sec
Coil Current PHA, Amp

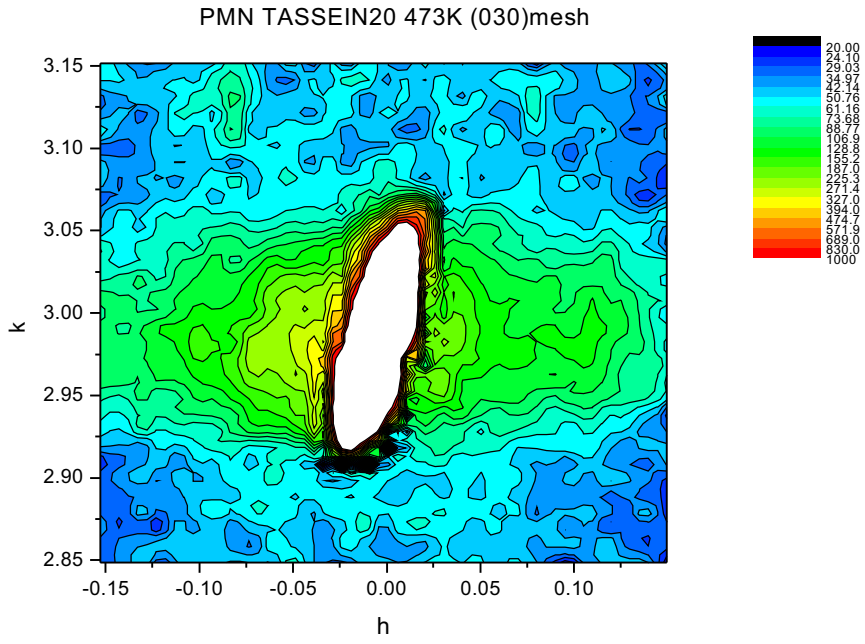
PMN TASSEIN20 473K (030)mesh
k
h

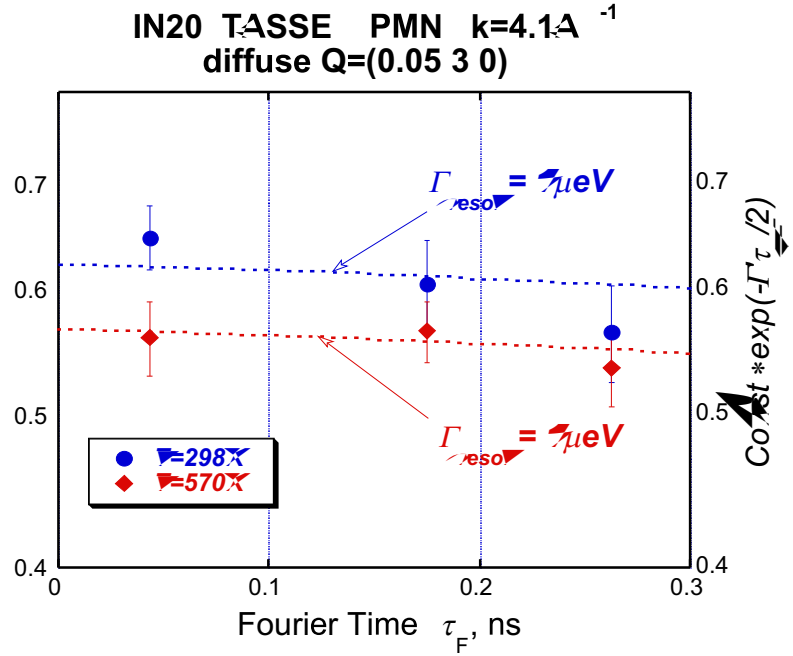
IN20 TASSE PMN k=4.1A^{-1}
diffuse Q=(0.05 3 0)
Γ_{resol} = 7μeV
Γ_{resol} = 7μeV
T=298K
T=570K
Const *exp(-$\Gamma\tau_F$/2)
Fourier Time τ_F, ns

Неупругое рассеяние СИ

Адиабатическое приближение

При смещении ядра атома все электроны движутся вместе с ним составляя одно целое

$$\rho(q) = \sum_i e^{-iq\cdot r_i} = \sum_\ell e^{-iq\cdot R_\ell}\left[\sum_{i(\ell)} e^{-iq(r_i - R_\ell)}\right]$$

$$\rho(q,t) = Zf(q)\sum_\ell e^{-iq\cdot R_\ell(t)} = Zf(q)\sum_\ell e^{-iq(\ell+u_\ell(t))}$$

Кинематика рассеяния

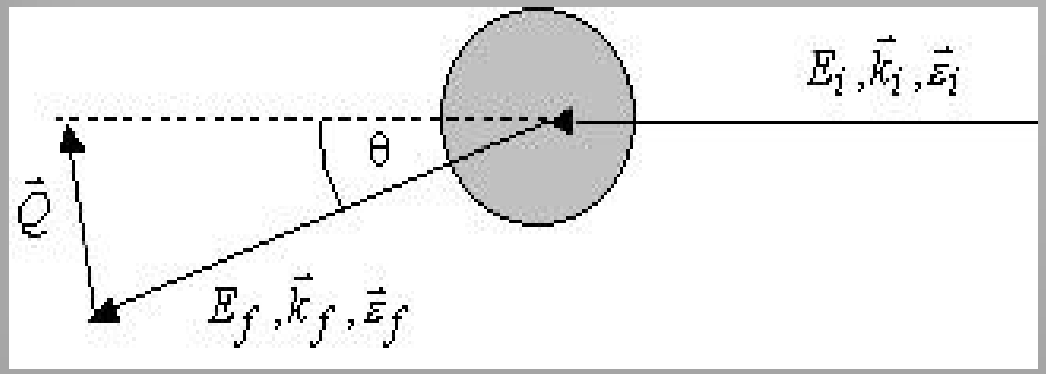

$Ki \approx Kf; \quad (Q/Ki) = 2\sin(\theta/2)$

Нет ограничений на передачу энергии

S(Qω) λ_i=4.8A SiC NIST

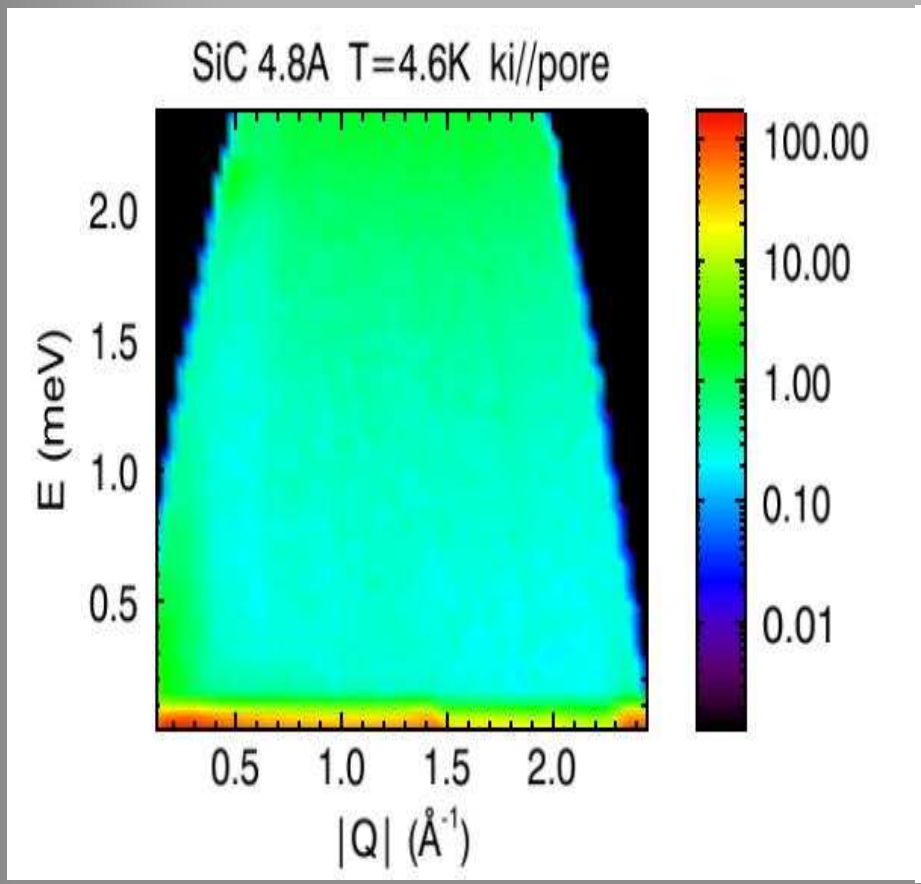

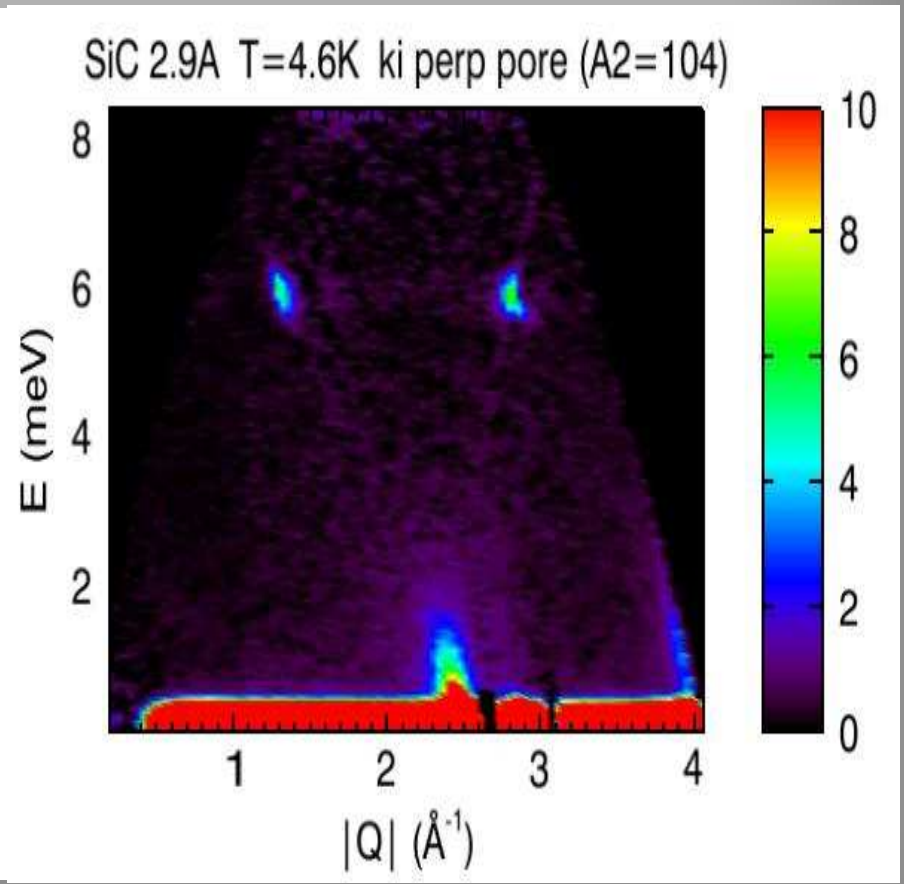

ID28 Spectrometer (ESRF)

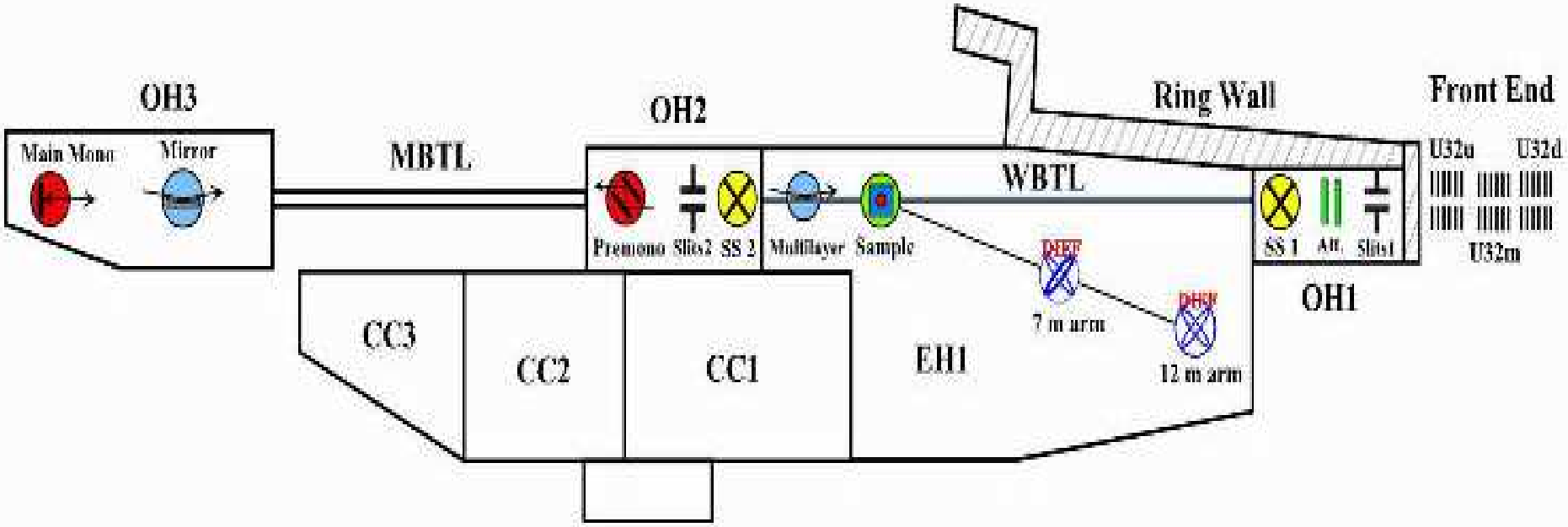

Высокое разрешение достигается за счет геометрии обратного рассеяния

$\lambda=2d\sin(\Theta)$; $\Delta\lambda/\lambda=\Delta d/d+\Delta\Theta\,\mathrm{ctg}(\Theta)$

Тепловое сканирование

ID28 Spectrometer (ESRF)

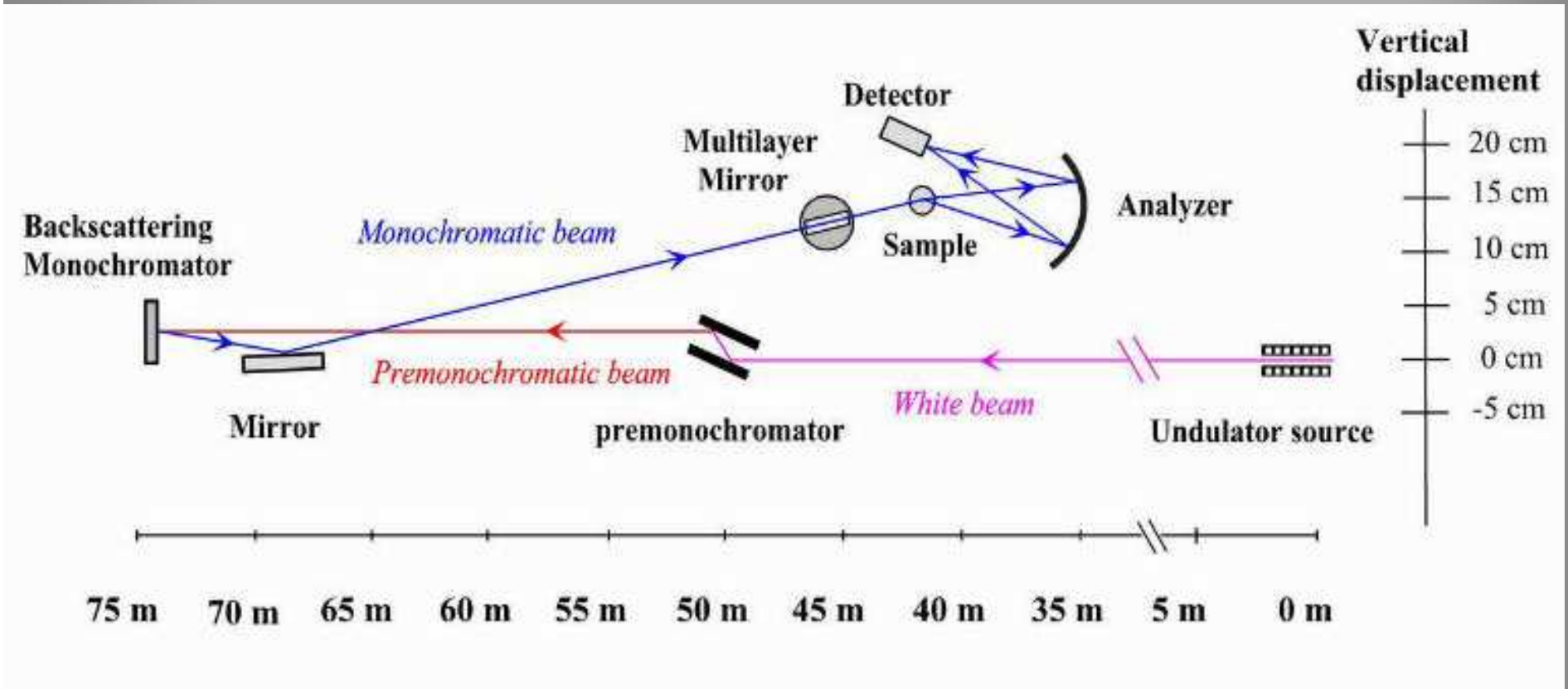

Ioffe Physico-Technical Institute

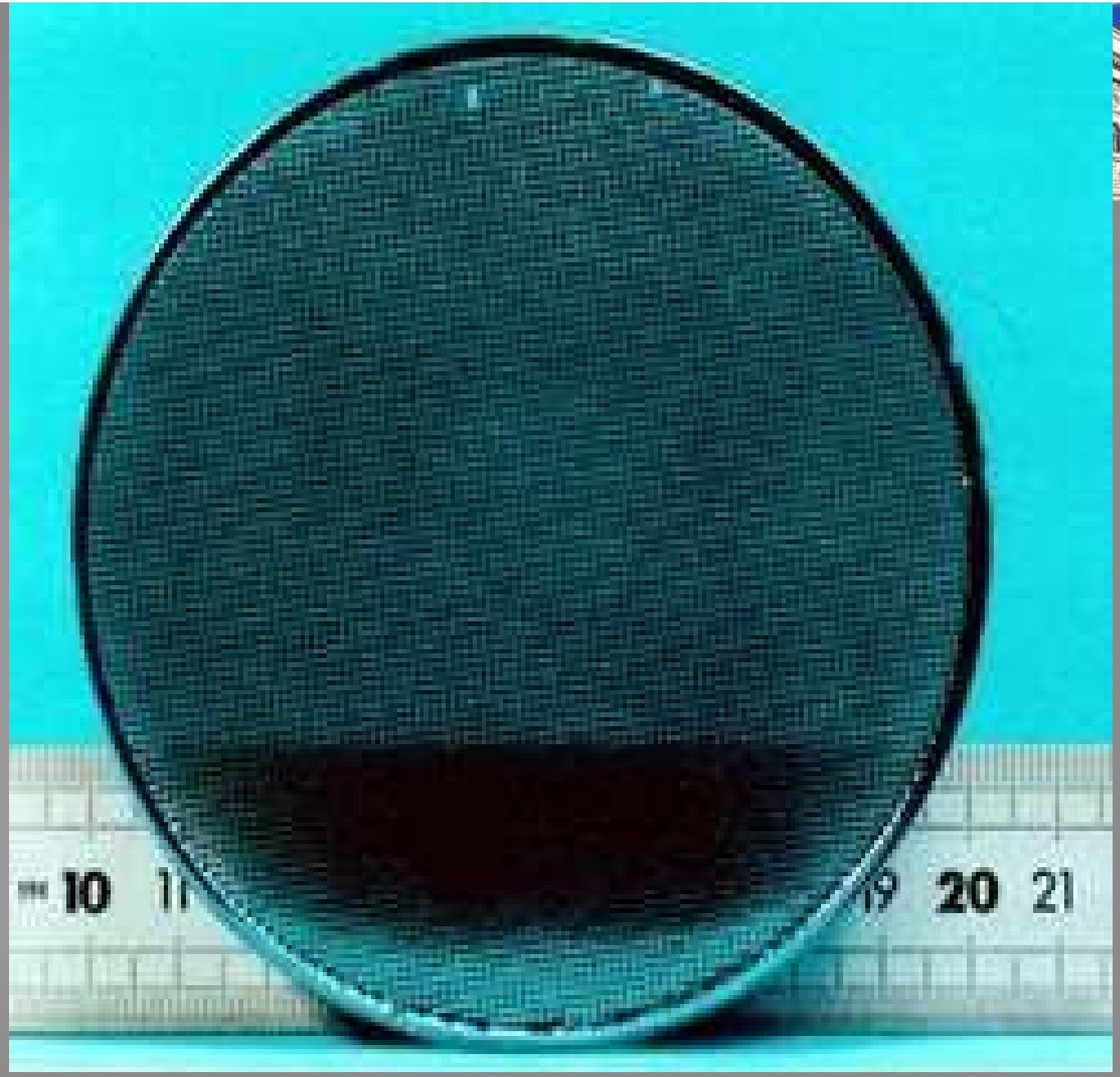

Сферический кристалл анализатор

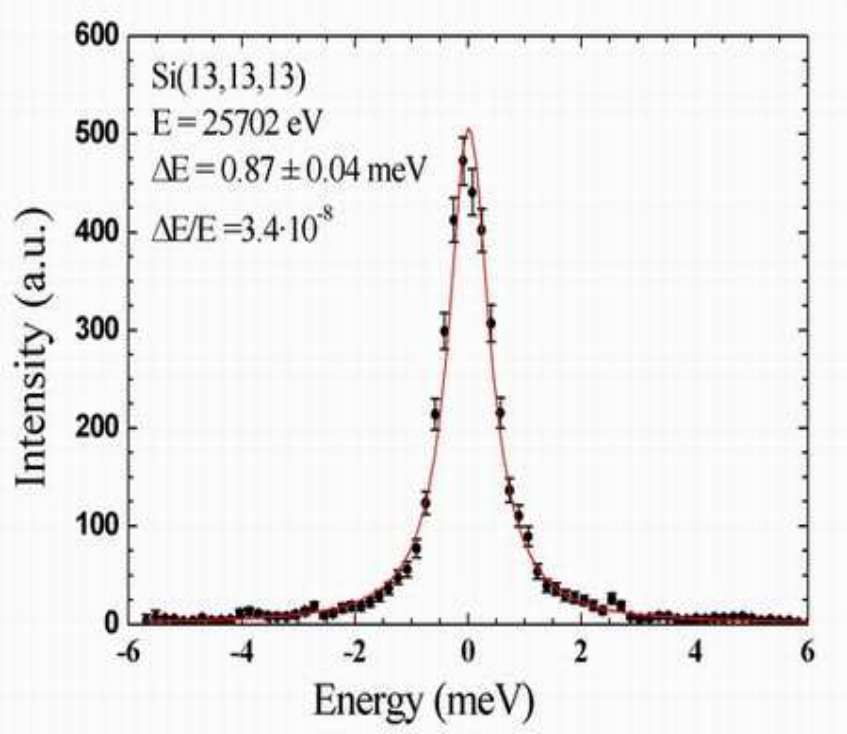

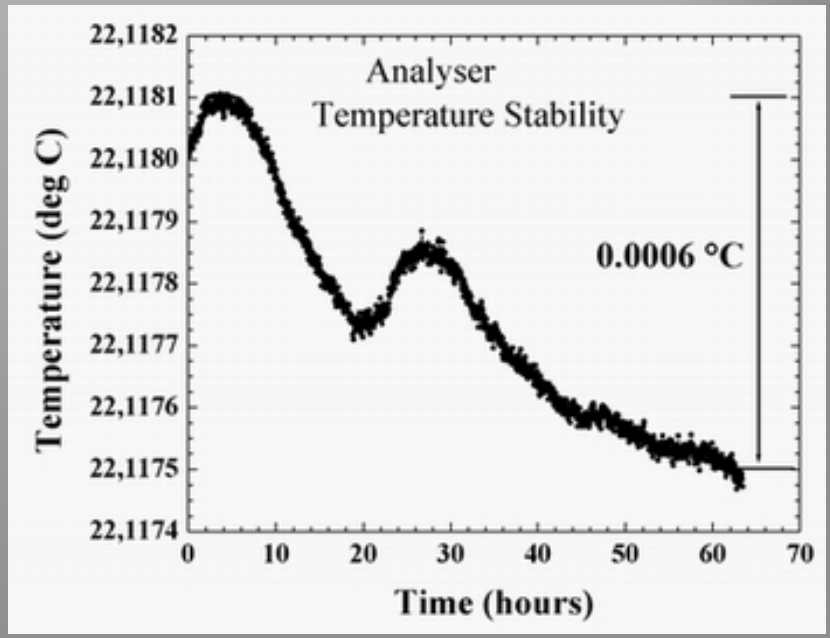

The main characteristics of the ID28 Beamline with the 7-m arm:

Reflection	Energy [keV]	E [meV]	Q_{max} [nm-1]	Q_{min} [nm-1]	ΔQ [nm-1]	Flux [ph./s/ 200 mA]
Si(7,7,7)	13.840	7.6 ± .2	64	1	1.89	$10.5 \cdot 10^{10}$
Si(8,8,8)	15.817	5.5 ± .2	74	1	2.16	$9.00 \cdot 10^{10}$
Si(9,9,9)	17.794	3.0 ± .2	83	1	2.43	$2.70 \cdot 10^{10}$
Si(11,11,11)	21.747	1.5 ± .1	101	1	3.00	$6.60 \cdot 10^{9}$
Si(12,12,12)	23.725	1.3 ± .1	111	1	3.24	$5.85 \cdot 10^{9}$
Si(13,13,13)	25.704	1.0 ± .1	120	1	3.50	$1.47 \cdot 10^{9}$

Photon **Flux** values are measured at the sample goniometer with the following experimental conditions: two 1.6 m U32 undulators; ring current: 200 mA; primary slits aperture: 1.6 mm (horizontal) x 0.7 mm (vertical); secondary slits aperture: 2.4 mm (horizontal) x 1.0 mm (vertical). The **Qmin** depends strongly from the beam divergence (40μrad hor. x 20μrad ver.) and from the aperture of the slits in front of the first analyser. The **focal spot size at the sample is** 250μ hor. x 80μ ver. using the toroidal part of the focussing mirror and 25μm hor. x 60μm ver. using the cylindrical part of the mirror for the vertical focussing and the multilayer mirror for the horizontal focussing

Эксперимент твердый раствор CdS/CdSe

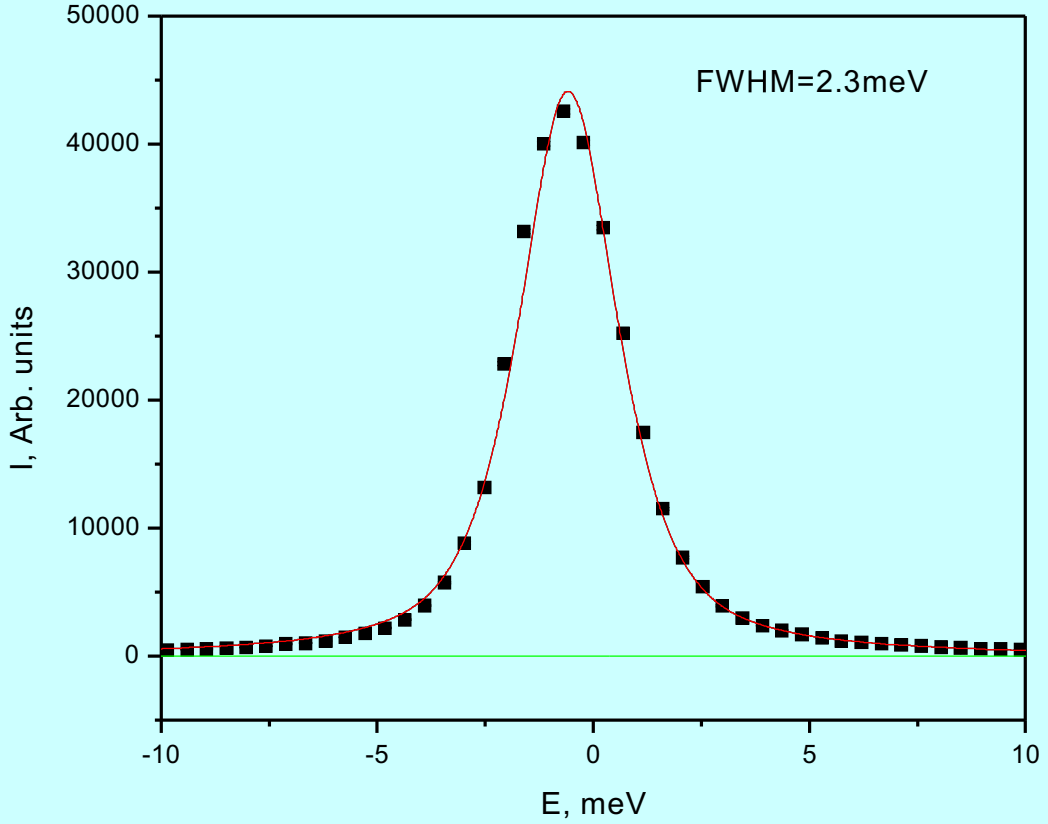

- Монохроматор: Si(999)
- E=17.8keV
  ΔE=2.3mev
- Room temperature

продольных и поперечных фононах

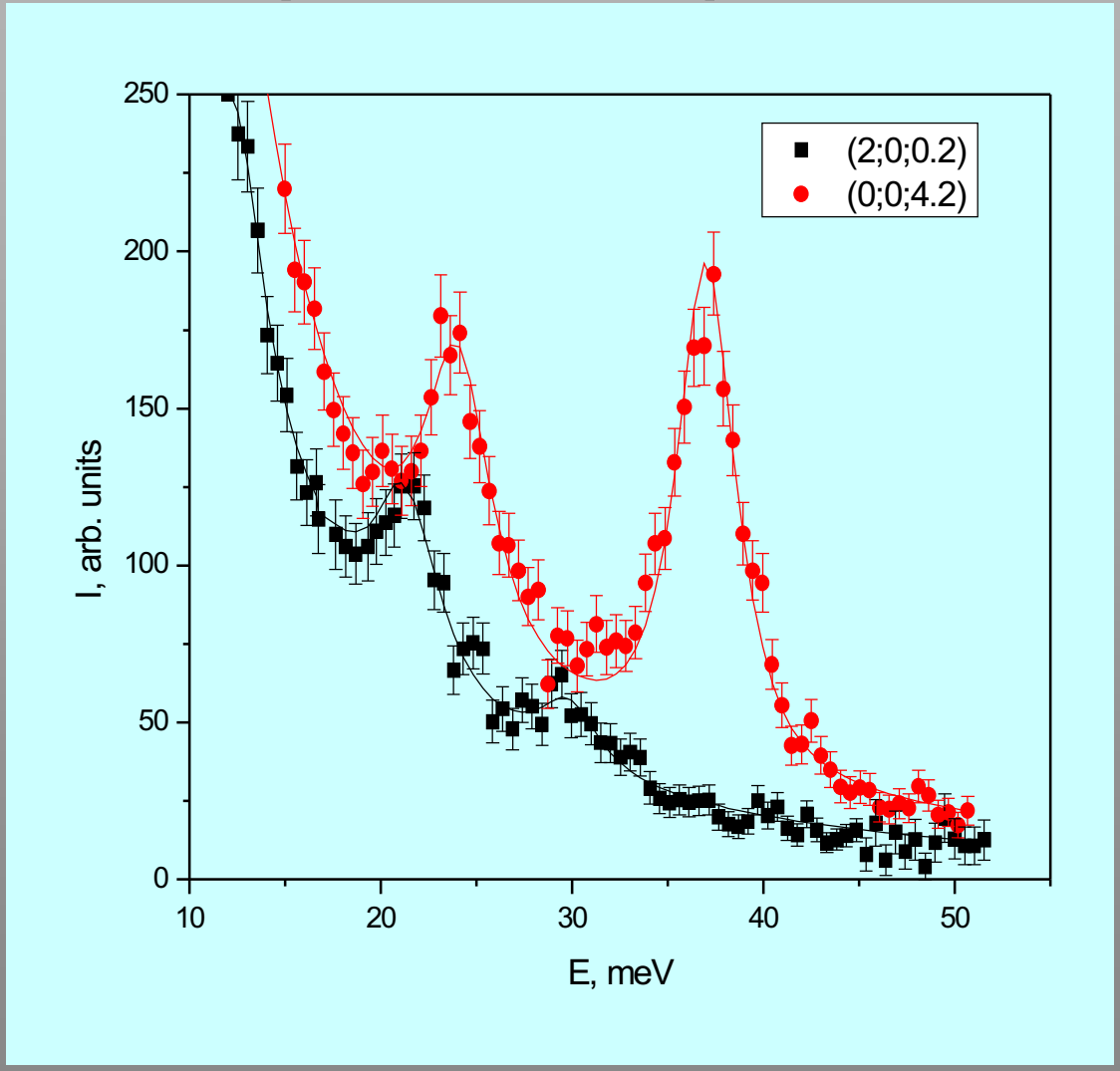

Зависимость от вектора обратной решетки

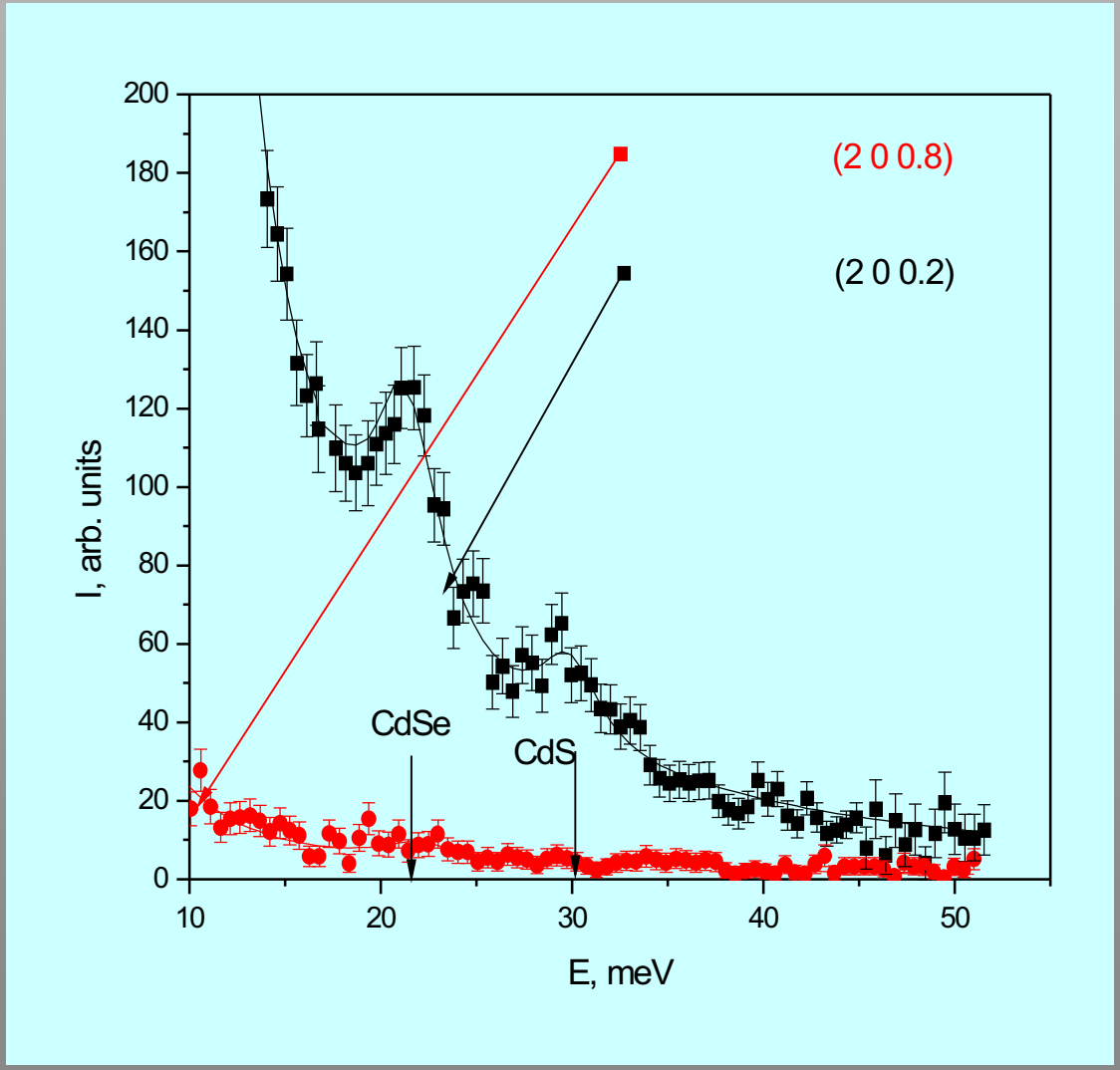

diffuse scattering in perovskite

Piezoelectrics $Li_x(K_{0.5}Na_{0.5})_{1-x}NbO_3$

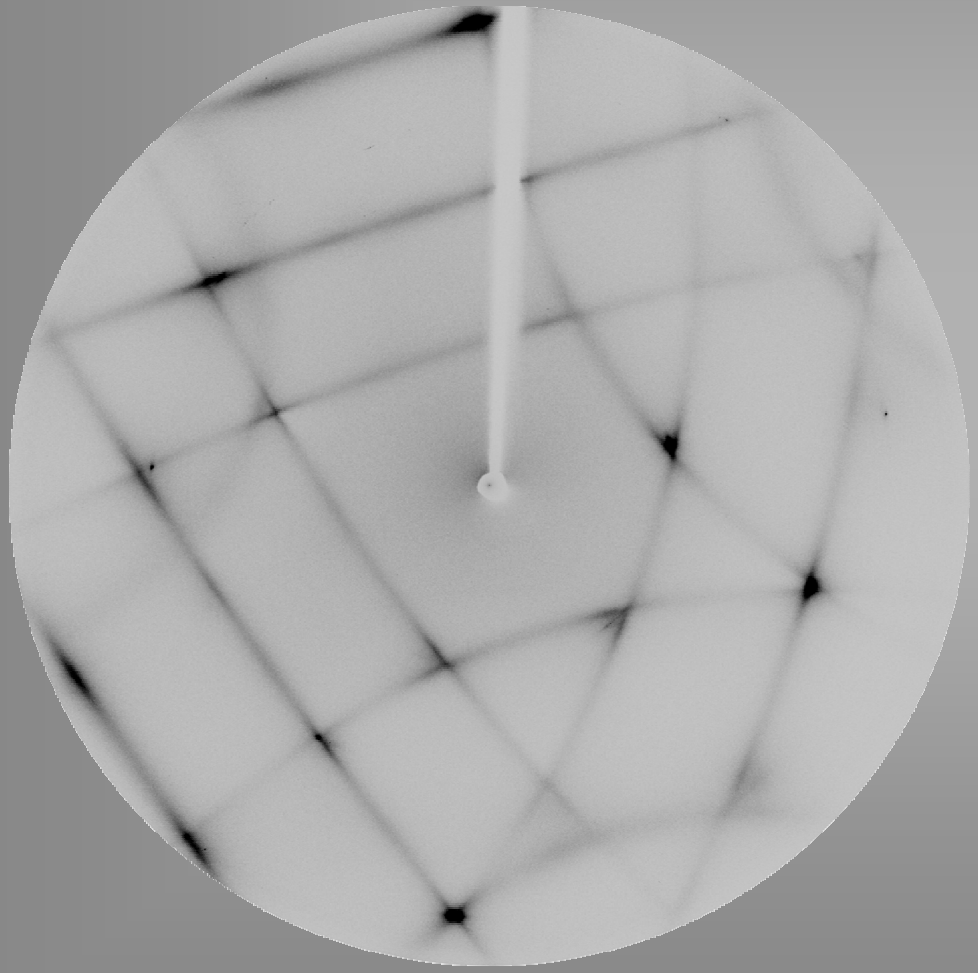

Collaboration:
A. Bosak
ESRF
D. Chernyshov
SNBL
D. Damjanovic
EPFL, Lausanne
M. Korablev-Dyson
SpbGPU, St. Petersburg
S.Vakhrushev
A.F. Ioffe PTI, St. Petersburg

High temperature:
cubic phase, three families of diffuse planes normal to <100>, <010>, <001>

diffuse scattering in perovskite

Piezoelectrics $Li_x(K_{0.5}Na_{0.5})_{1-x}NbO_3$

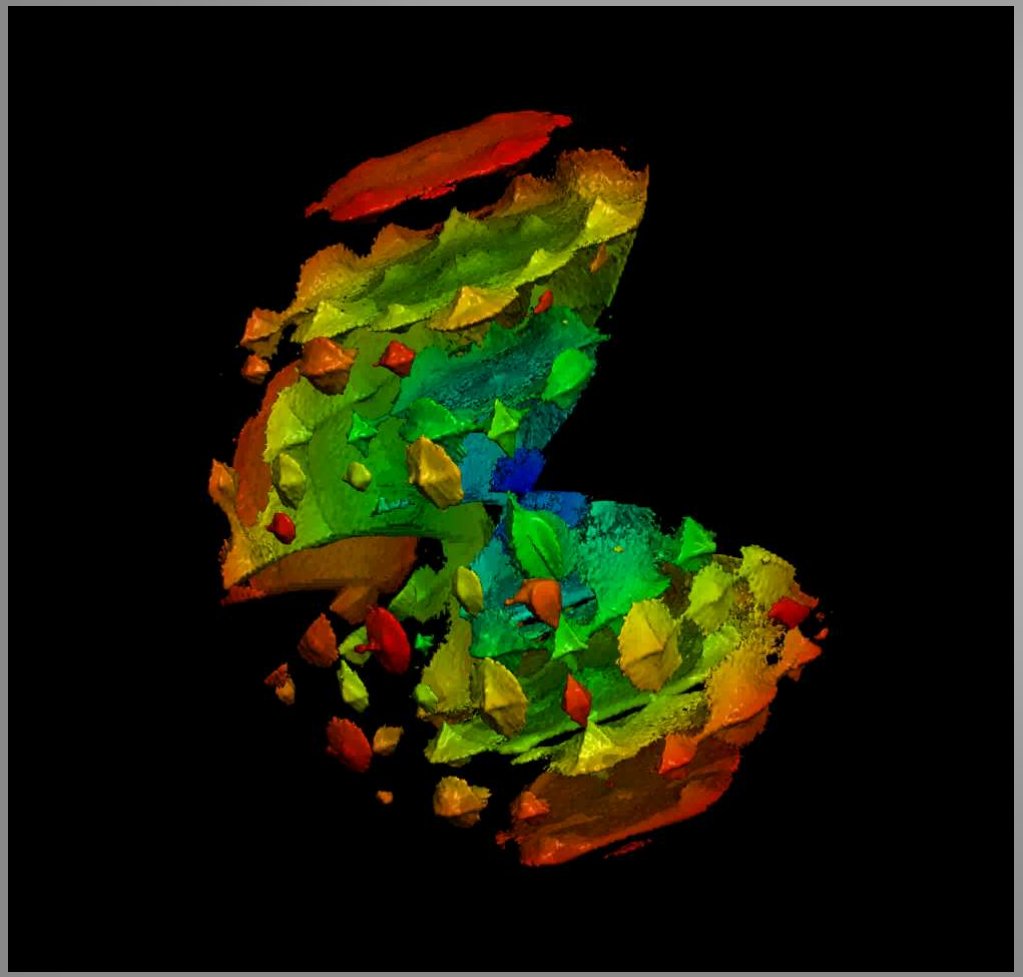

Collaboration:
A. Bosak
ESRF
D. Chernyshov
SNBL
D. Damjanovic
EPFL, Lausanne
M. Korablev-Dyson
SpbGPU, St. Petersburg
S.Vakhrushev
A.F. Ioffe PTI, St. Petersburg

High temperature:
cubic phase, three families of diffuse planes normal to <100>, <010>, <001>

Двумерное распределение интенсивности в NBT ДН-2 Дубна

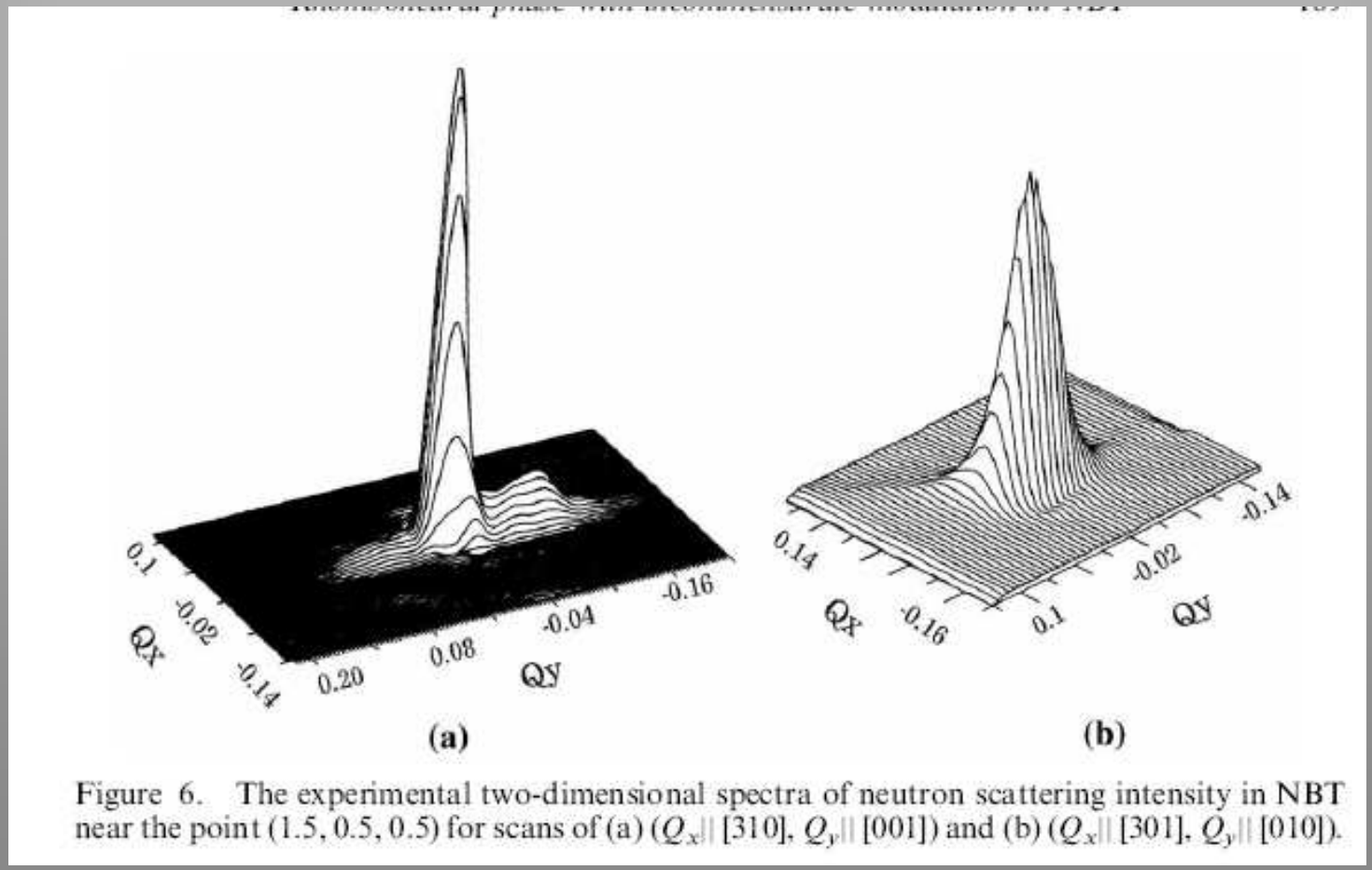

Figure 6. The experimental two-dimensional spectra of neutron scattering intensity in NBT near the point (1.5, 0.5, 0.5) for scans of (a) (Q_x|| [310], Q_y|| [001]) and (b) (Q_x|| [301], Q_y|| [010]).

Phonons only: no static disorder

Ambient temperature:
orthorhombic phase, only one family of diffuse planes normal to <001> survives

elastic or inelastic?
IXS @ ID28!

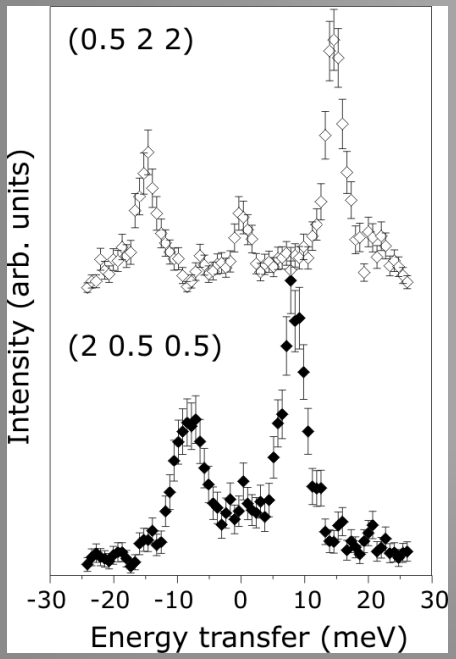

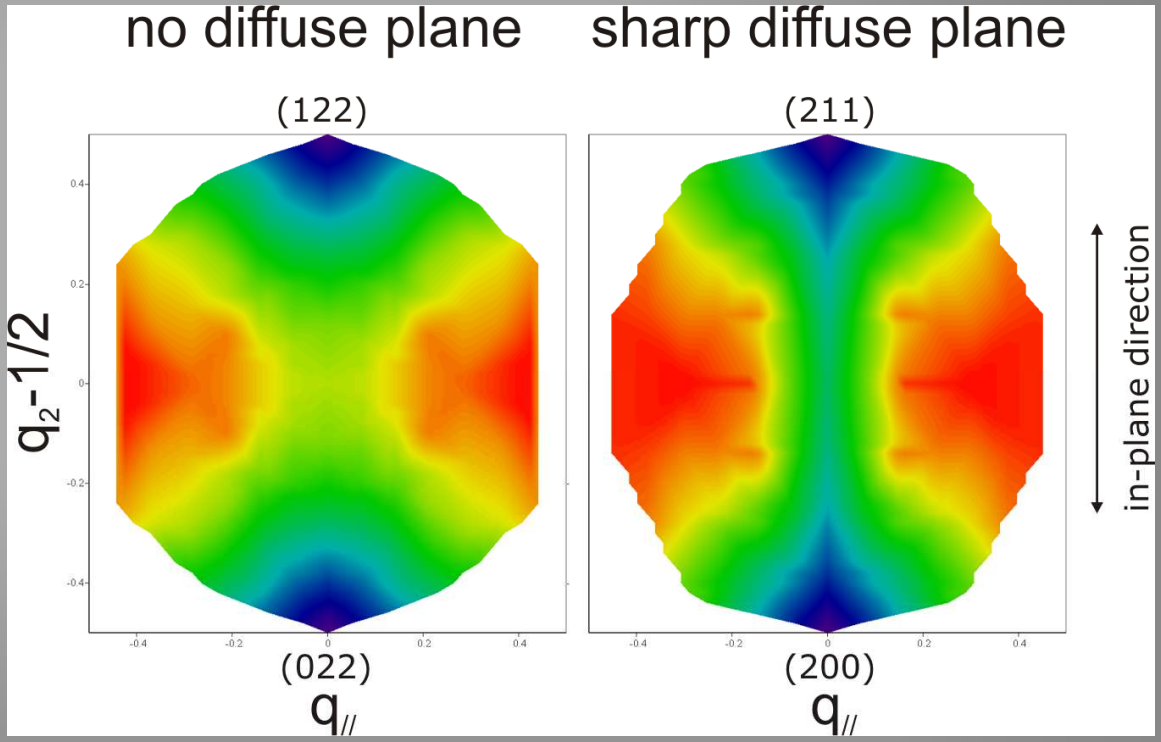

sharp diffuse features correspond to strong phonon softening

Phonons only: no static disorder

Ambient temperature:
orthorhombic phase, only one family of diffuse planes normal to <100> survives

elastic or inelastic?
IXS @ ID28!

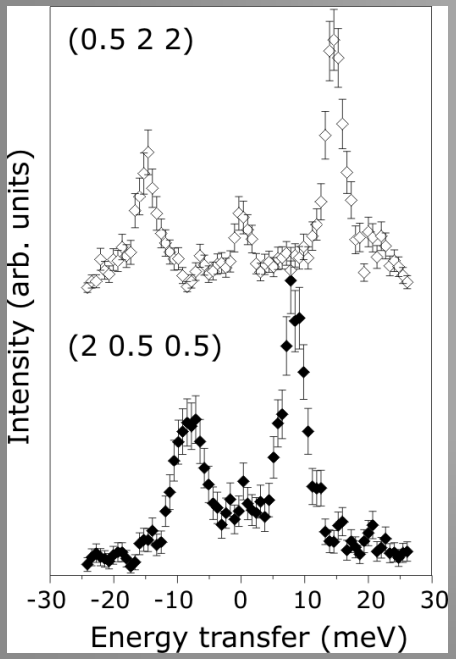

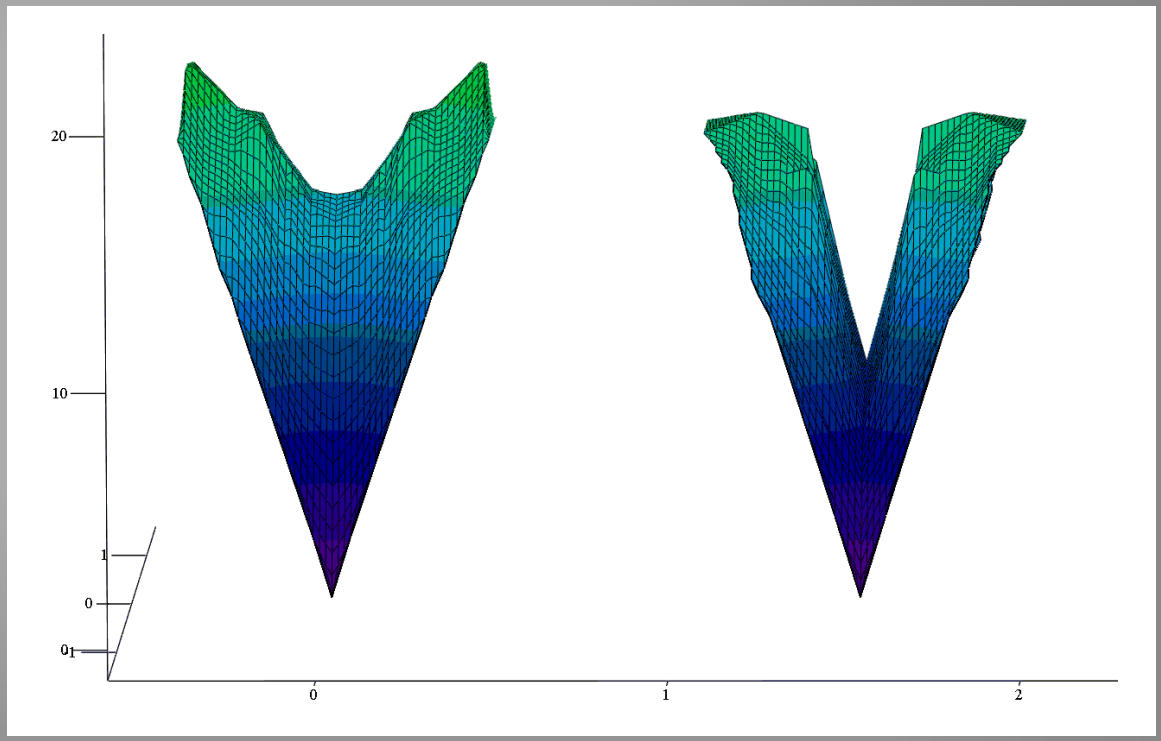

sharp diffuse features correspond to strong phonon softening

ПЛЕНКИ

Phonons in 100nm film

PMN film (0.25 2 0) "large" tilt (inside film?)

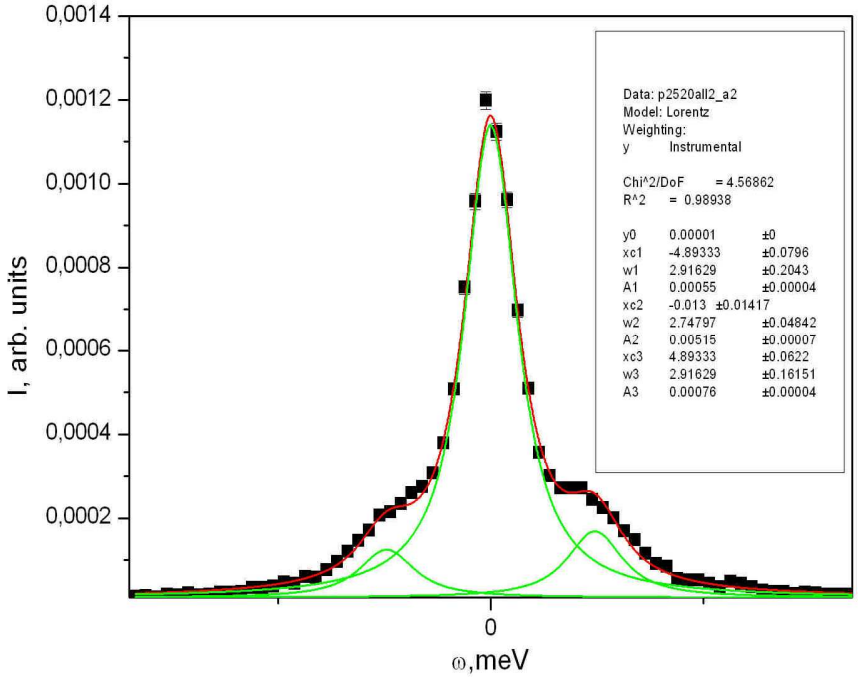

Figure 1

PMN film (0.25 2 0) small tilt (near surface?)

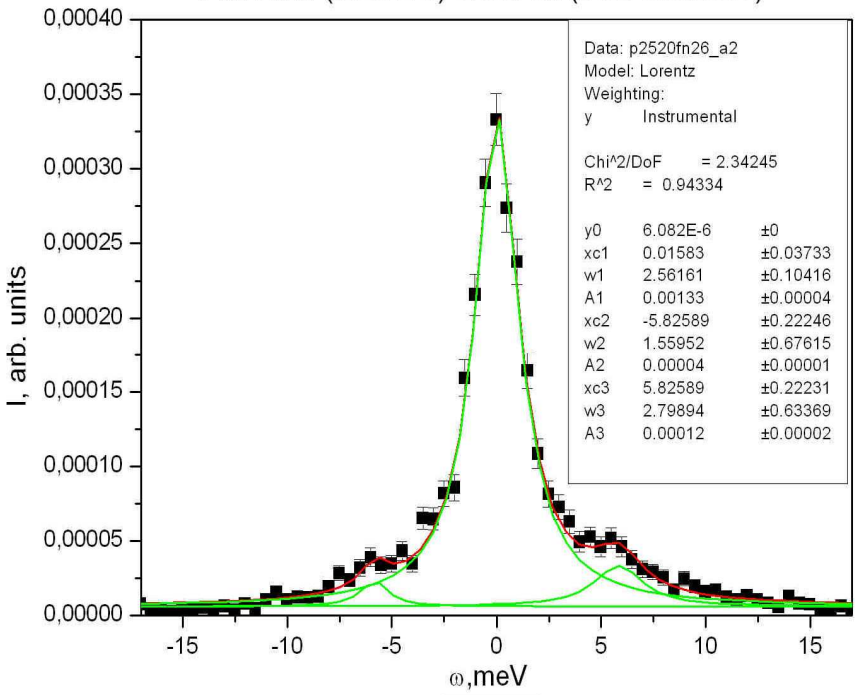

Figure 2

PMN film 80nm
BL35XU V=800μ^3

PBMN 600C (0.25 2 0) dQ = (0.007 0.07 0.45) horizontal slit opened

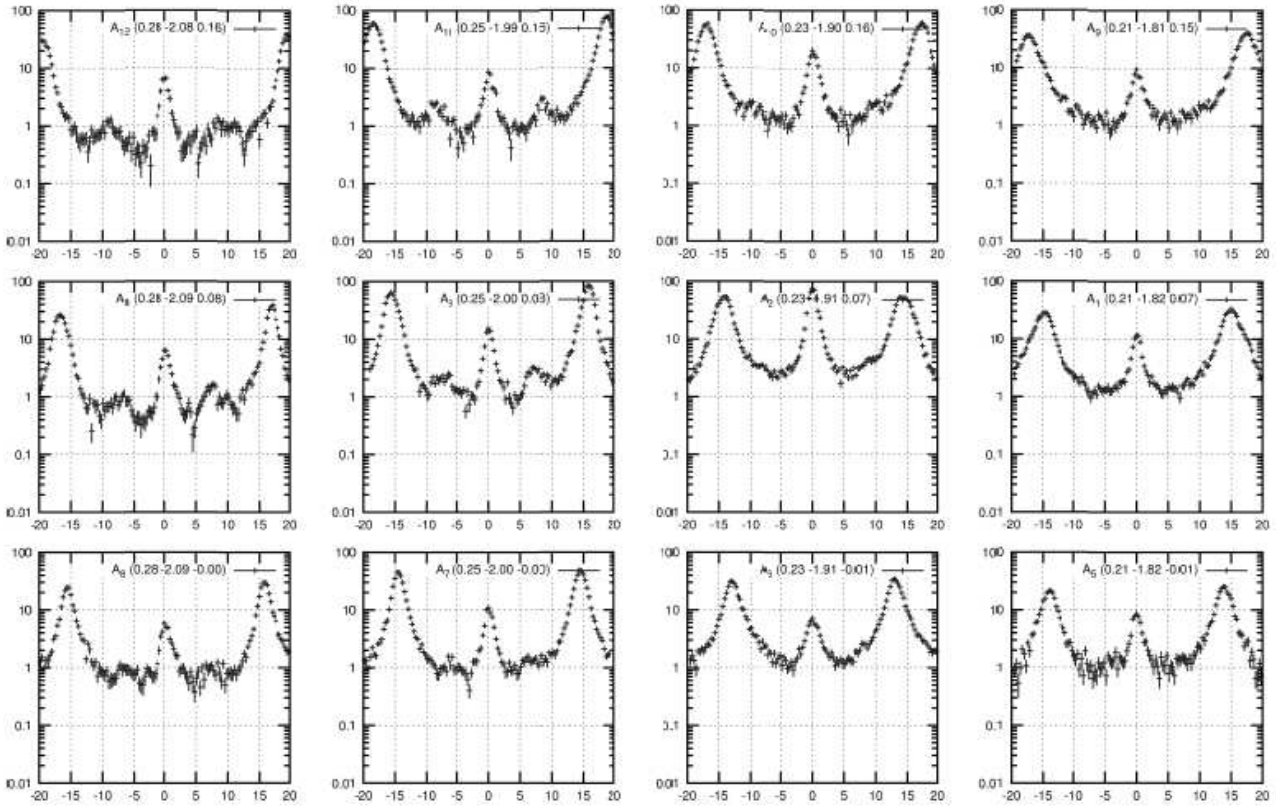

Локальная Структура и динамика

Ioffe Physico-Technical Institute

Static PDF

- Dynamic structure factor:

$$S(\boldsymbol{Q},\omega)=\frac{1}{N\langle b\rangle^2}\sum_{\nu,\mu}b_\nu b_\mu\int\left\langle\left\langle e^{i\boldsymbol{Q}\cdot\left(\boldsymbol{R}_\nu(0)-\boldsymbol{R}_\mu(t)\right)}\right\rangle\right\rangle e^{-i\omega t}dt$$

- Elastic structure factor ($\omega = 0$) describes the average structure:

$$S(\boldsymbol{Q},0)=\frac{1}{N\langle b\rangle^2}\sum_{\nu,\mu}b_\nu b_\mu\left\langle\left\langle e^{i\boldsymbol{Q}\cdot\left(\boldsymbol{R}_\nu-\boldsymbol{R}_\mu\right)}\right\rangle\right\rangle$$

Instantaneous PDF

- Energy integrated structure factor describes the instantaneous (snap-shot) structure:

$$S_{total}(\boldsymbol{Q}) = \int_{-\infty}^{\infty} S(\boldsymbol{Q},\omega)\,d\omega$$

$$= \frac{1}{N\langle b\rangle^2} \sum_{\nu,\mu} b_\nu b_\mu \int\int \left\langle\left\langle e^{i\boldsymbol{Q}\cdot\left(\boldsymbol{R}_\nu(0)-\boldsymbol{R}_\mu(t)\right)}\right\rangle\right\rangle e^{-i\omega t}\,dt\,d\omega$$

$$= \frac{1}{N\langle b\rangle^2} \sum_{\nu,\mu} b_\nu b_\mu \left\langle\left\langle e^{i\boldsymbol{Q}\cdot\left(\boldsymbol{R}_\nu(0)-\boldsymbol{R}_\mu(0)\right)}\right\rangle\right\rangle$$

Дифракция без анализа по энергии

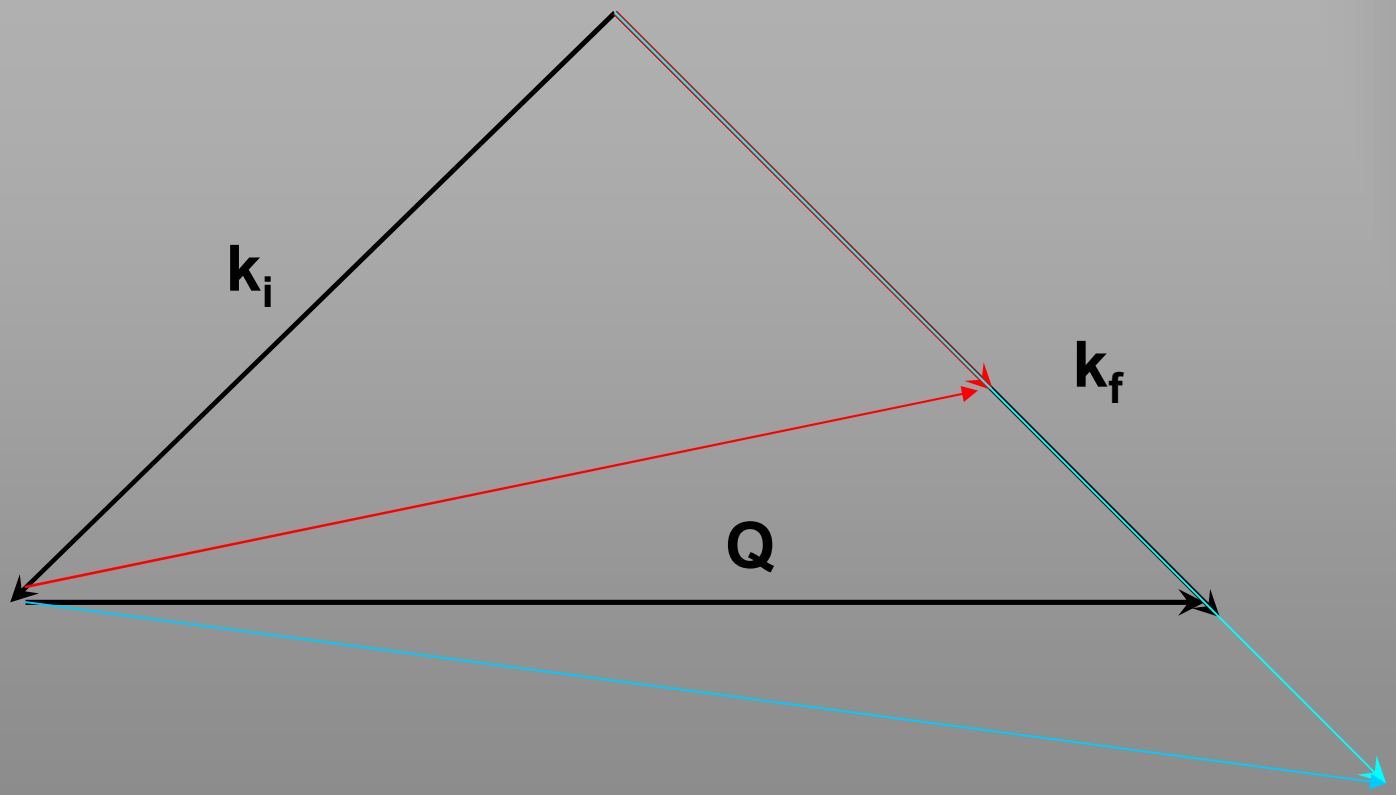

Pb polarization

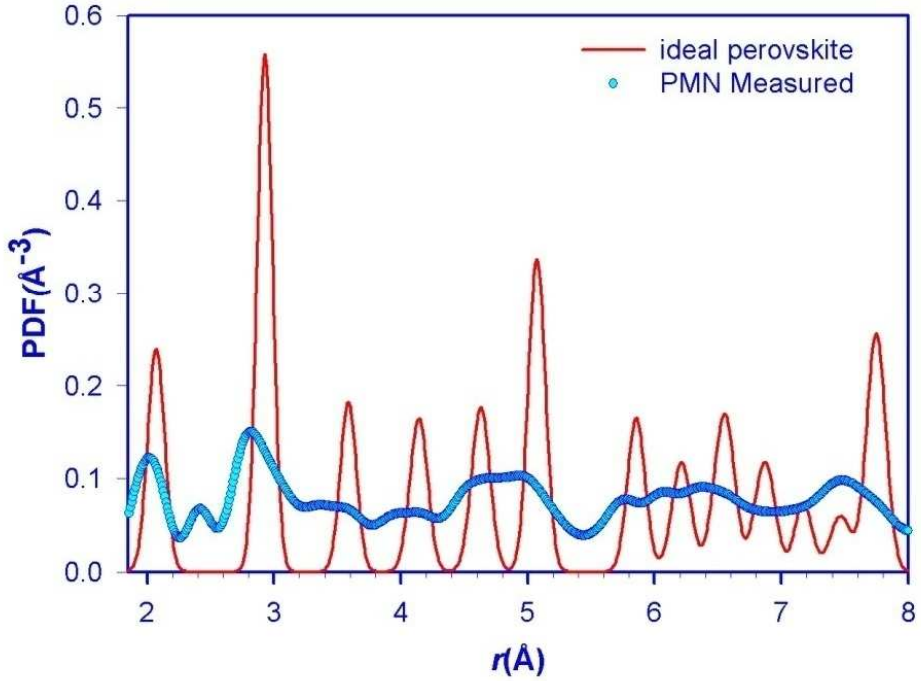

- **PDF of PMN**

Pb^{2+} in $PbZrO_3$

Pb is off-centered by 0.5 Å in the O_{12} cage

Lone-pair *s-p* electrons of Pb

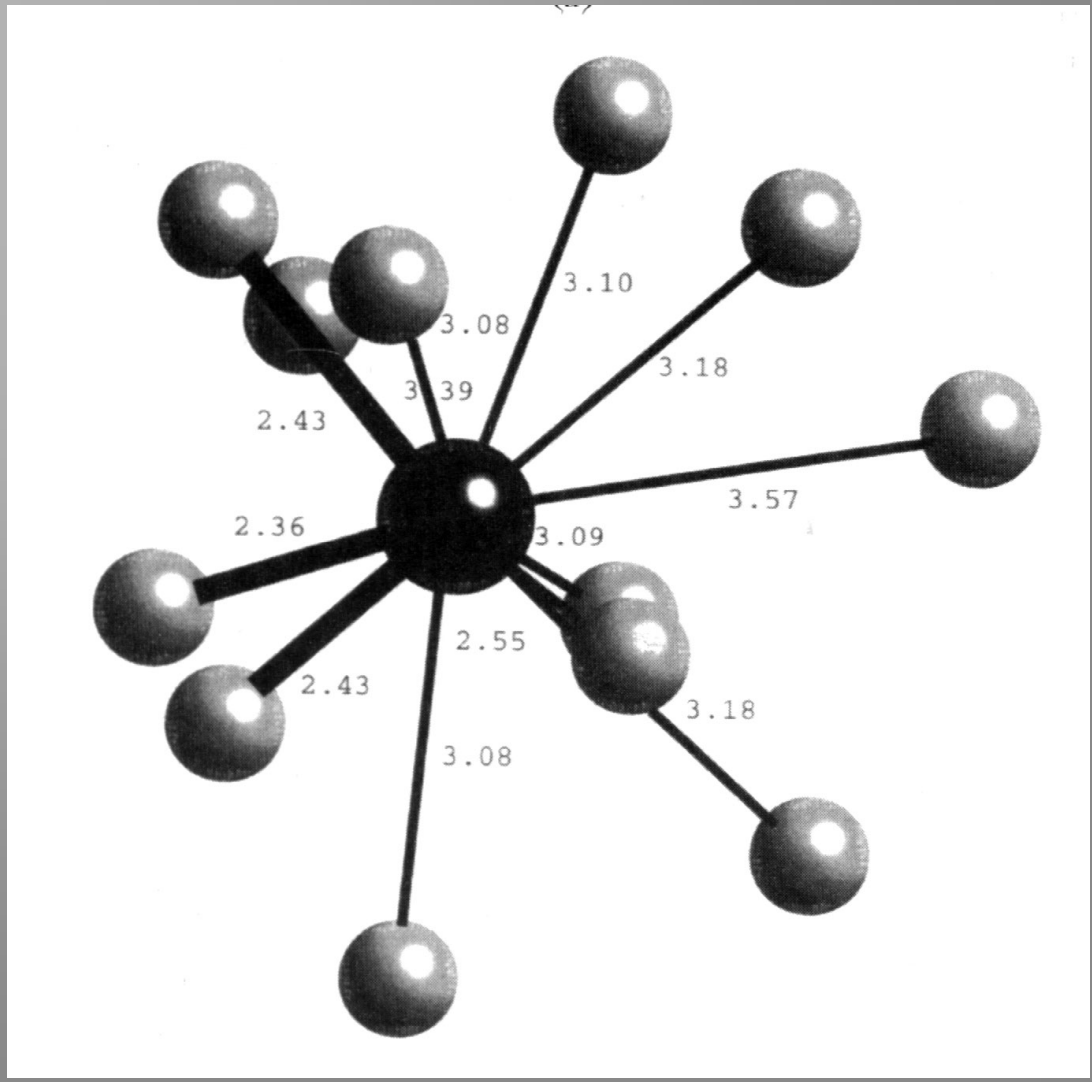

S(Q,w) PMN, T = 450 K

Uusually it is implicitly supposed that time-averaged and instanteneous structures are equivalent

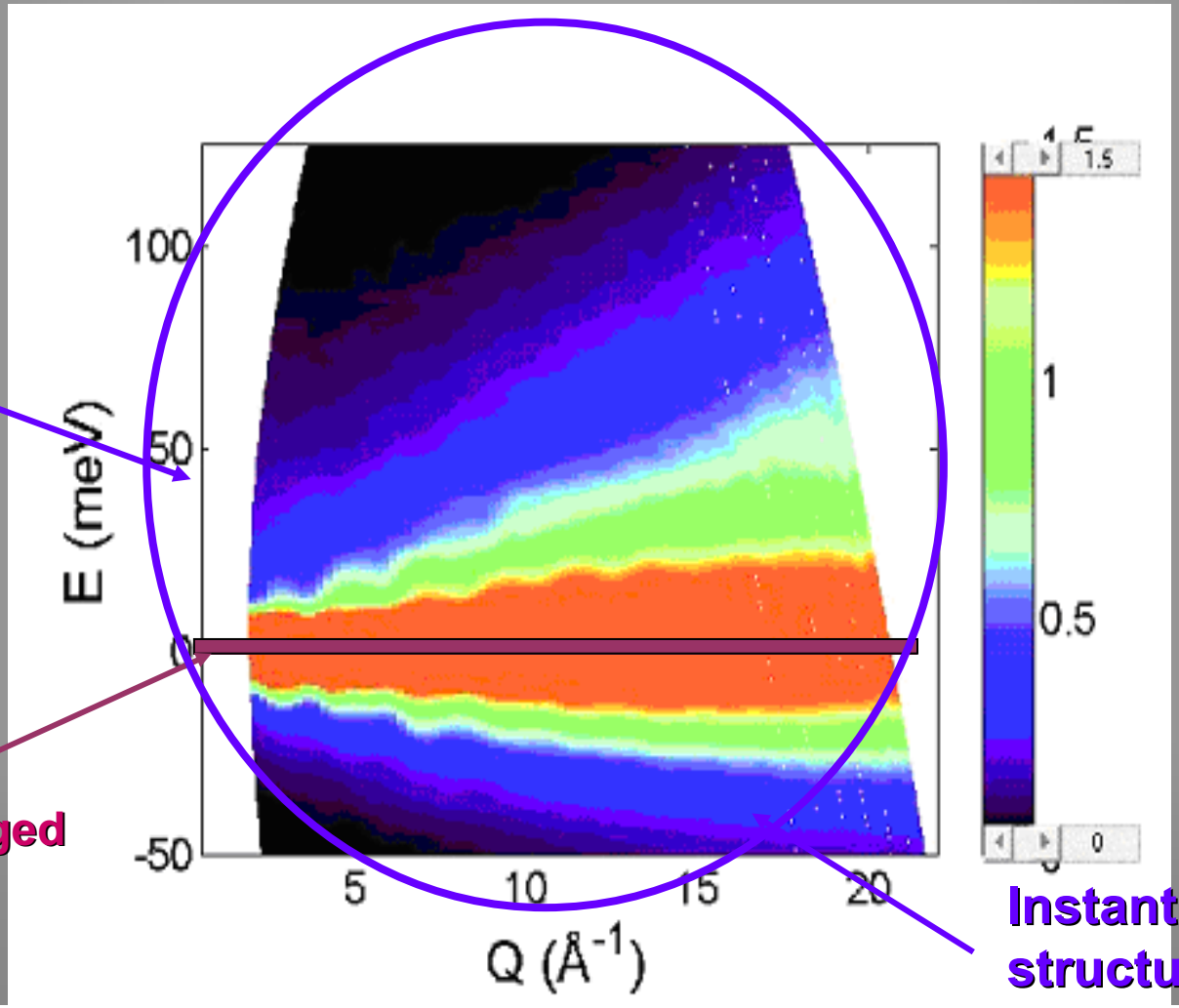

Elastic (average) and energy-integrated (instantaneous) pair distribution functions for Pb in PMN

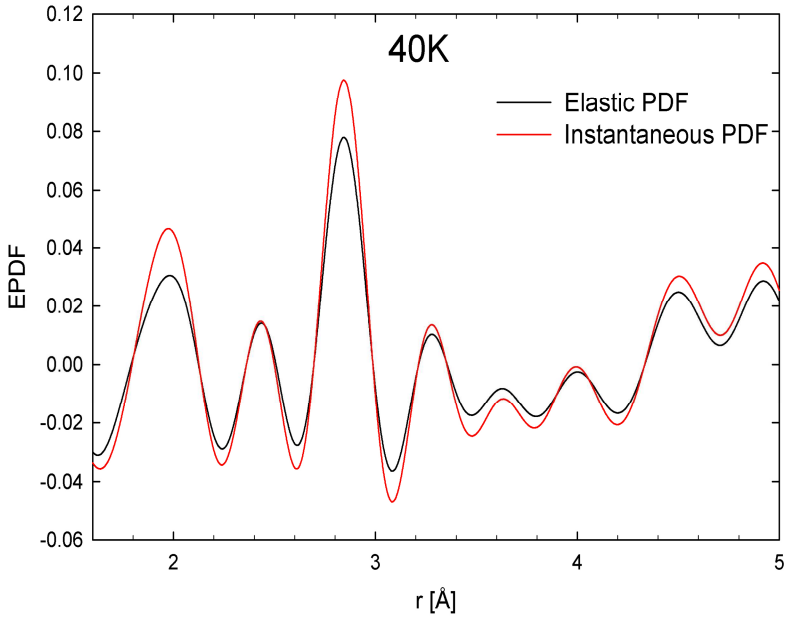

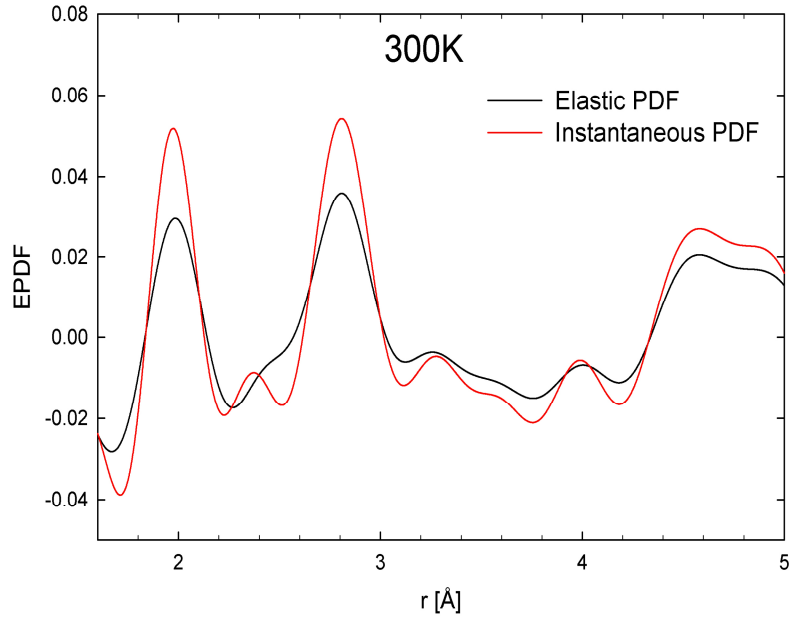

Dynamic PDF of PMN at 450 K.

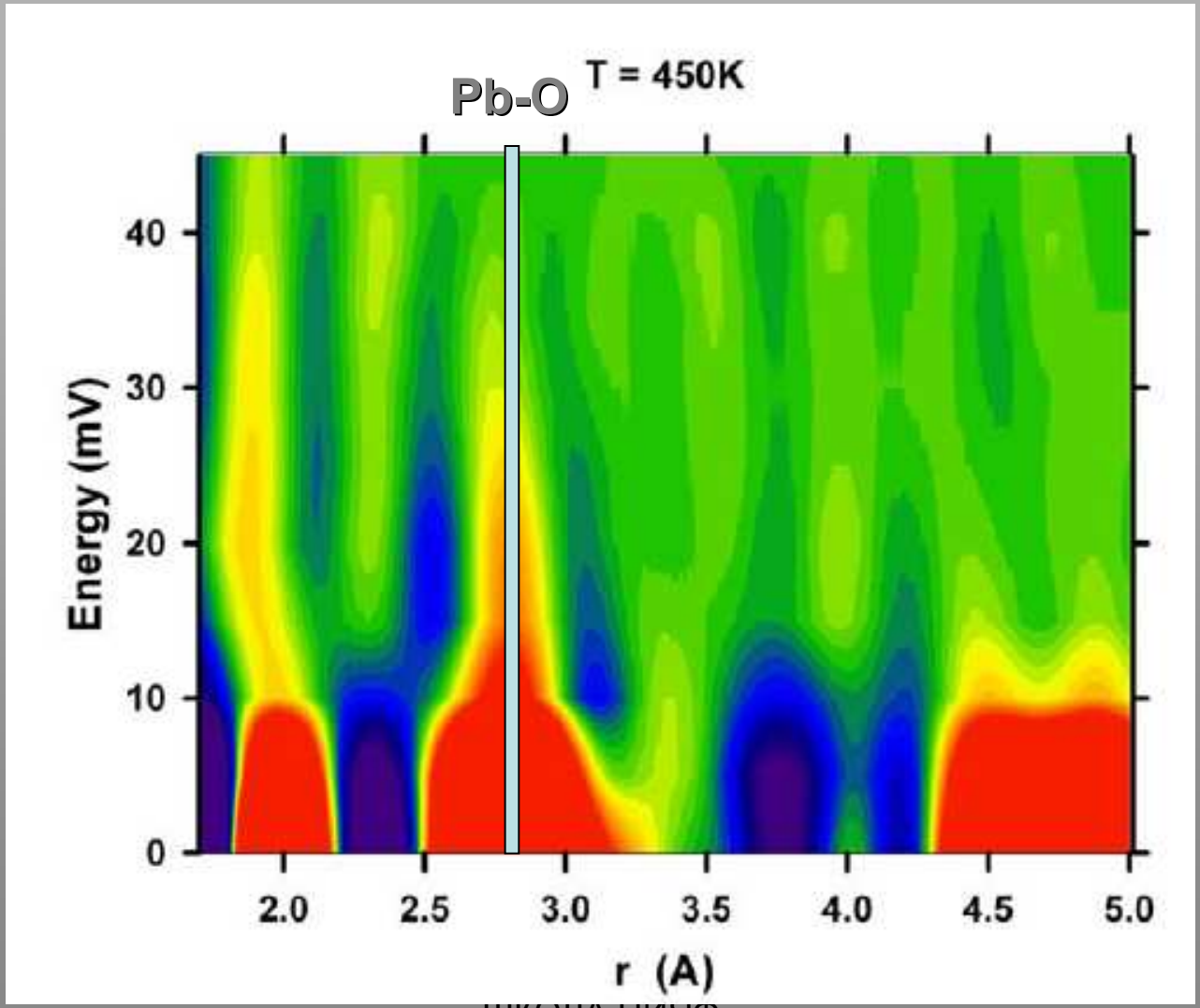

Temperature evolution of average local structure

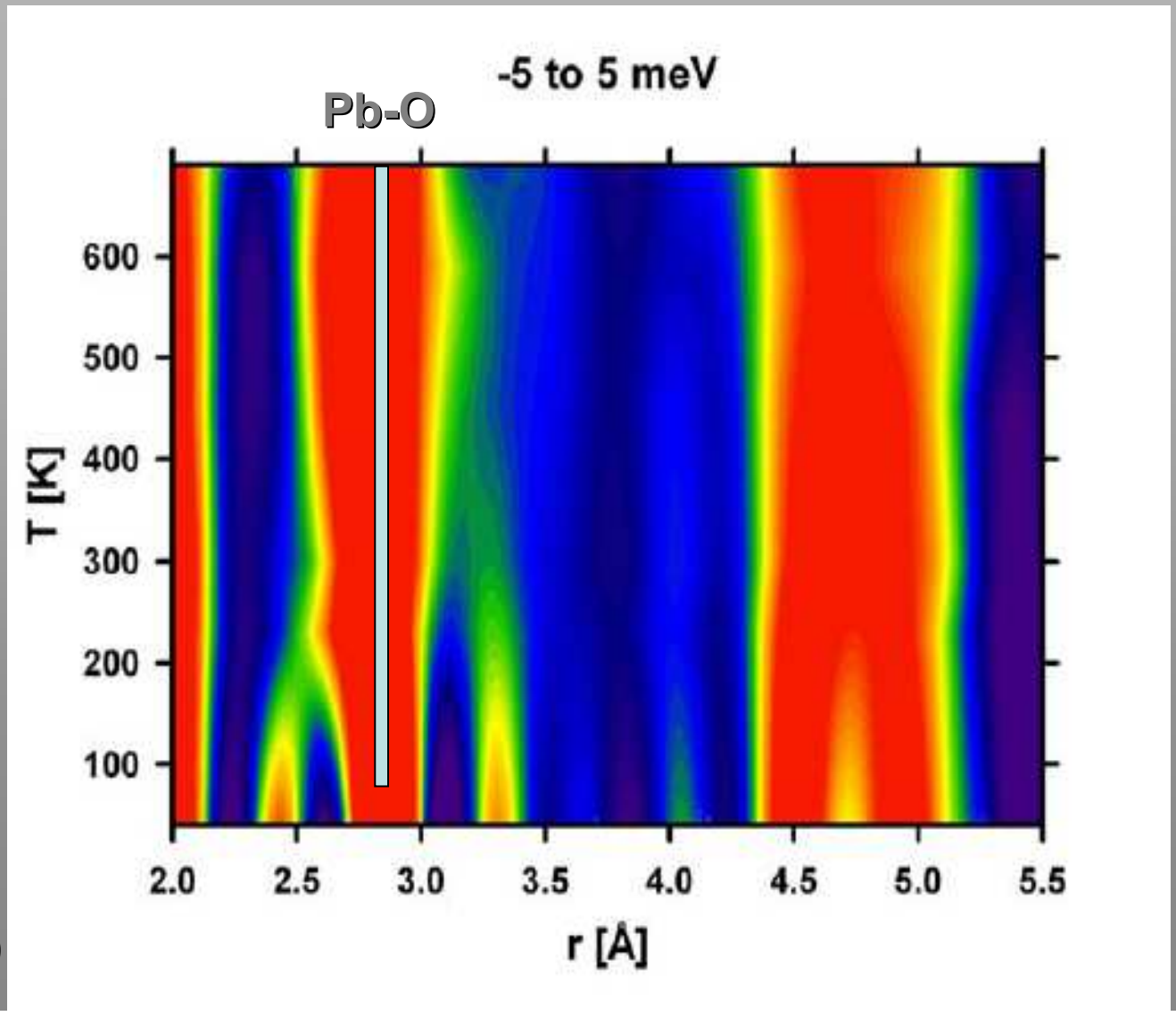

Temperature evolution of the dynamic structure

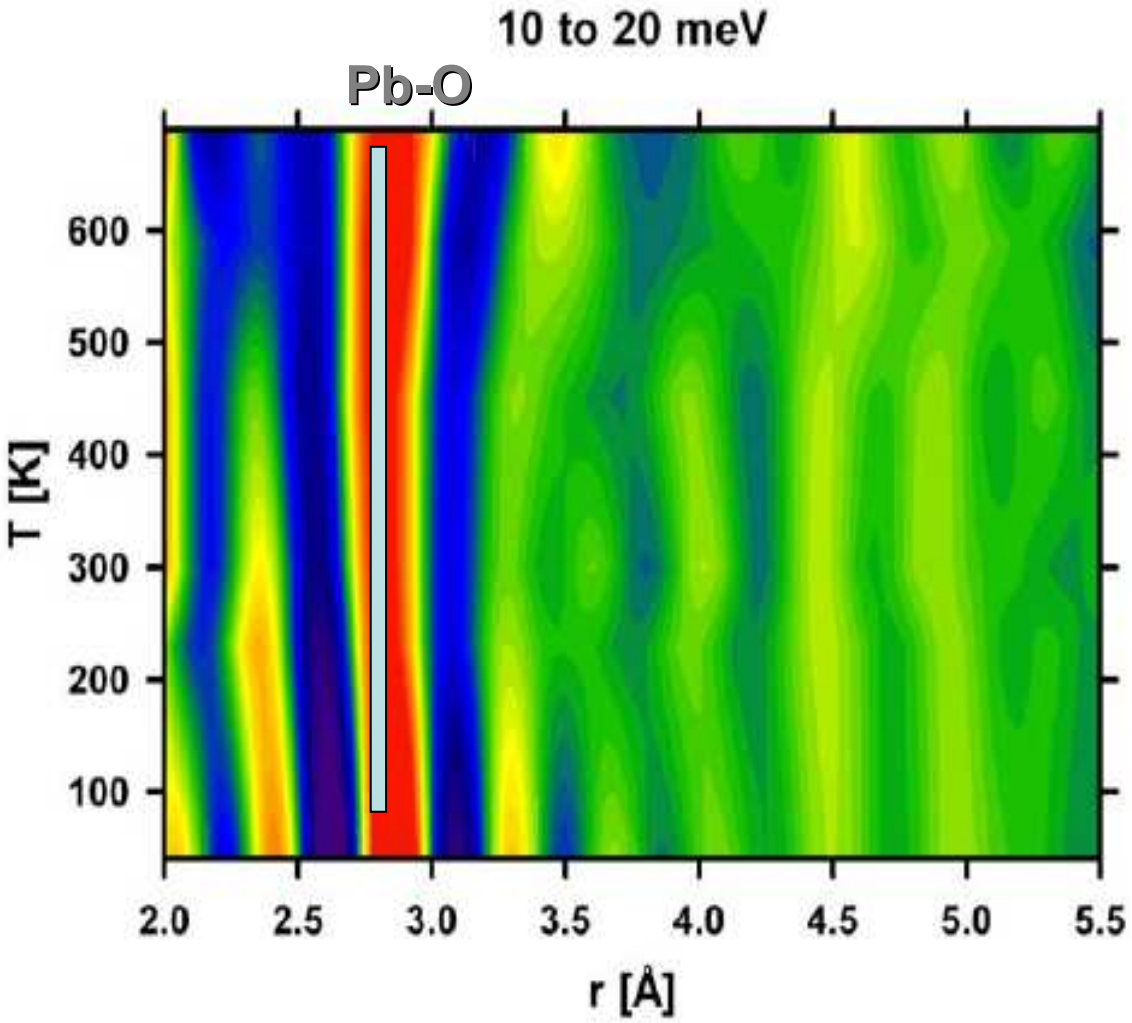

Мезоструктура. Почему рассеяние

- Макроскопические методы не дают микроскопической картины
- Оптическая микроскопия – не дает достаточного разрешения и не чувствительна к смещениям отдельных ионов
- Электронная микроскопия – только тонкие слои и нарушает структуру
- PFM – сильные поля

Немного о рассеянии

$$\left(\frac{d\sigma}{d\Omega}\right)_{l|i} = \frac{k}{k_o N}\sum_{\nu}^{N}\sum_{\nu'}^{N} b_\nu b_{\nu'} \left\langle i\left|e^{i\vec{Q}\vec{r}_\nu}\right|l\right\rangle\left\langle l\left|e^{-i\vec{Q}\vec{r}_{\nu'}}\right|i\right\rangle$$

в кристалле мы можем записать:

$$\hat{r}_\nu \equiv \hat{r}_{nj} = \vec{R}_n + \vec{\rho}_j + \hat{u}_{nj}$$

Тогда, после усреднения:

$$\left(\frac{d\sigma}{d\Omega d\omega}\right)_{coh} = \frac{1}{m}\sum_{j}^{m}\sum_{j'}^{m} b_{jcoh} b_{j'coh} e^{i\vec{Q}(\vec{\rho}_j - \vec{\rho}_{j'})} \frac{1}{N}\sum_{n}^{N}\sum_{n'}^{N} e^{i\vec{Q}(\vec{R}_n - \vec{R}_{n'})}\varphi_{\nu\nu'}(T)$$

$$\left(\frac{d\sigma}{d\Omega d\omega}\right)_{inc} = \frac{1}{m}\sum_{j}^{m} b_{jinc}^2 \frac{1}{N}\sum_{n}^{N}\varphi_{\nu\nu}(T)$$

От какого объема мы получаем картину рассеяния?

- На самом деле суммирование ведется НЕ ПО ОБЪЕМУ ОБРАЗЦА и НЕ ПО РАЗМЕРУ ПУЧКА, а по некому «когерентному объему» определяемому параметрами пучка излучения.

4.2.2. Пространственная когерентность и площадь когерентности

Теперь рассмотрим вкратце интерференционный эксперимент типа опыта Юнга, используя квазимонохроматический свет от протяженного источника σ (рис. 4.2). Предположим, что σ представляет собой *тепловой* источник, такой, как раскаленное вещество или газовый разряд. Для простоты рассмотрим симметричную схему с источником в форме квадрата со стороной Δs. Если отверстия P_1 и P_2 расположены достаточно близко к оси симметрии, вблизи центральной точки P в плоскости наблюдения $\mathscr{B}$ будут наблюдаться интерференционные полосы. Возникновение полос является, как говорят, проявлением *пространственной когерентности* между двумя пучками, приходящими в точку P от двух отверстий P_1 и P_2, поскольку контраст между полосами зависит от расстояния между этими отверстиями (расстояние P_1P_2). Экспериментально установлено, что при достаточно большом расстоянии между источником и плоскостью $\mathscr{A}$, в которой расположены отверстия, интерференционные полосы вблизи P будут наблюдаться в том случае, если

$$\Delta\theta\,\Delta s \leq \bar{\lambda}, \tag{4.2.5}$$

где $\Delta\theta$ — угол, под которым виден отрезок P_1P_2 из источника, и $\bar{\lambda} = c/\bar{\nu}$ — средняя длина волны. Если через R обозначить расстояние между источником и плоскостью, в которой расположены отверстия, то оказывается, что для наблюдения полос вблизи P отверстия должны быть расположены на плоскости $\mathscr{A}$ в пределах области с центром в точке Q и площадью

$$\Delta A \sim (R\Delta\theta)^2 \sim \frac{R^2\bar{\lambda}^2}{S}, \tag{4.2.6}$$

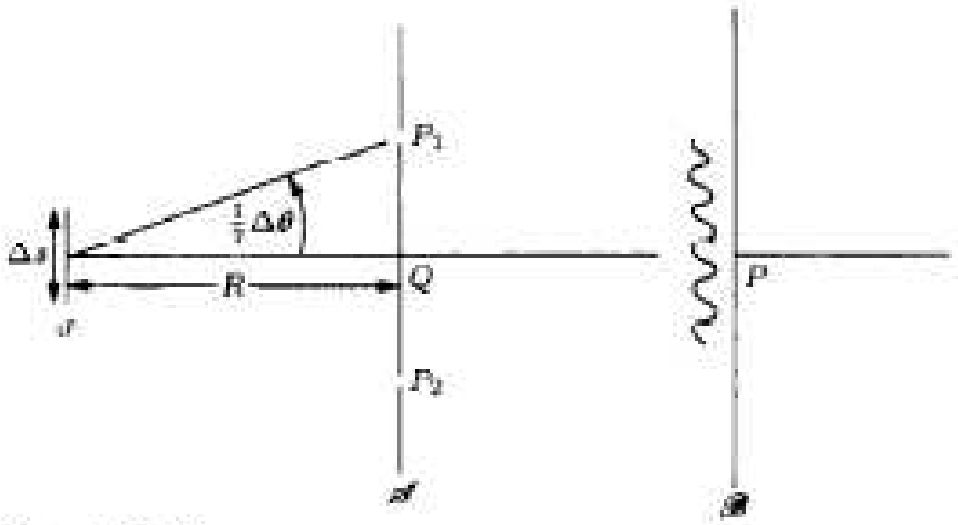

Рис. 4.2. Пространственная когерентность, иллюстрируемая интерференционным опытом Юнга для света от теплового источника σ

где $S = (\Delta s)^2$ — площадь источника. Эта область называется *площадью когерентности* света в плоскости $\mathscr{A}$ вблизи точки Q, а квадратный корень от площади когерентности иногда называют *поперечной длиной когерентности*. Следует отметить, что согласно (4.2.6) площадь когерентности будет тем больше, чем

For classical X-ray scattering experiments, the diffraction of large beams with many coherence volumes is observed. In each coherence volume $\mathcal{D}_i$, a wave $A_i(\mathbf{q})$ is diffracted. Only an incoherent sum of the intensities over a large number of domains N is measured:

$$I(\mathbf{q}) = \sum_{i \in N} |A_i(\mathbf{q})|^2. \qquad (1)$$

With the new synchrotron sources, the high brilliance and the small source size open the possibility of obtaining coherent X-ray beams of reasonable intensity and of nearly macroscopic spatial extension. As the X-ray source is not coherent, the method consists in selecting, in the two transverse directions, a part of the incoherent beam which fulfils the conditions for diffraction:

$$\sigma\sigma' \simeq \lambda/4\pi, \qquad (2)$$

where σ' is the r.m.s. divergence of the beam and σ is the r.m.s. beam size. The equality in equation (2) corresponds to fully coherent Gaussian beams. Equation (2) is in fact another version of the Heisenberg equation, if one estimates $\Delta p = 2\pi\hbar\sigma'/\lambda$ and $\Delta x = \sigma$. In practice, owing to optics,

Характерное значение для рентгеновского излучения
$\sigma = 1.5*10^{-1}/4\pi/10^{-3} = 13$nm

F. Livet, Acta cryst. A63, 87-107 (2007)

Along the longitudinal direction, the diffracted waves can interfere if the FWHM path-length distribution of the waves in the irradiated sample $\Delta\mathcal{L}$ fulfils

$$\Delta\mathcal{L} \leq \Lambda_l = \lambda^2/2\delta\lambda, \qquad (4)$$

where Λ_l is the longitudinal (temporal) coherence length. The optics determines the experiment monochromaticity $\delta\lambda$. One

Характерное значение для рентгеновского излучения
$\Lambda=0.15/2/(d\lambda/\lambda=2*10^{-4})=400nm$

Для пучка размером 10*10 микрон мы должны иметь расходимость Порядка 10^{-5} радиана и монохроматичность порядка 10^{-5}

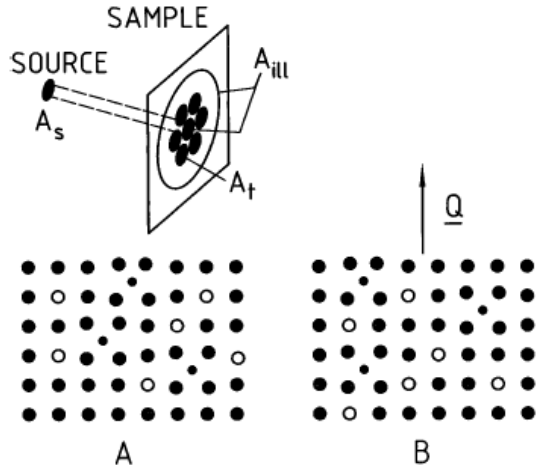

Fig. 4 Two sample areas with equal average periodic lattice, equal defect densities, equal short and long-range order but different individual arrangement of the defects. The *upper part* shows the transverse coherence area A_{tr} and two illuminated areas of different size

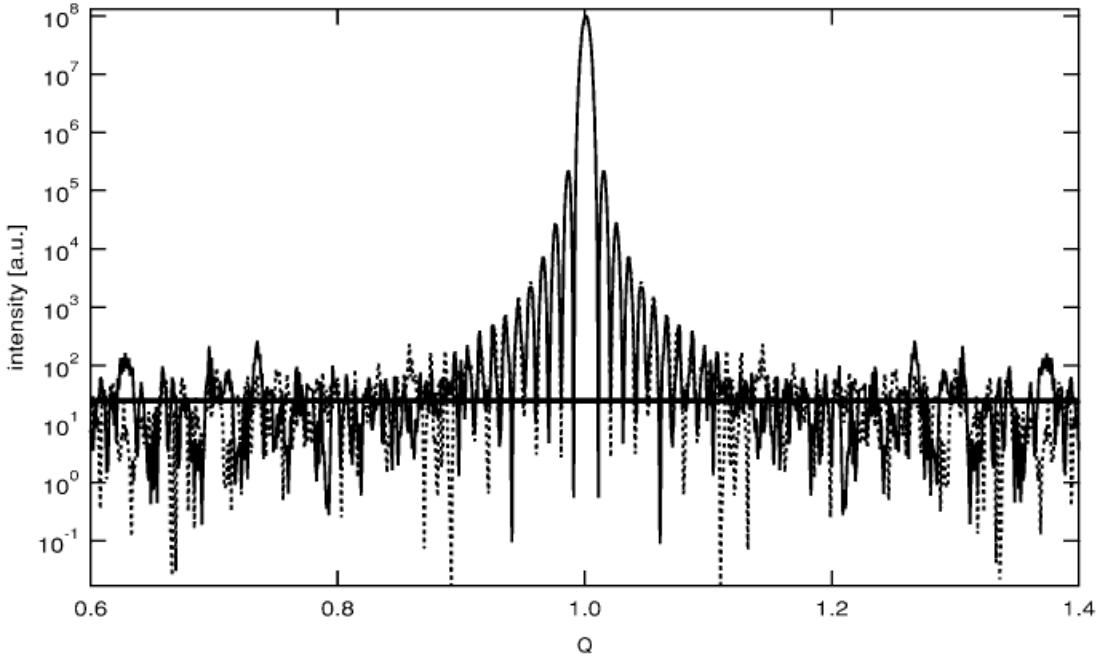

Double pinhole diffraction of white synchrotron radiation

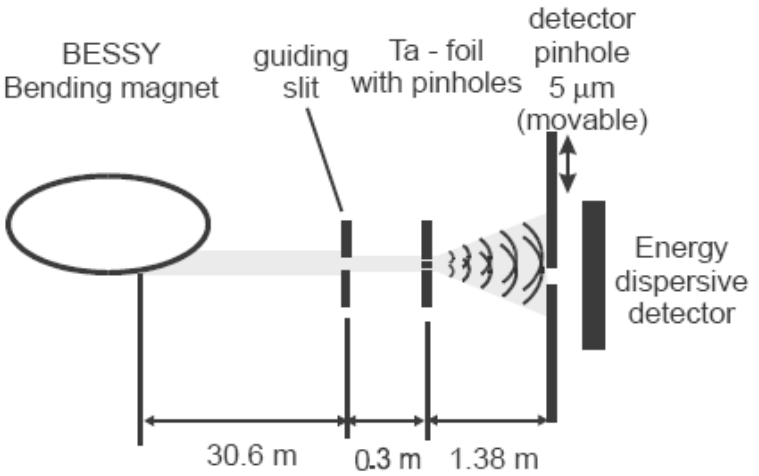

Fig. 1. Experimental set-up at the EDR-beamline at BESSY II.

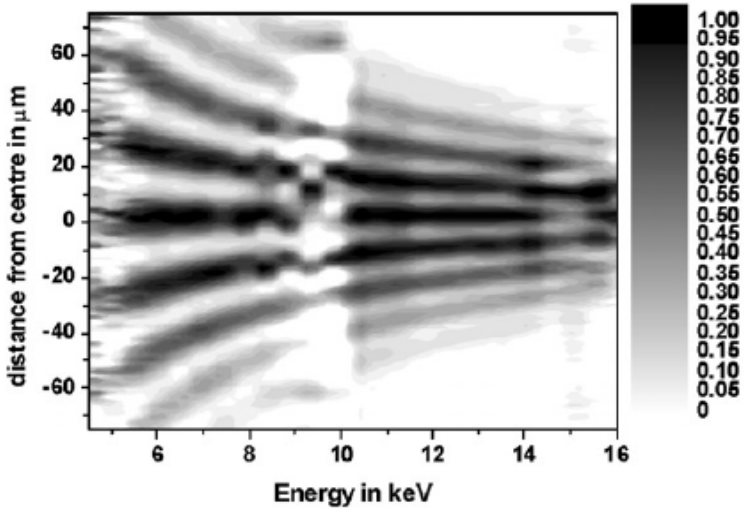

Fig. 3. Normalized diffracted intensity as a function of energy and the distance from the optical axis.

W. Leitenberger et al. / Physica B 336 (2003) 63–67

Double pinhole diffraction of white synchrotron radiation

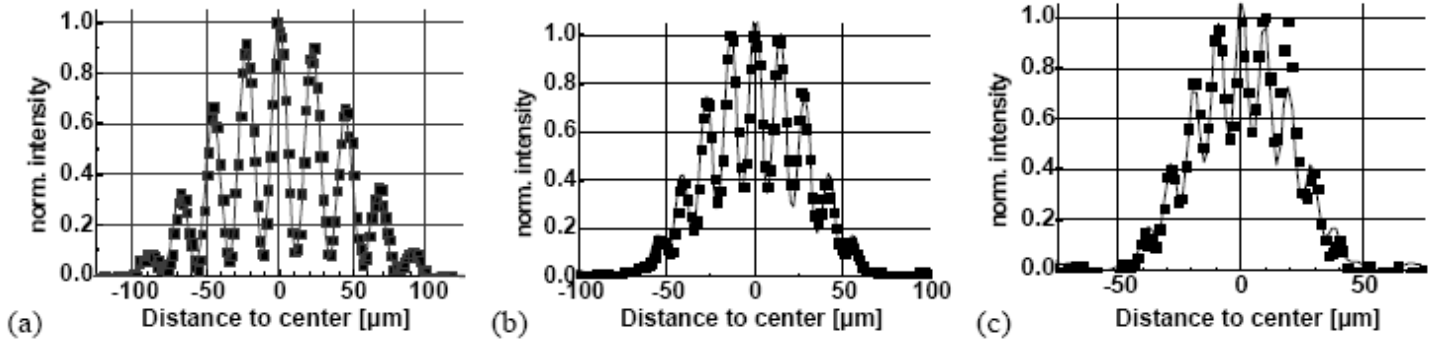

Fig. 4. Normalized interference fringes obtained with the double pinhole at three different energies (a)–(c) 6 keV, 10 keV and 14 keV. The squares indicate the measured data from Fig. 3 and the lines indicate the results of the best fit of Eq. (1).

W. Leitenberger et al. / Physica B 336 (2003) 63–67

Примеры

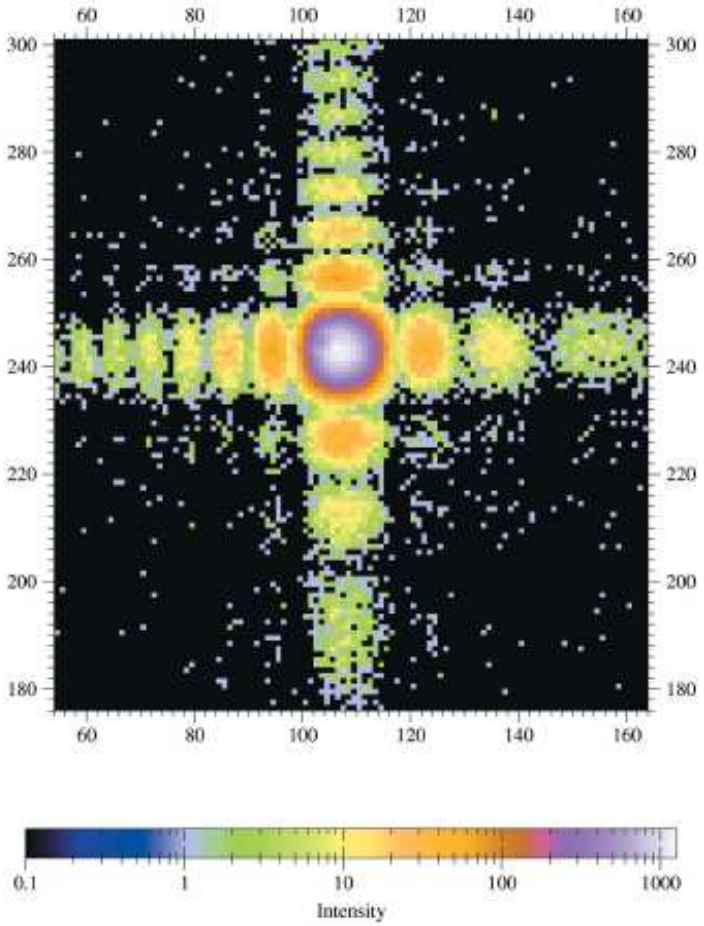

Figure 8
Diffraction from 1 μm asymmetric square slits, $\lambda = 1.58$ Å, detector with 22 μm pixels at 1.25 m. Slit edges are 1 mm distant along the beam path (unpublished results from the BM2 beamline of ESRF).

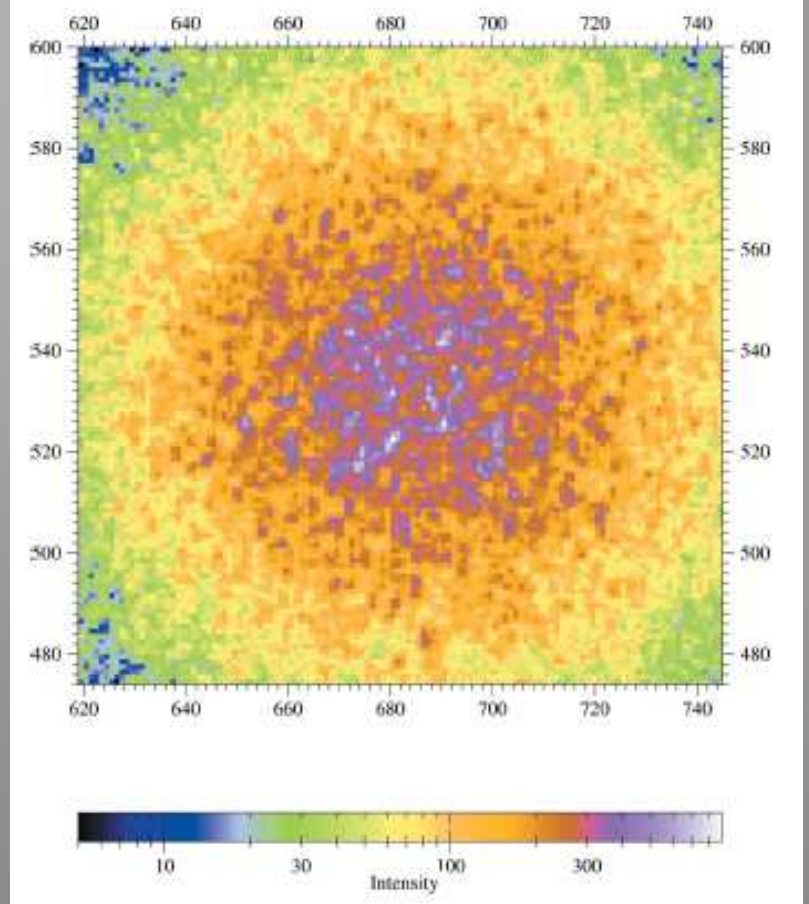

Figure 9
Diffraction from an ordered $AuAgZn_2$ alloy at the $(\frac{111}{222})$ Bragg superstructure position. $\lambda = 1.58$ Å, 12 μm^2 slits, detector with 22 μm pixels at 2 m (unpublished results from the ID10 beamline of ESRF).

Coherent X-ray scattering

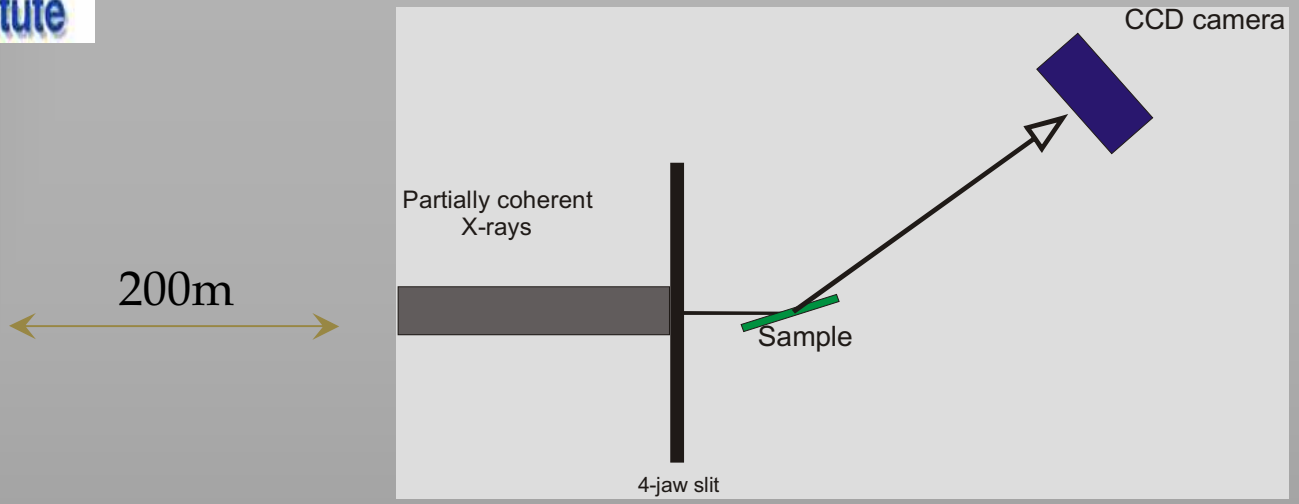

$$\gamma(x) = \frac{\int_{-\infty}^{\infty} \mathcal{T}^*(x'+x)\mathcal{T}(x')dx'}{\int_{-\infty}^{\infty} \mathcal{T}^*(x')\mathcal{T}(x')dx'}.$$

Simplified (Following R.Z.Tai et al., PRL 89,257602 (2002))

$$\gamma(x) = \mathbf{F}(I(q)) / \mathbf{F}(I_{sp}(q))$$

Diffraction image from perfect crystal and its FFT

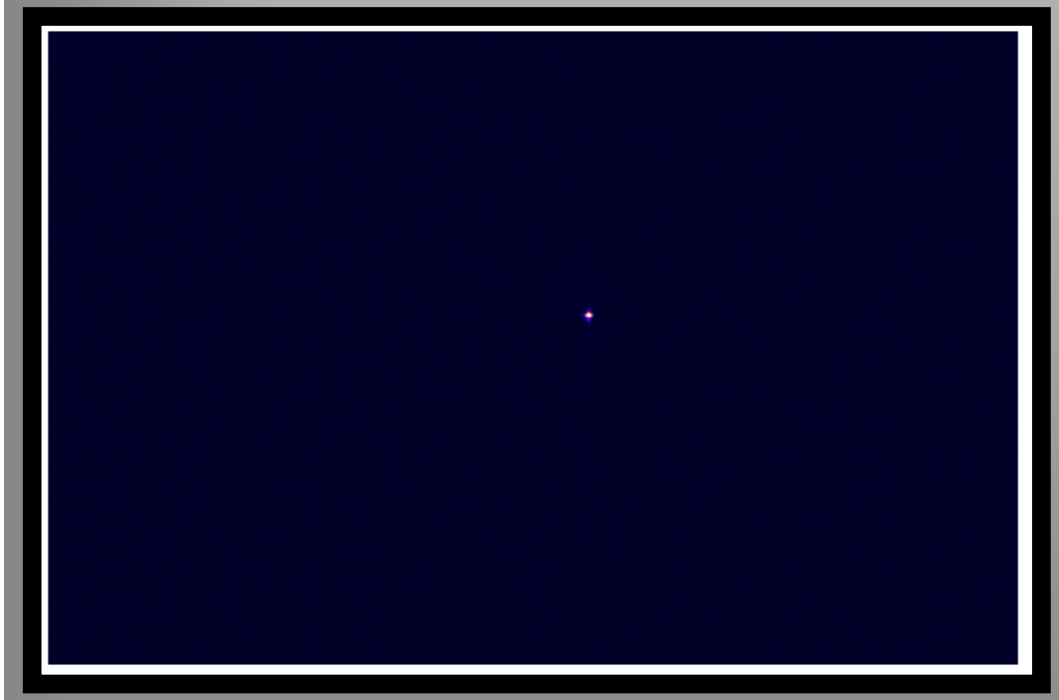

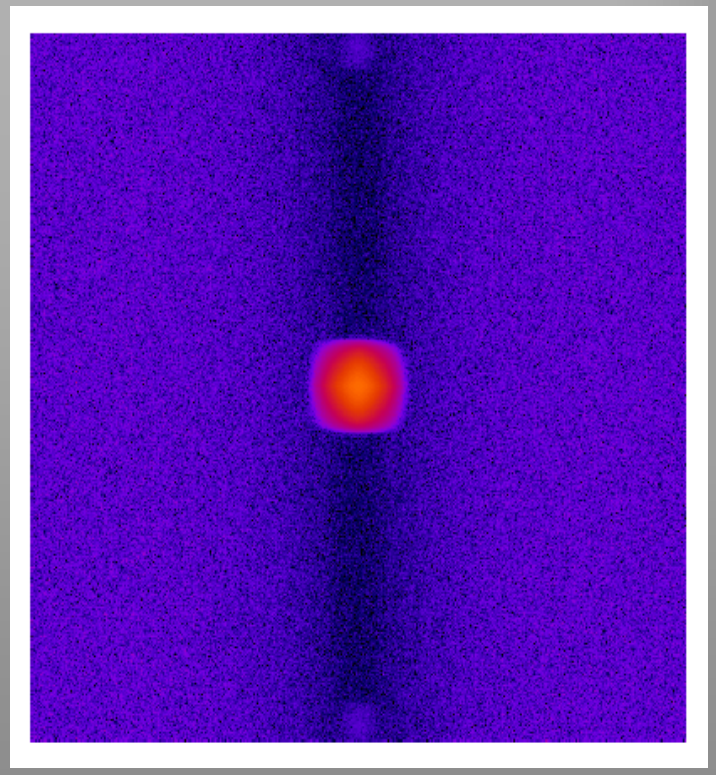

Геометрия рассеяния

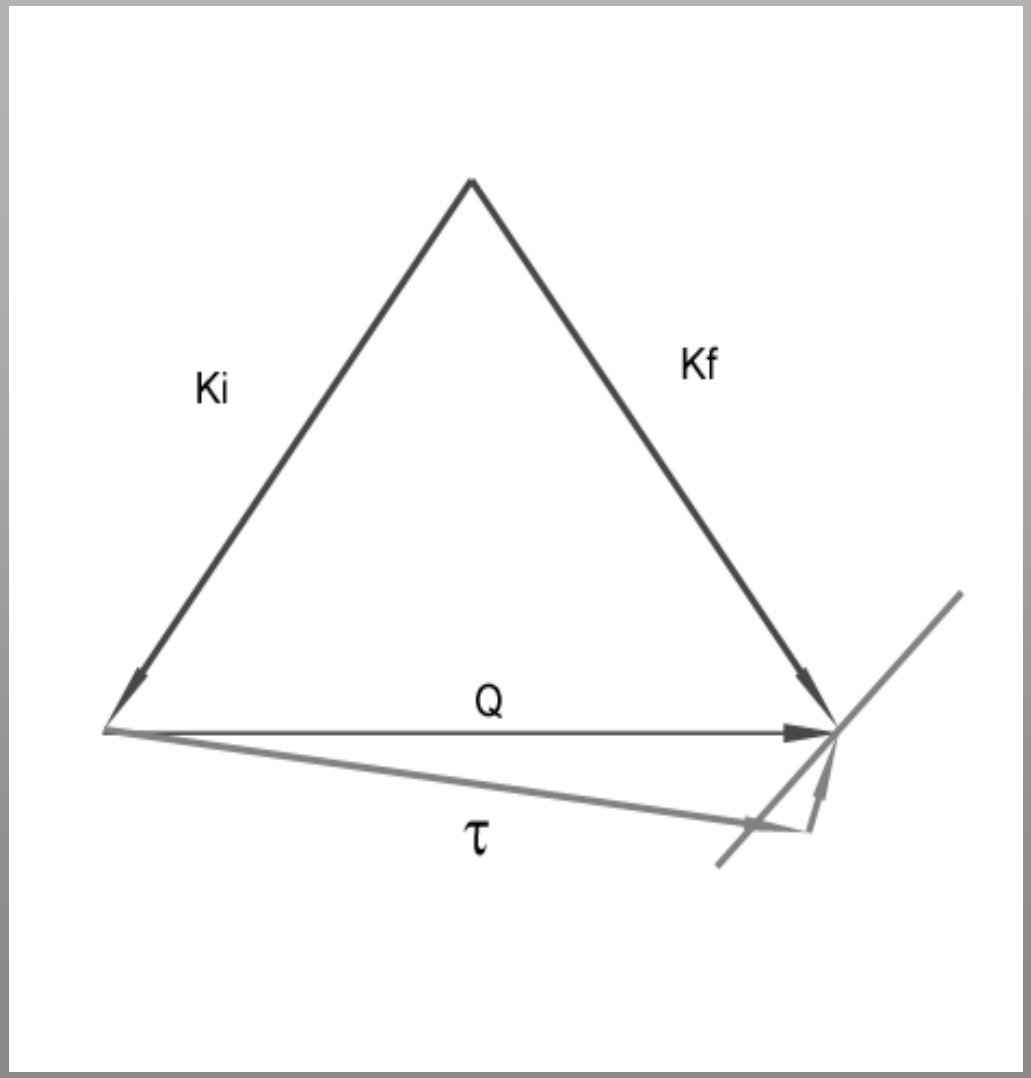

Бреговское рассеяние
370 K

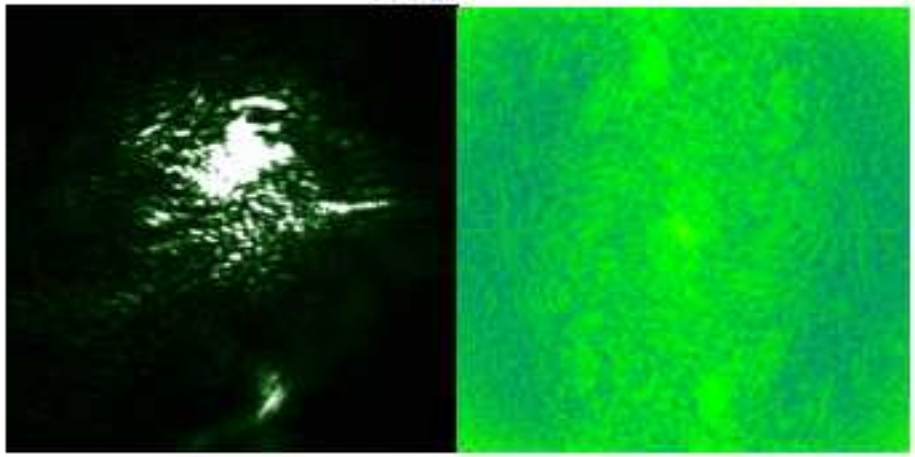

0°

-15°

Бреговское рассеяние
300 K

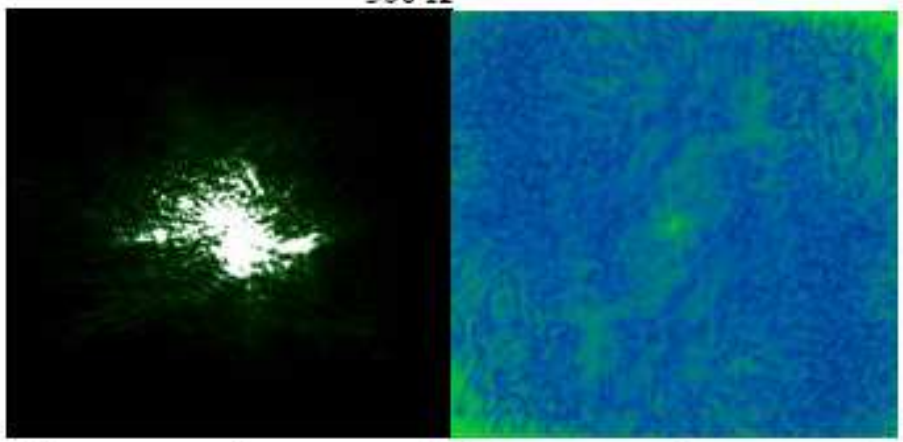

0°

10°

Ioffe Physico-Technical Institute

Бреговское рассеяние
250 K

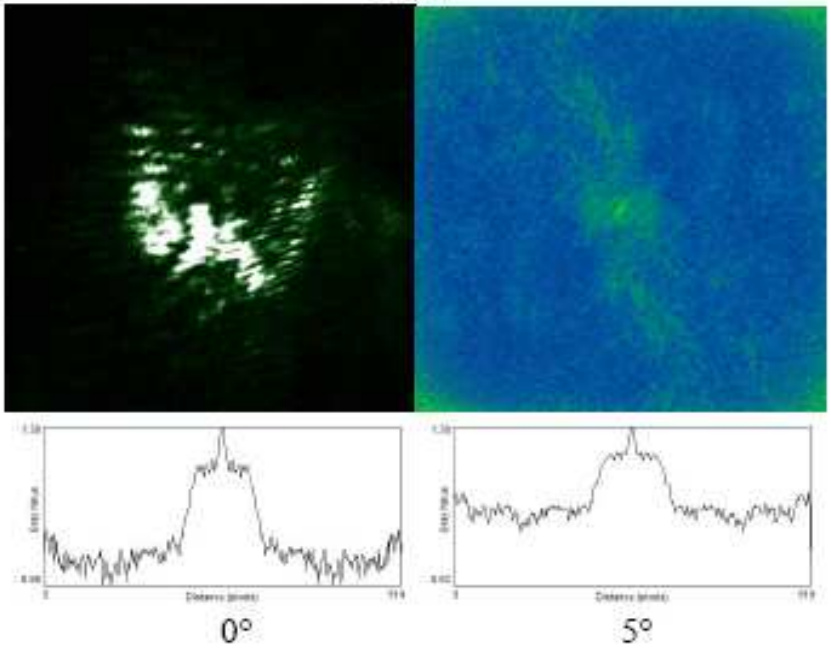

0°

5°

Бреговское рассеяние
230 K

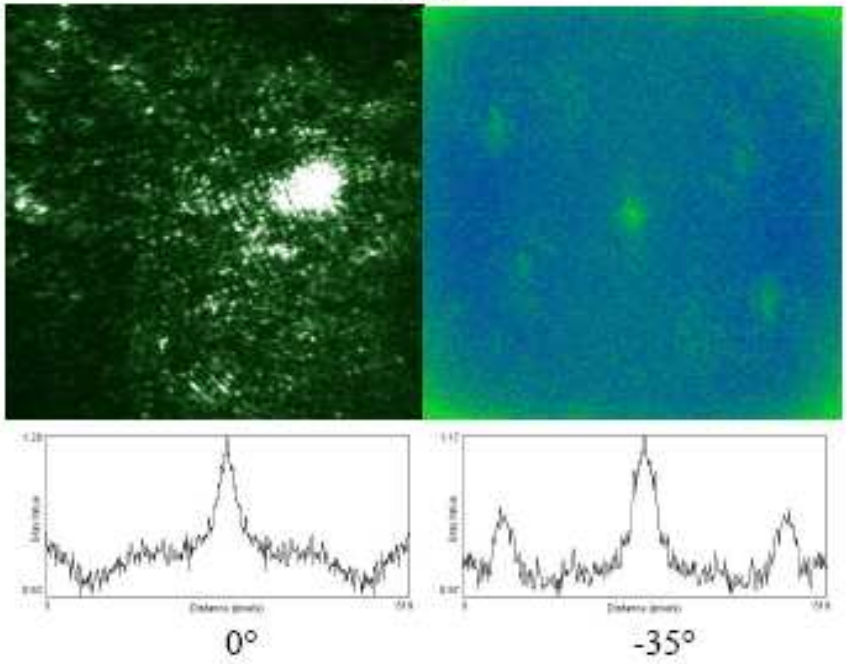

0°

-35°

Ioffe Physico-Technical Institute

Береговское рассеяние

200 К

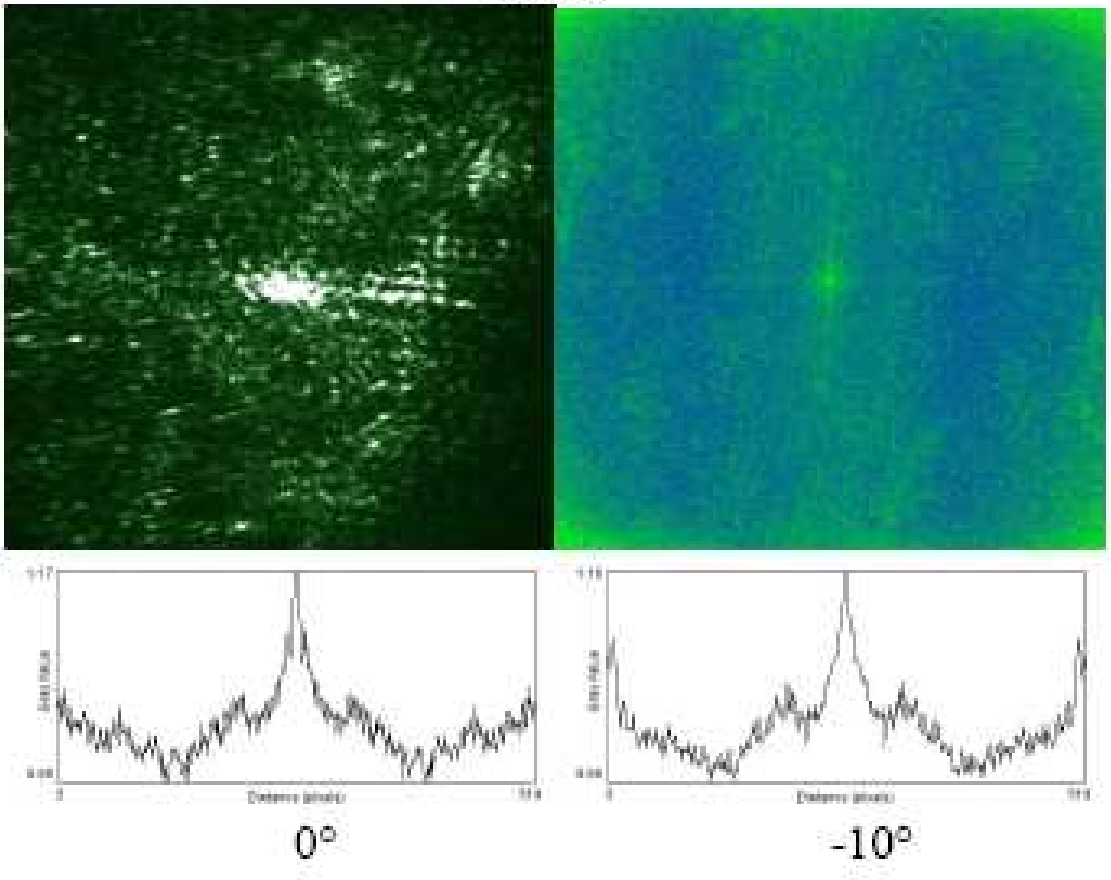

0°

-10°

Ioffe Physico-Technical Institute

Диффузное рассеяние
370 K

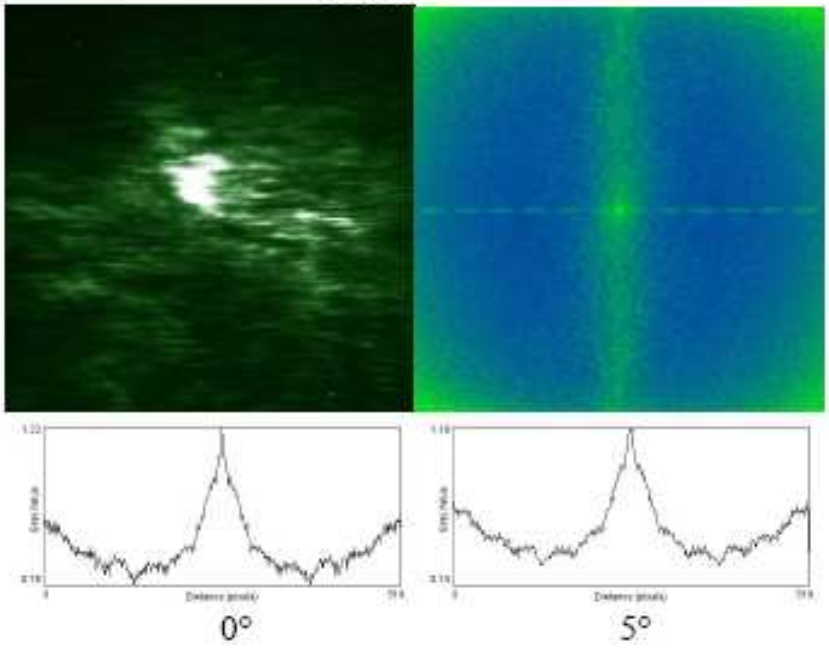

0°

5°

Диффузное рассеяние
320 K

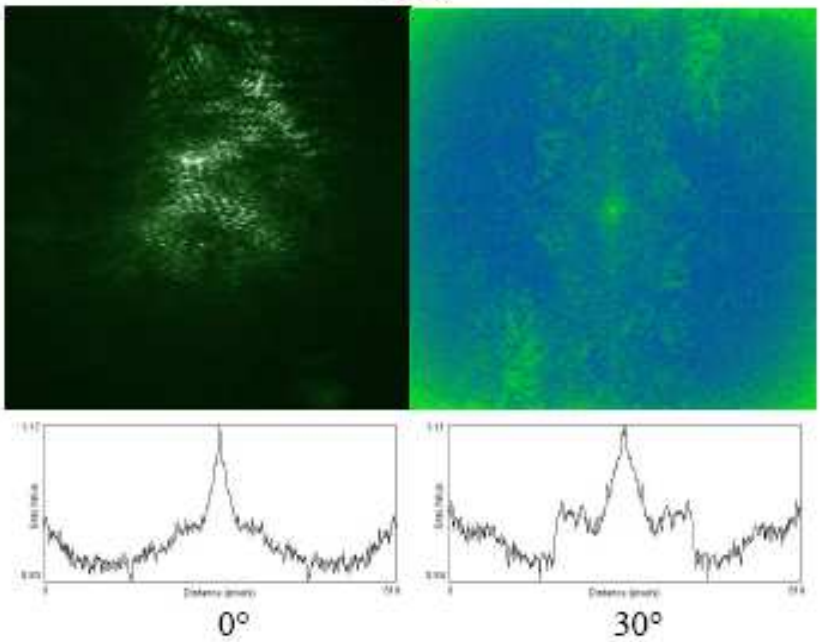

0°

30°

Ioffe Physico-Technical Institute

Диффузное рассеяние
270 K

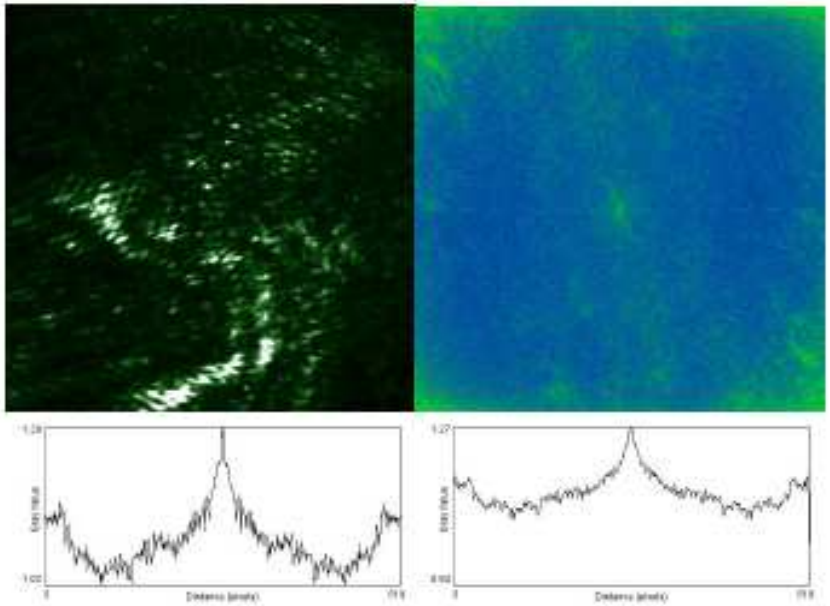

0°

5°

Диффузное рассеяние
250 K

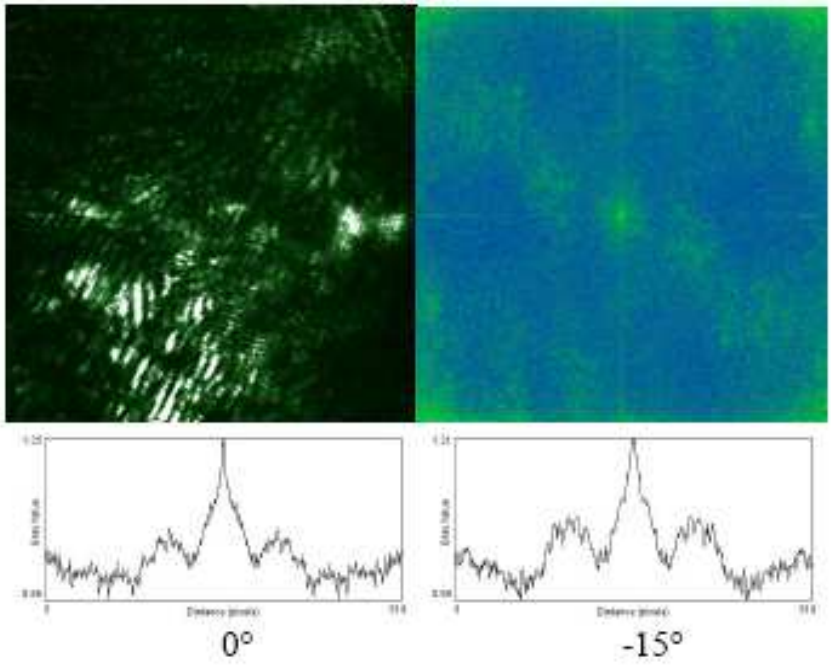

0°

-15°

SBN61 480K брэгговский пик

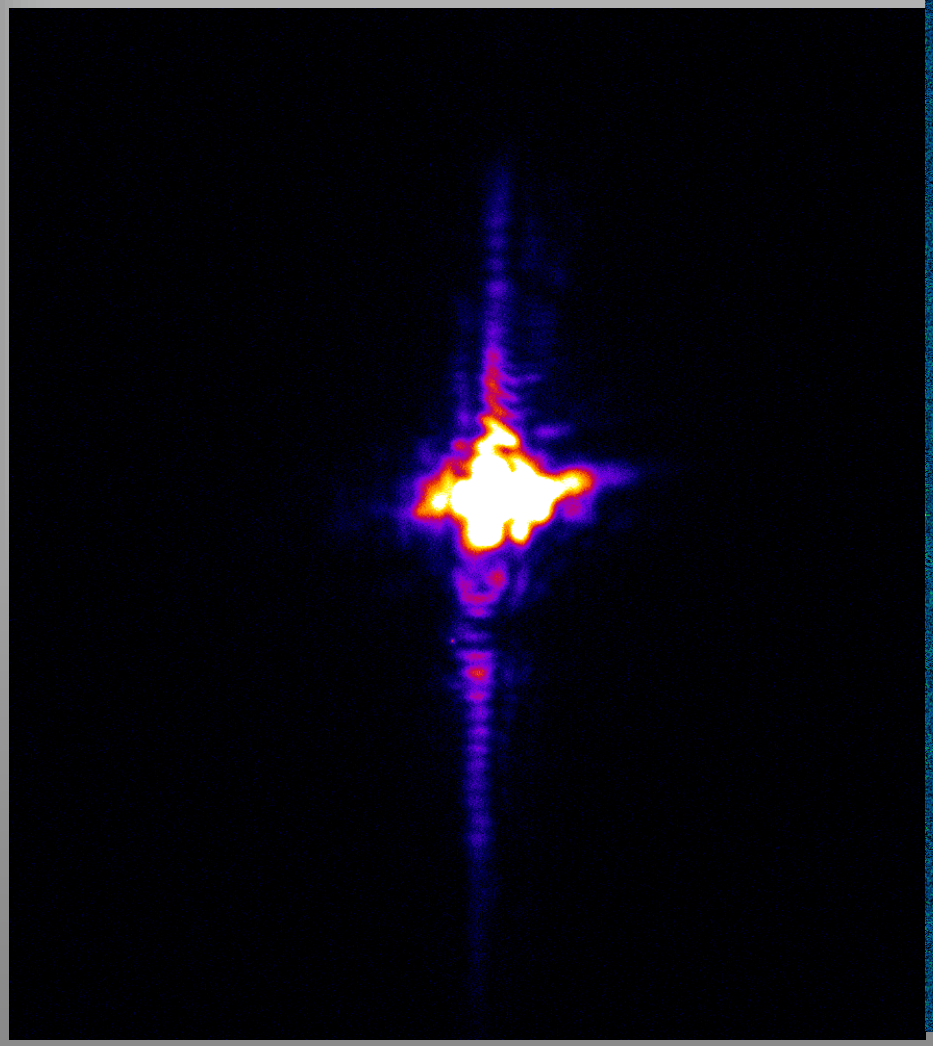

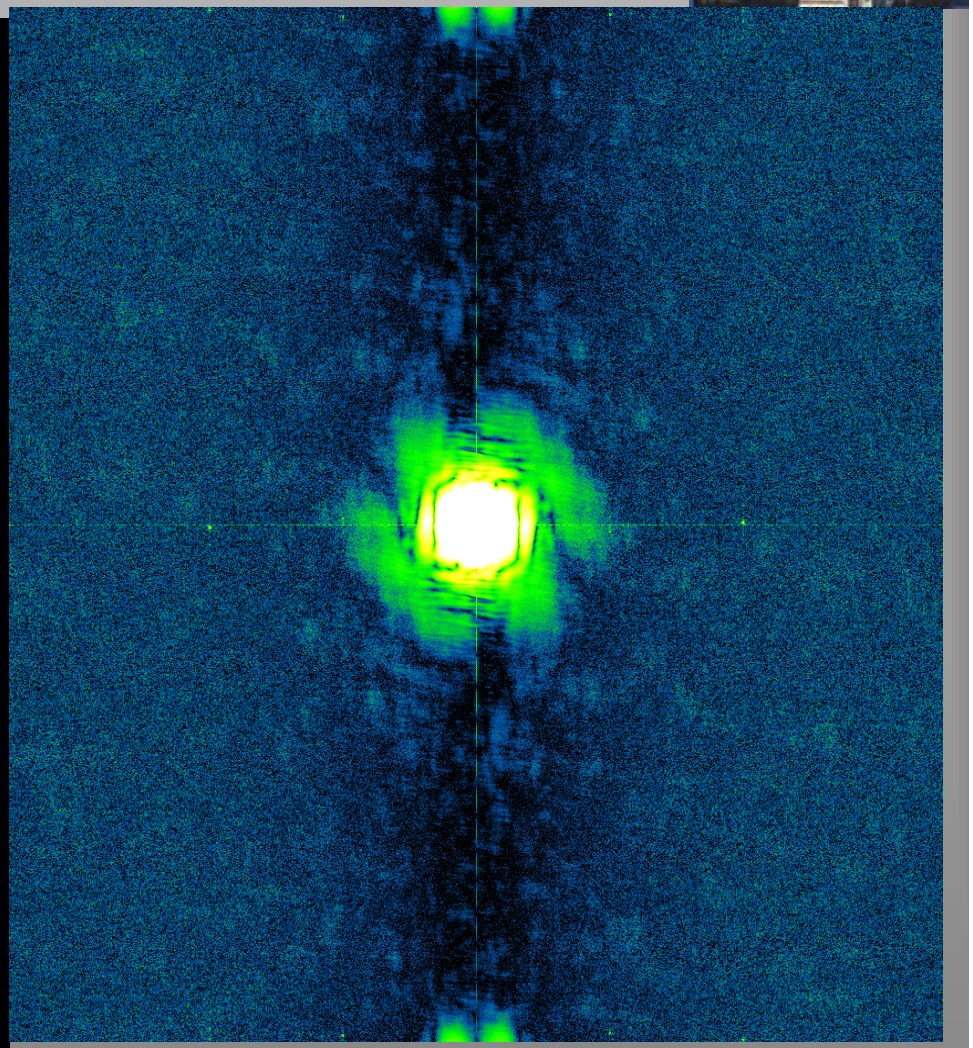

Дифракция на щели в вертикальном направлении

Фурье образ

230 K diffuse

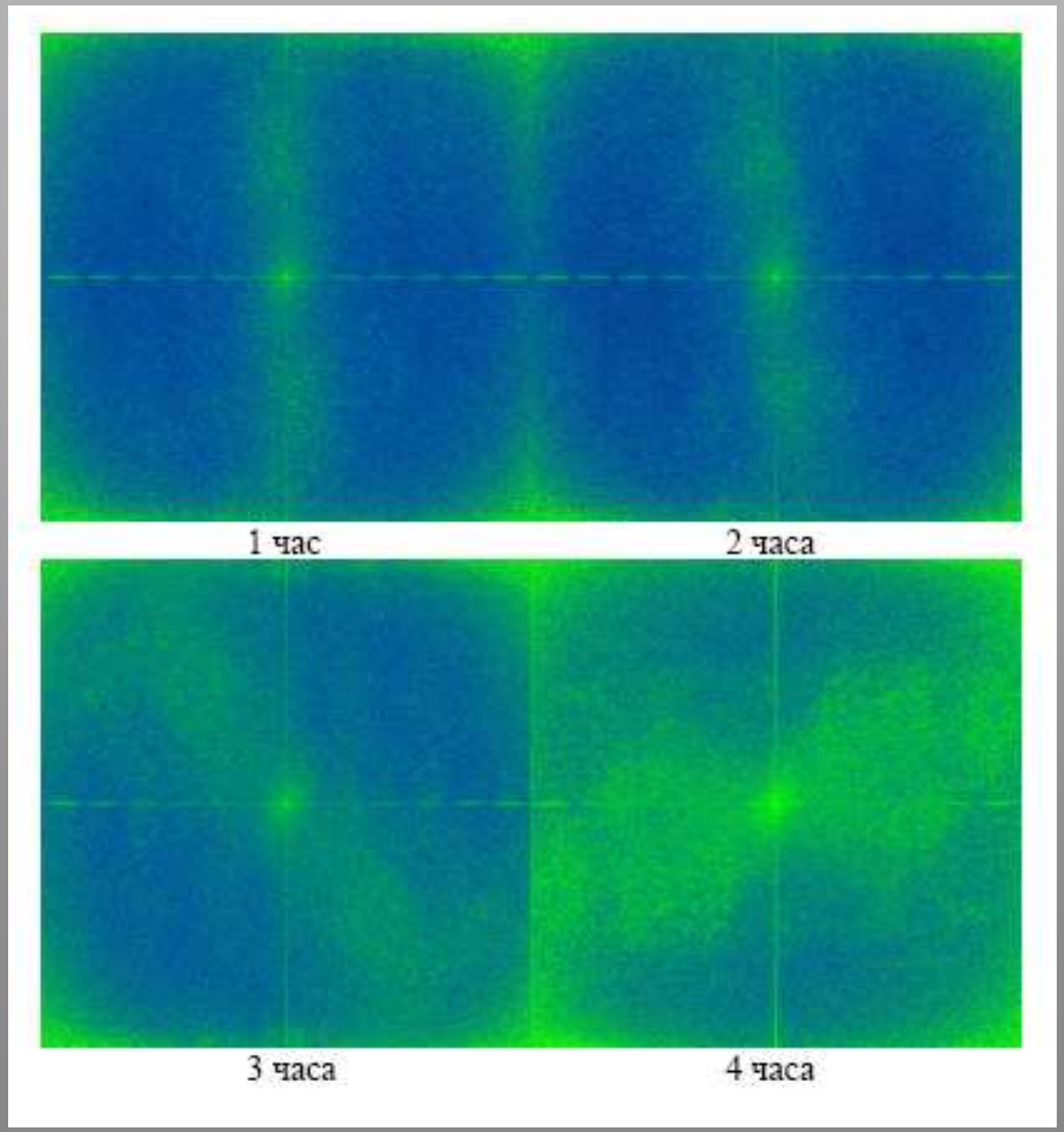

230K diffuse

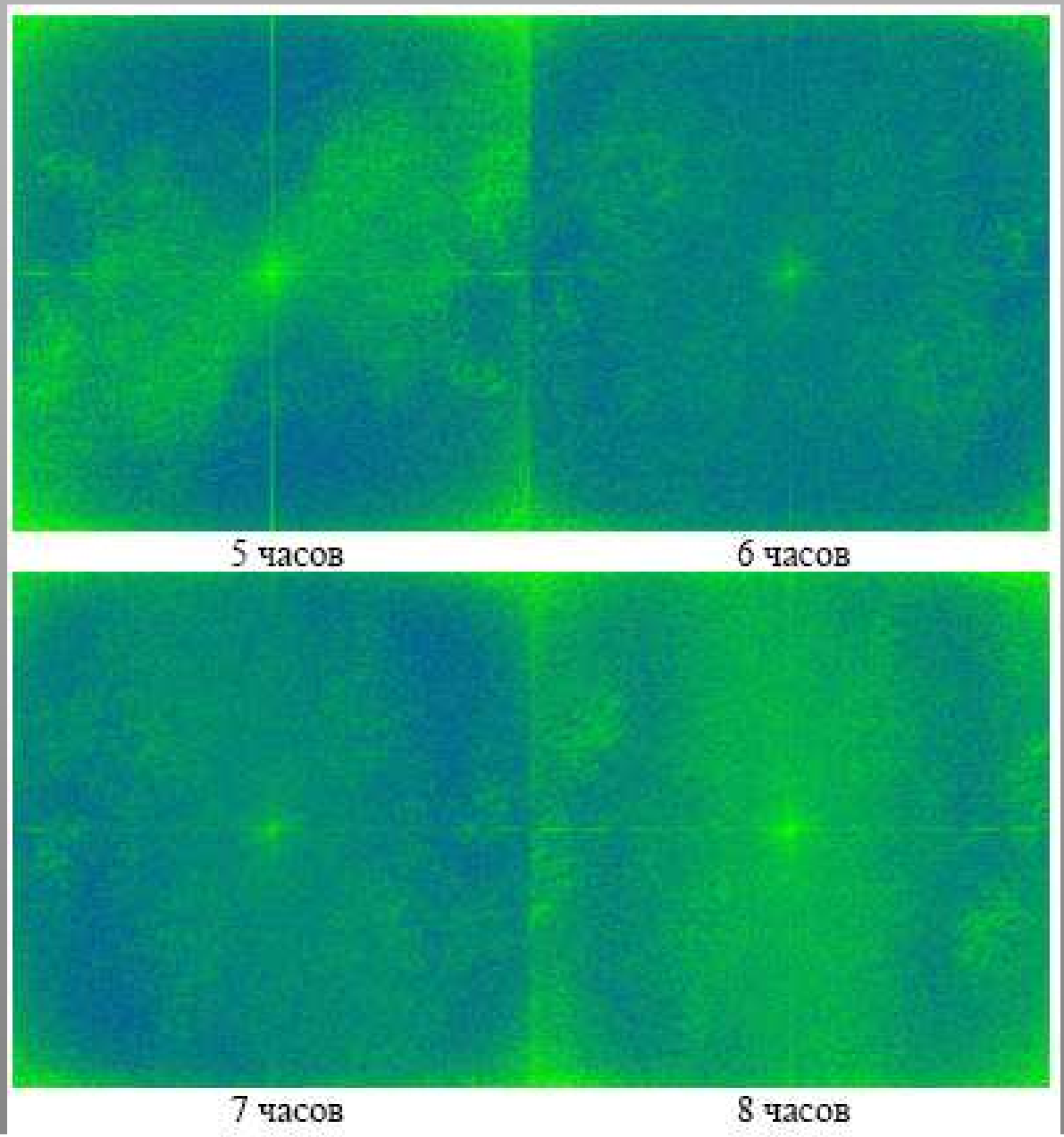

Bragg diffraction image 200K

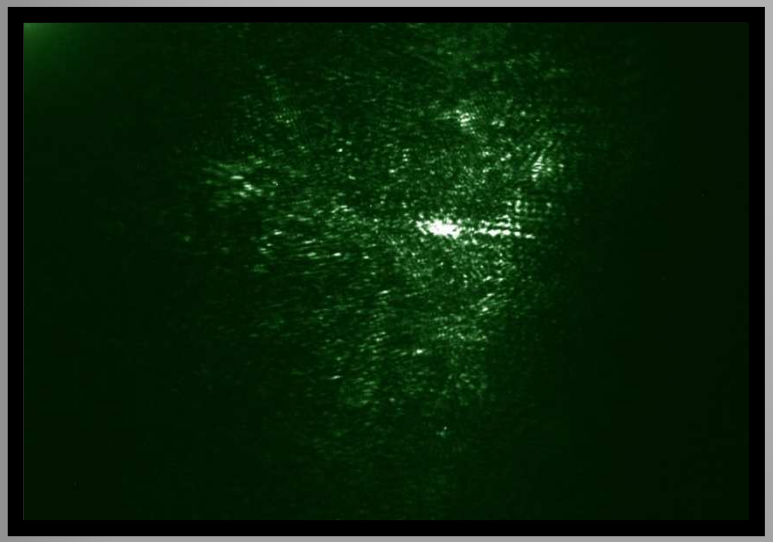

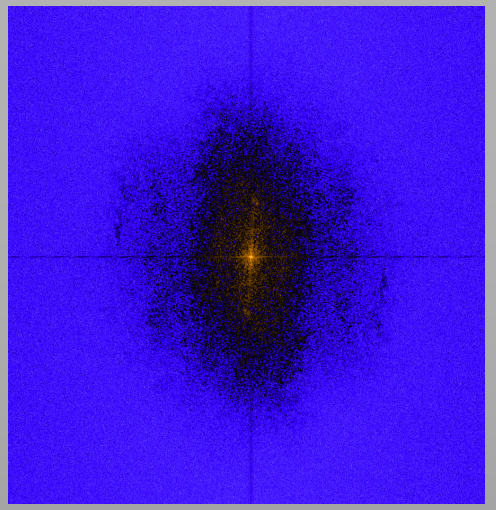

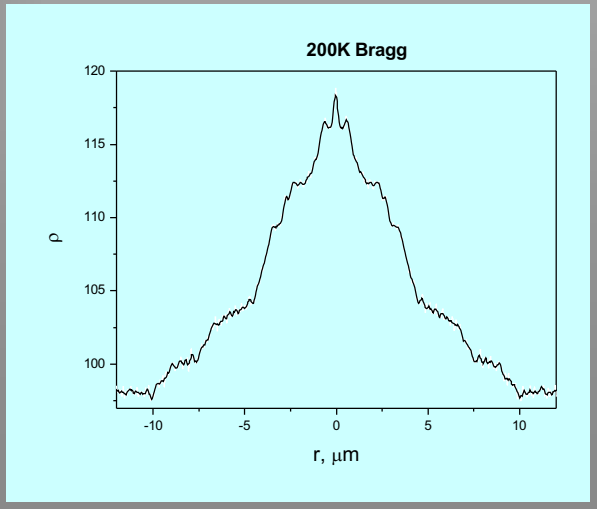

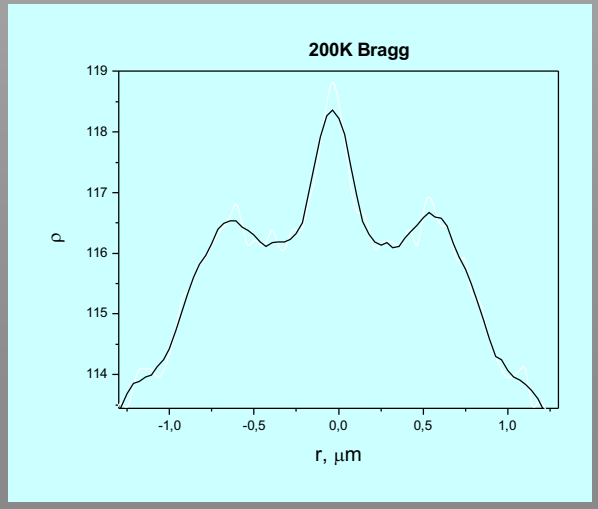

Ioffe Physico-Technical Institute

XPCS
Рентгеновская фотонная корреляционная спектроскопия

$$1 + \beta(q) g^{(2)}(q, t) = \langle\langle I(\mathbf{q}, t') I(\mathbf{q}, t + t')\rangle_{t'}\rangle_{\mathbf{q}} / \langle\langle I(\mathbf{q}, t')\rangle_{t'}^2\rangle_{\mathbf{q}},$$

Ioffe Physico-Technical Institute

Slices position

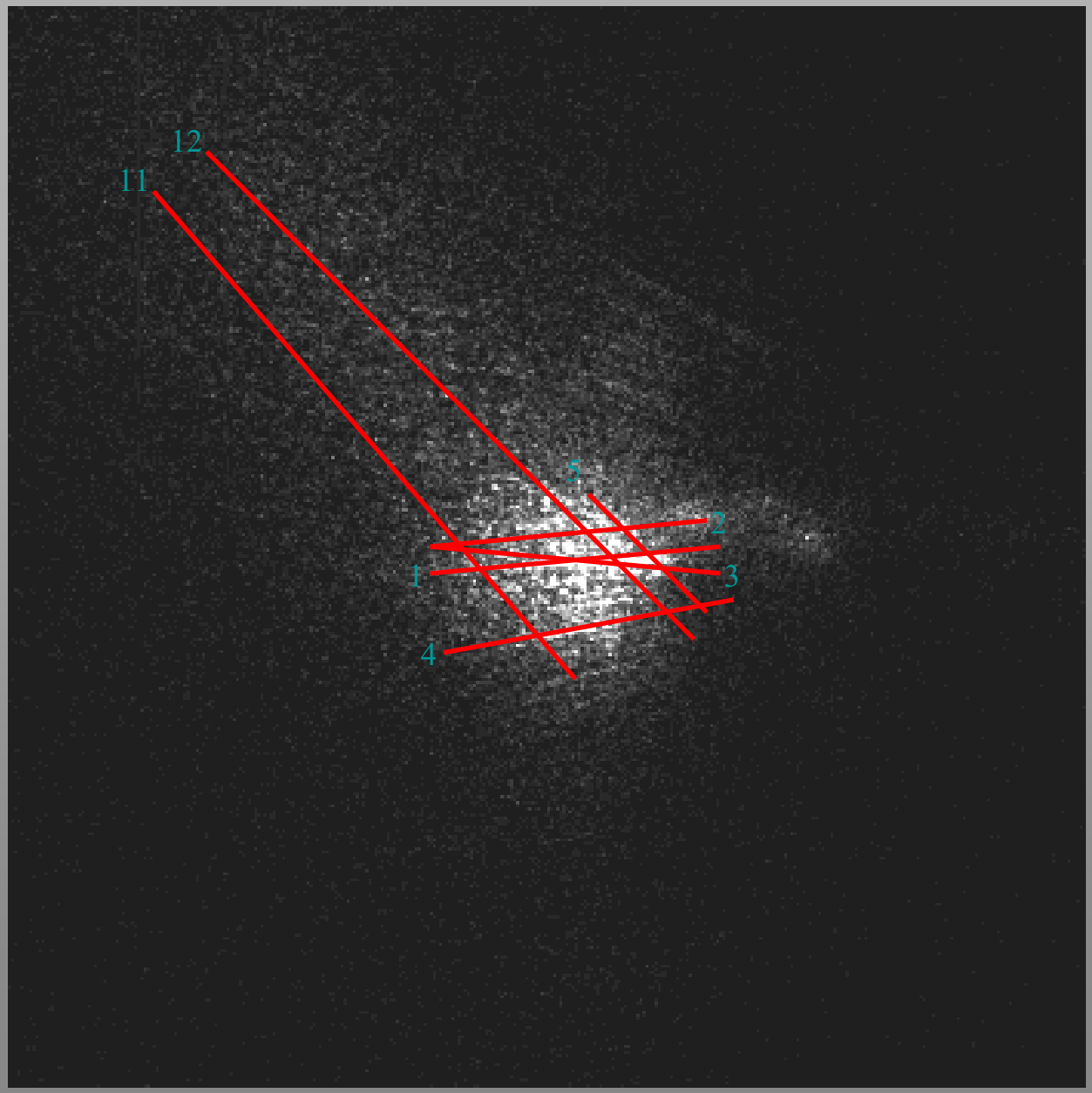

360K

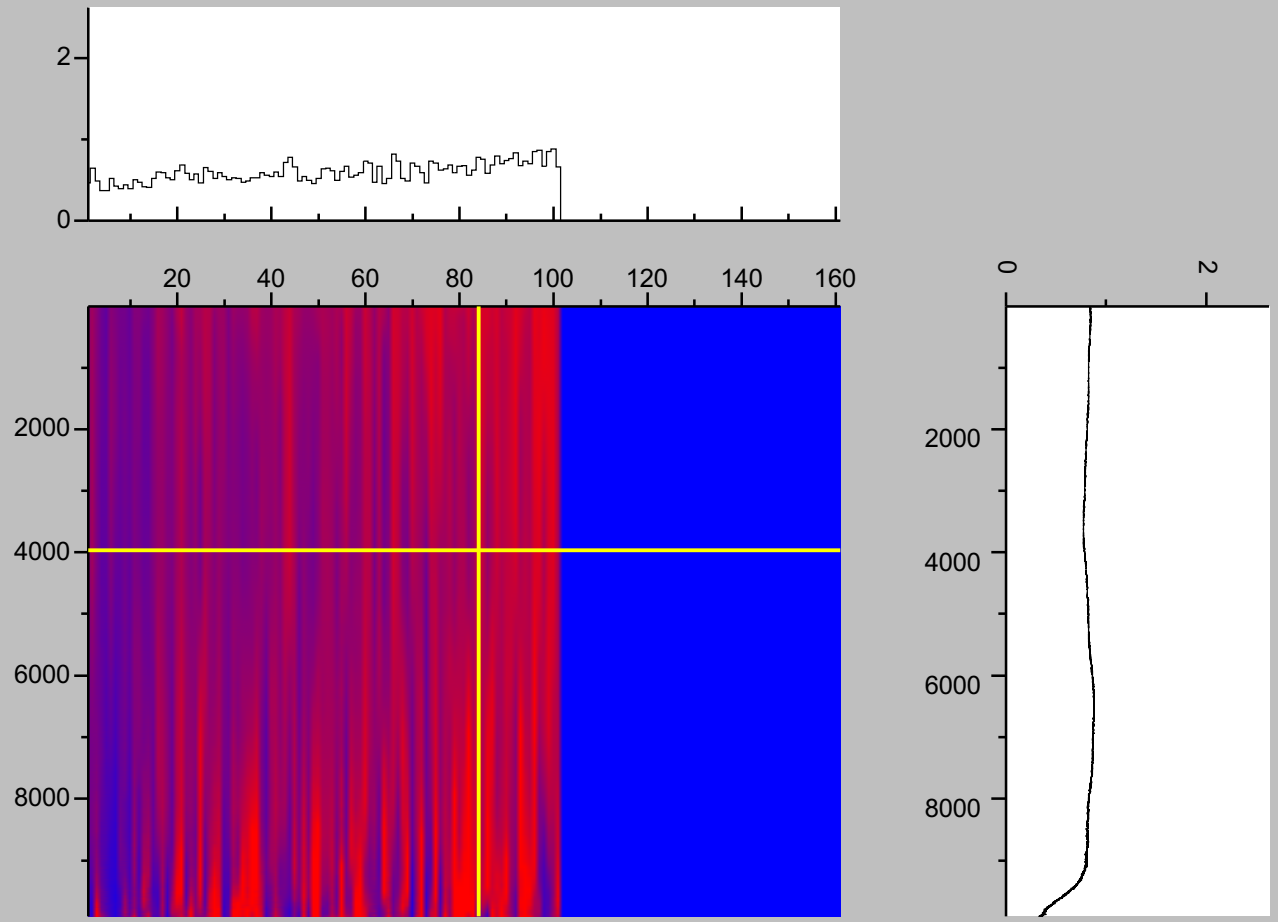
2
0
20
40
60
80
100
120
140
160
2000
4000
6000
8000
0
2
2000
4000
6000
8000

340K

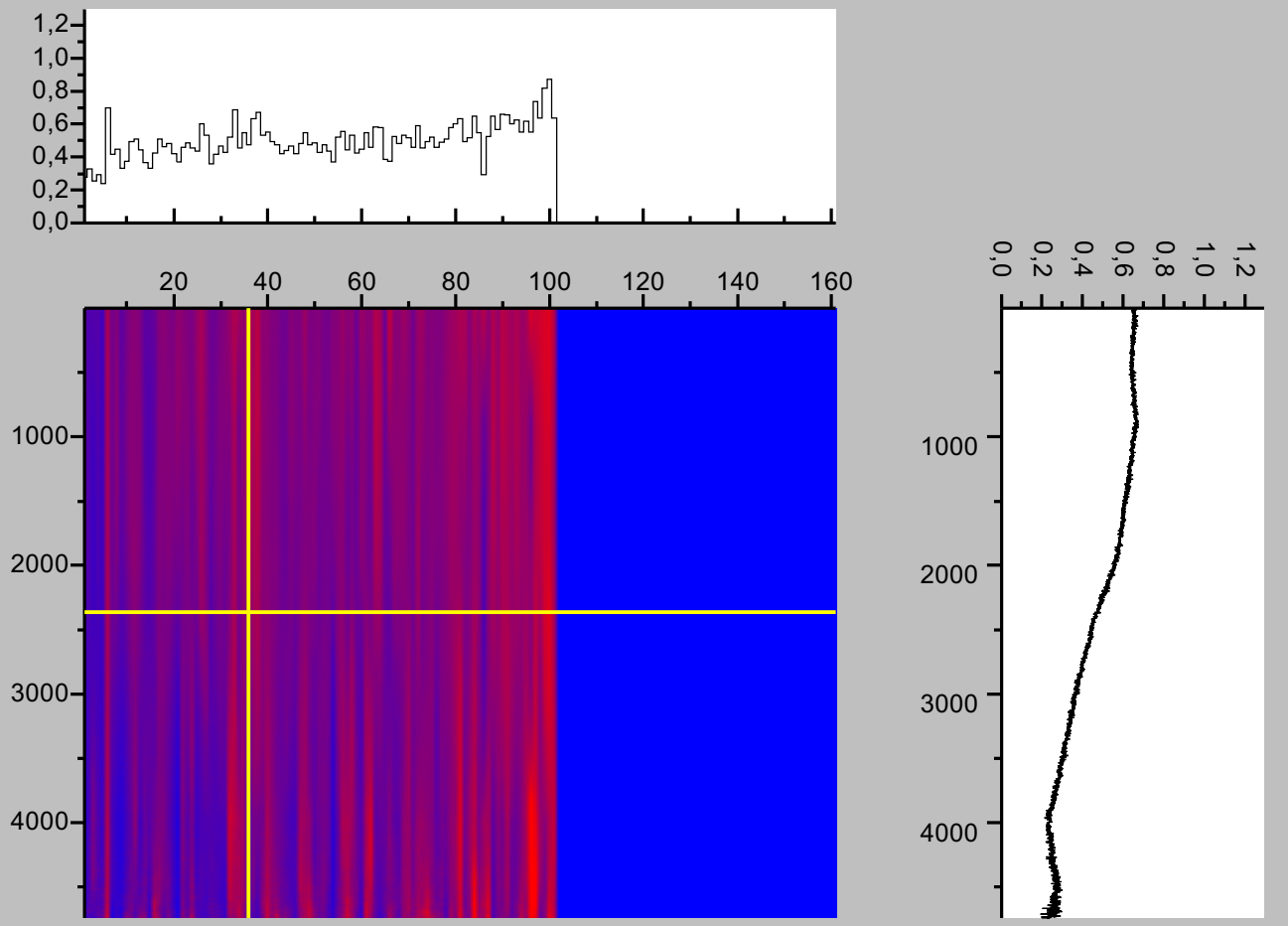
1,2
1,0
0,8
0,6
0,4
0,2
0,0
20
40
60
80
100
120
140
160
1000
2000
3000
4000
0,0
0,2
0,4
0,6
0,8
1,0
1,2
1000
2000
3000
4000

Ioffe Physico-Technical Institute

PMNPT10 XPCS 210K

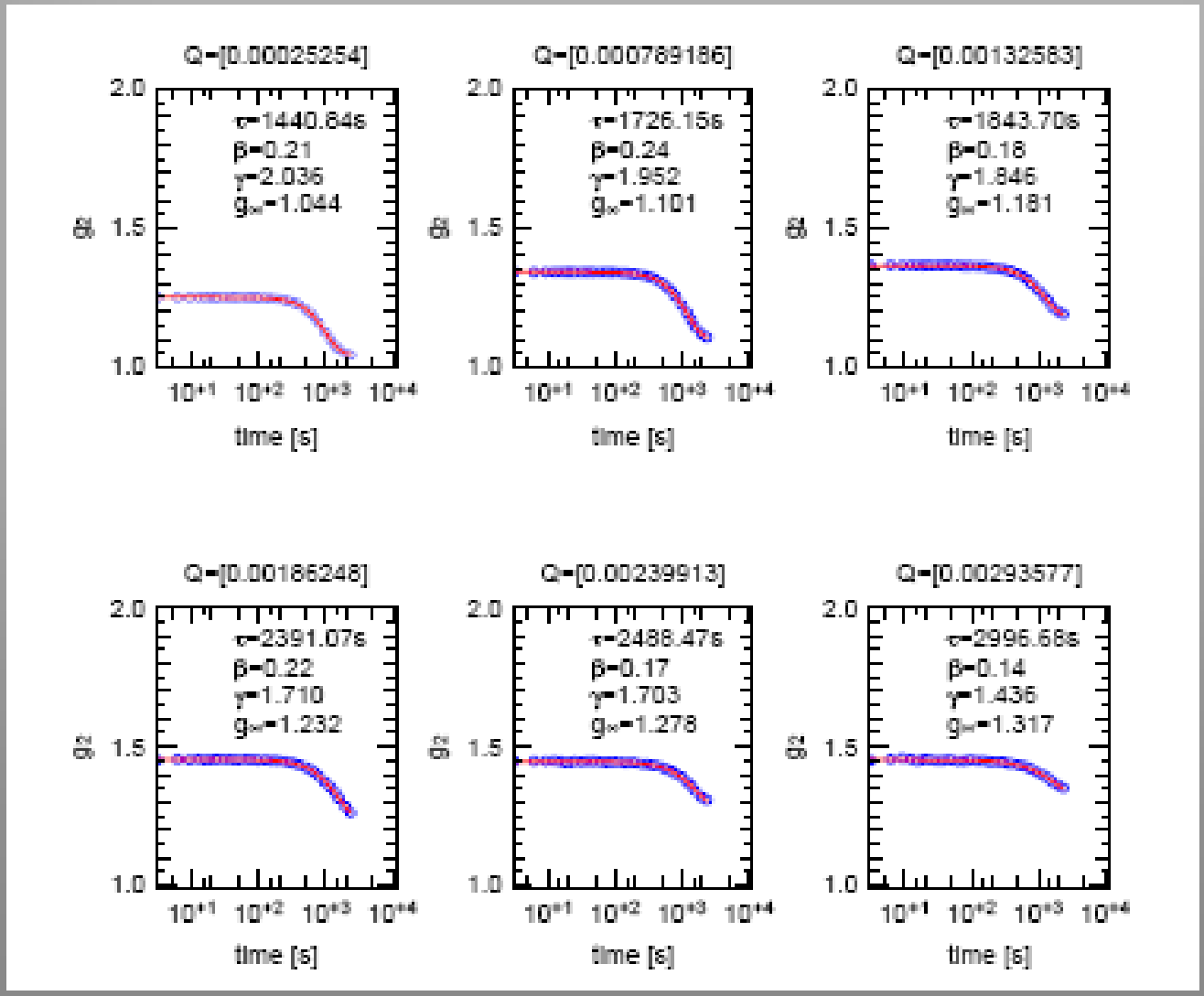

Вода

Нейтроны - диффузия

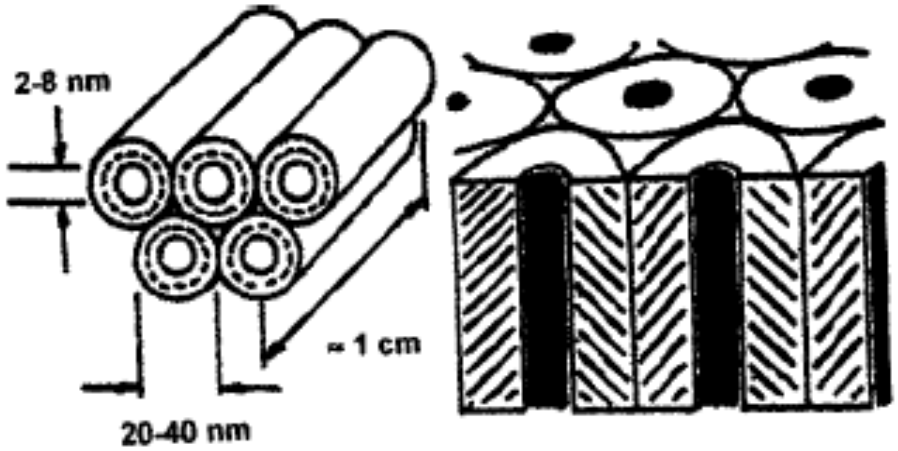

FIG. 1. A schematic picture of a bundle of chrysotile asbestos fibers.

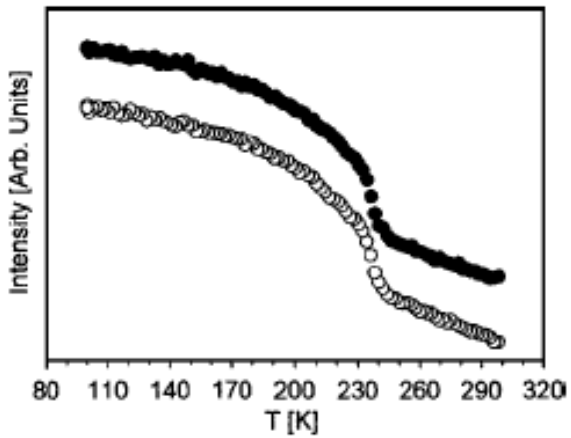

FIG. 2. The elastic scattering intensity measured in the fixed-window mode as a function of temperature and summed up over all Q values. Open circles: "Q-parallel" orientation. Filled circles: "Q-perpendicular" orientation. An arbitrary vertical offset of the baselines is applied for clarity. The increase in the elastic scattering at about T=237 K is due to the freezing of water in the fibers.

Замедление динамики больше чем на порядок

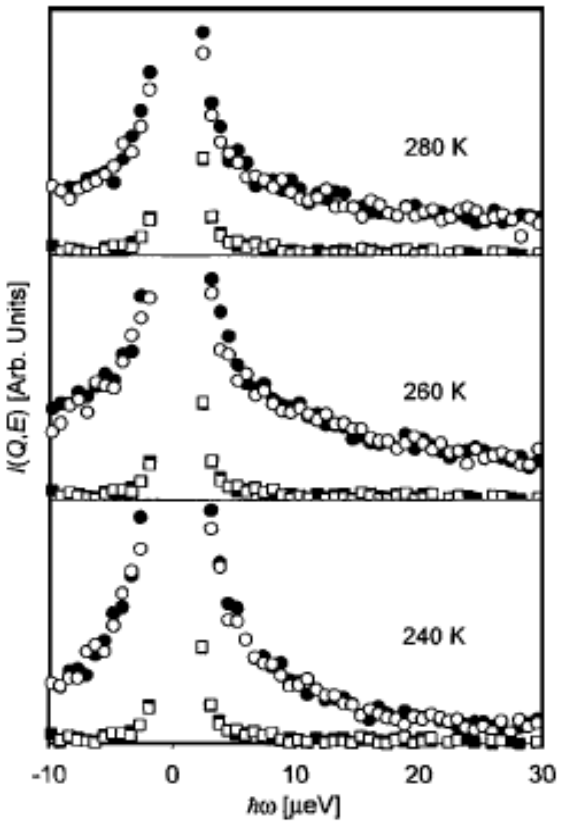

FIG. 3. The scattering intensities measured in the energy space at the 90° detector (Q=1.42 Å^{-1}). The elastic peaks at zero energy transfer are truncated to better demonstrate the quasielastic signal. The 100 K data used as a resolution function are plotted on every graph and shown with squares. Open symbols: "Q-parallel" orientation. Filled symbols: "Q-perpendicular" orientation.

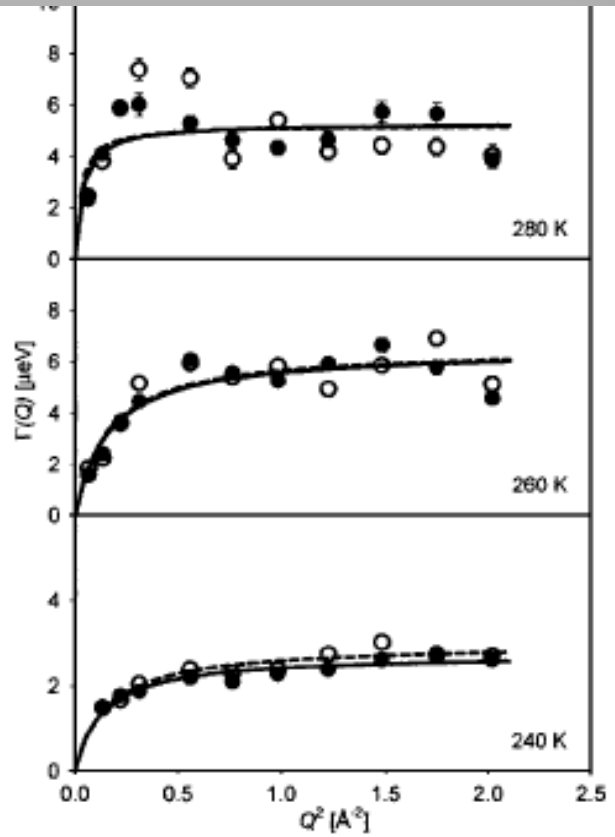

FIG. 4. The Q dependence of the parameter $\Gamma(Q)$ obtained from fitting the data using Eqs. (1) and (2) and its fit with Eq. (3). Open circle data points and dashed line fitting curves: "Q-parallel" orientation. Filled circle data points and solid line fitting curves: "Q-perpendicular" orientation.

Дифракция СИ в асбесте

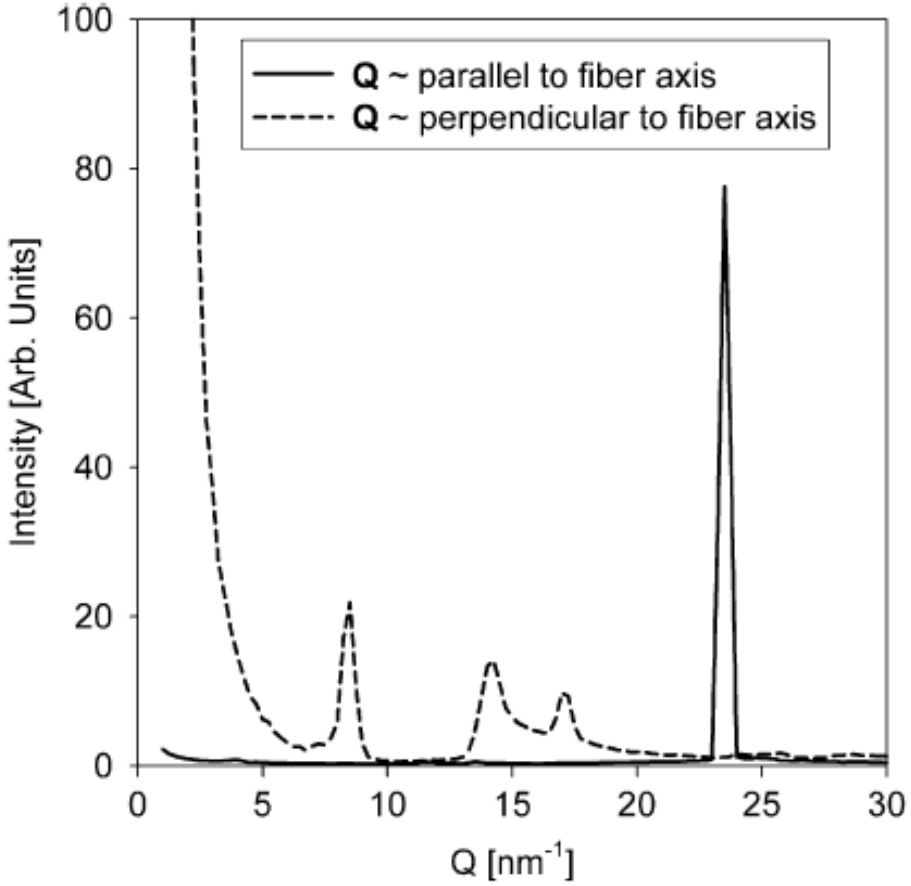

Fig. 2. Diffraction patterns measured with the scattering vector aligned nearly parallel and perpendicular to the long axis of the chrysotile asbestos fiber.

Неупругое рассеяние СИ

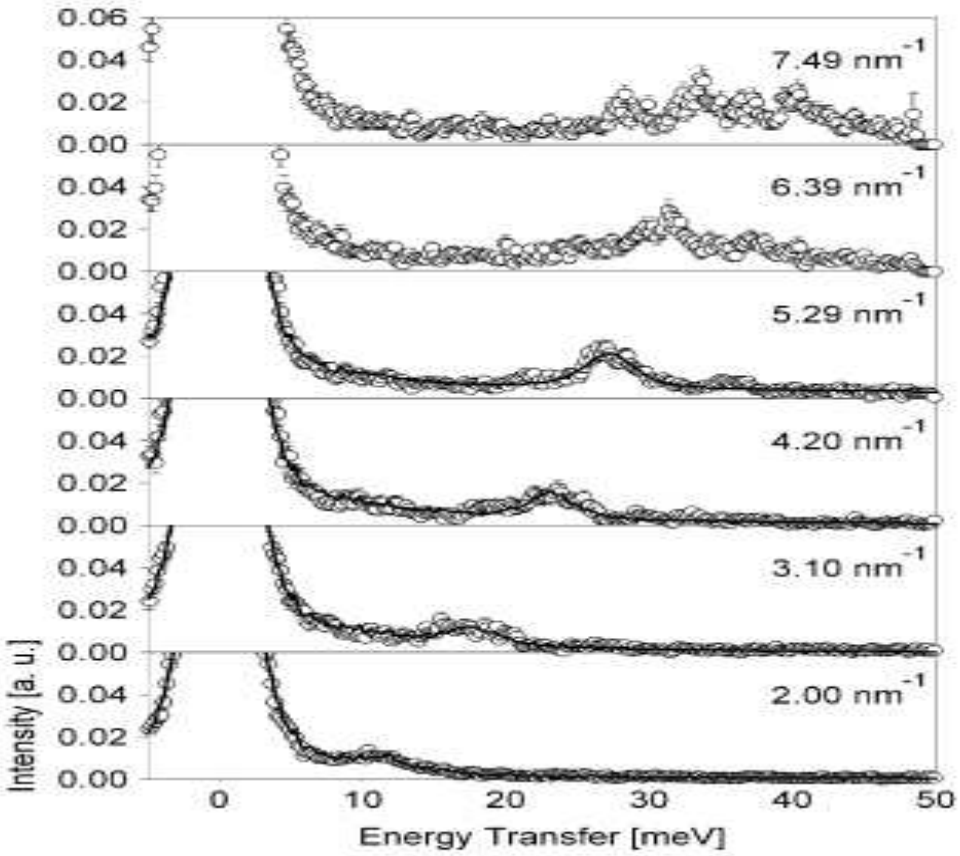

Fig. 3. Symbols: Inelastic x-ray scattering spectra measured with the scattering vector aligned along [1 0 0] direction of the reciprocal lattice (that is, nearly parallel to the long axis of the chrysotile asbestos fiber, which coincides with [1 0 0] direction of the direct lattice). Lines: Fits with Eqs. (1) and (2) (for the four lowest Q values). The spectra are normalized to have the same height of the elastic peak at all Q values.

IN1 вода в асбесте

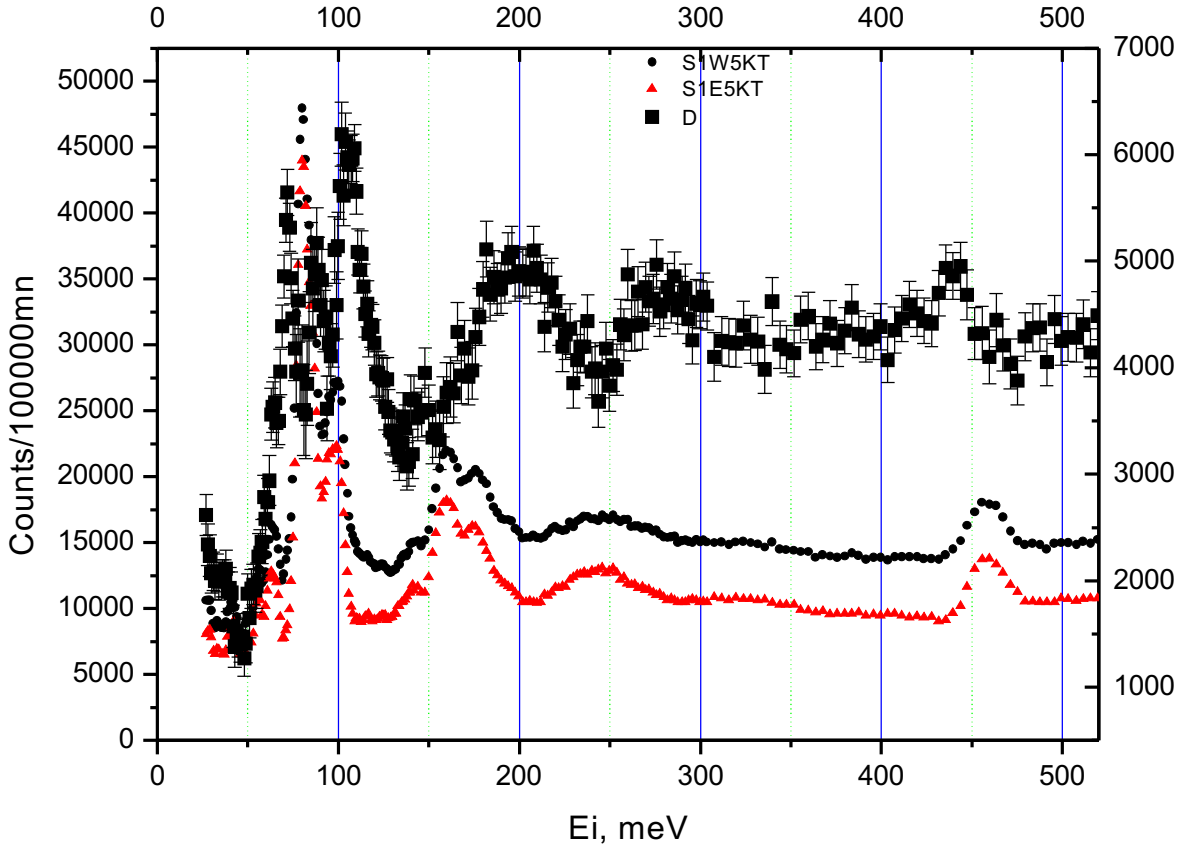

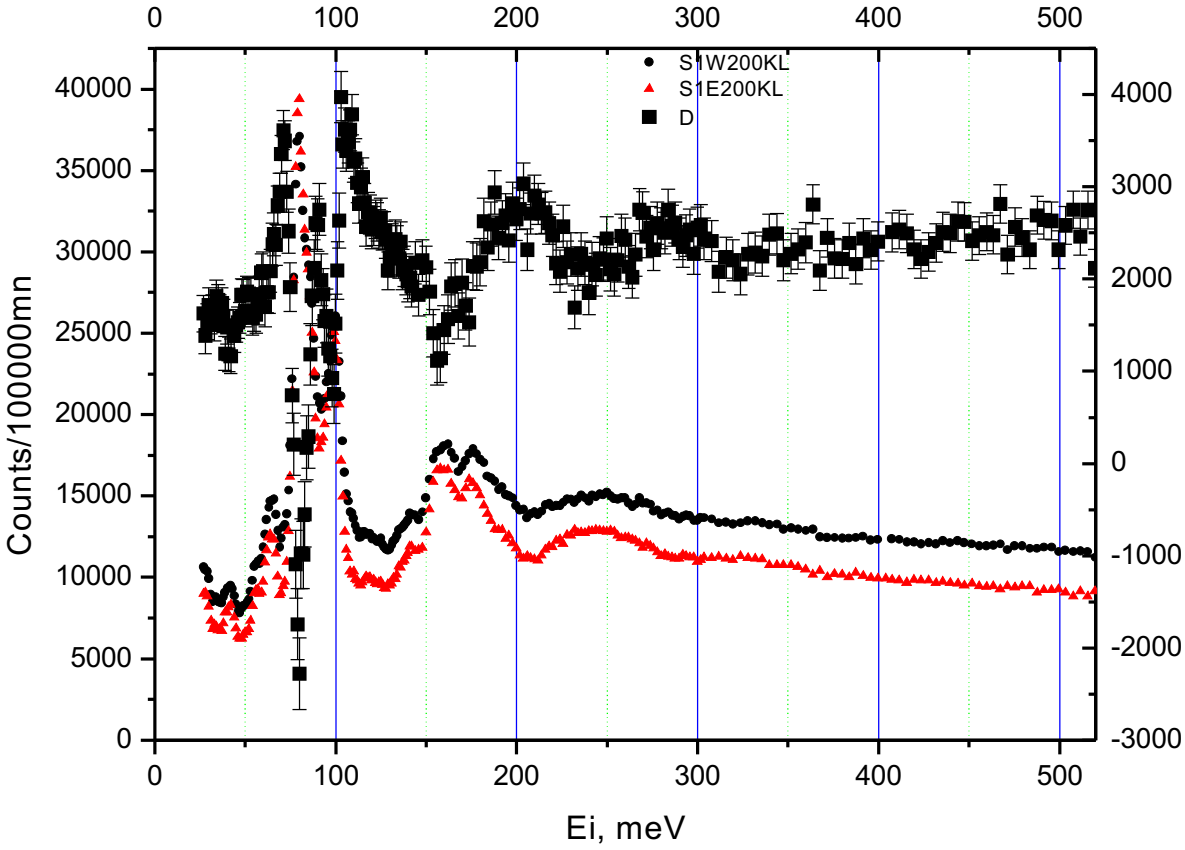
S#1 200K a3=8 (along Ki) Cu220
S1W200KL
S1E200KL
D
Counts/100000mn
Ei, meV
0
100
200
300
400
500
40000
35000
30000
25000
20000
15000
10000
5000
4000
3000
2000
1000
-1000
-2000
-3000

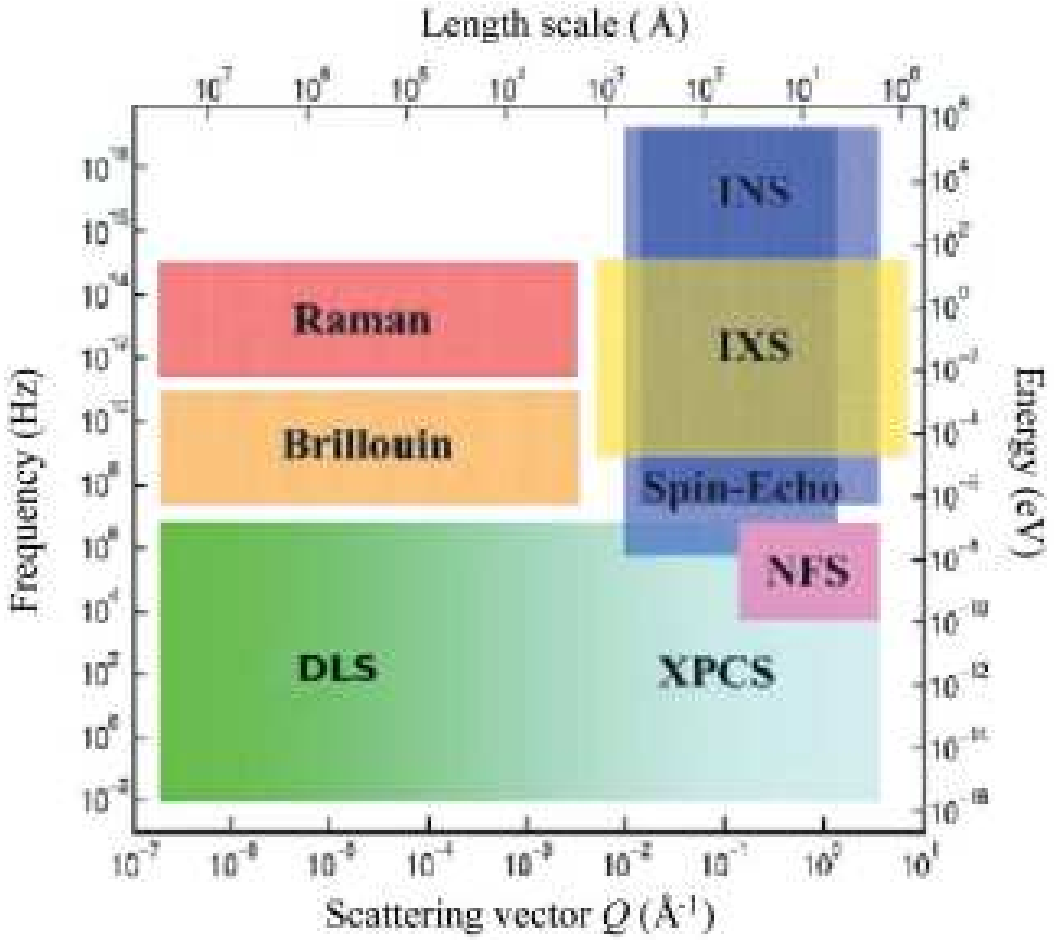

Figure 1
The frequency–scattering vector domains of available techniques for dynamic studies [adapted from Grübel & Zontone (2004)]. The XPCS domain can be extended down to $q \simeq 3 \times 10^{-4}$ Å^{-1} and $\nu \simeq 10^{-4}$ Hz, overlapping with DLS. The other techniques are inelastic neutron scattering (INS), inelastic X-ray scattering (IXS) and nuclear forward scattering (NFS).